2012

Multi-scale hydrogeomorphic influences on bull trout spawning habitat in snowmelt-dominated headwater streams

Jared Robinson Bean
The University of Montana

Multi-scale hydrogeomorphic influences on bull trout spawning habitat in snowmelt-dominated headwater streams

by
Jared Robinson Bean
Bachelor of Arts, Middlebury College, Middlebury, VT 2010

Thesis
Presented in partial fulfillment of requirements of the degree of

Master of Science
in Geosciences

The University of Montana
Missoula, MT

Fall 2012

Approved by:

Sandy Ross, Dean of the Graduate School
Graduate School

Dr. William W. Woessner, Co-Chair
Department of Geosciences

Dr. Andrew C. Wilcox, Co-Chair
Department of Geosciences

Dr. Clint C. Muhlfeld
USGS Northern Rocky Mountain Science Center &
Flathead Lake Biological Station

Acknowledgements

I would like to thank the individuals and organizations that helped make this study possible. I thank my co-advisors, William Woessner and Andrew Wilcox, for the opportunity to work on this project and for their guidance and encouragement. Thank you also to Clint Muhlfeld for helping land the project and guide me through the process. Thank you to my lab group colleagues for your comments and suggestions at various points during this study. Thank you to Johnnie Moore for useful insights on my research proposal. Thank you to everyone who assisted me in the field: Ali White, Franklin Dekker, Sharon Bywater-Reyes, Nicholas Banish, Allie Tincher, Ben Gardner, Thomas Pallin, Zack Rambo, Rob Livesay, Thomas Bean, Lisa Bean, Andy Bean, and Phil Ehrlich. Thank you to Vin D'Angelo for helping with logistics. Thank you to Carter Fredenberg, Brady Miller, Ben Galloway, Tommy Peterson, and Joe Giersch for helping to show me the ropes in the Park. Thank you to Chris Downs, John Fraley, and Mark Deleray for letting me tag-along on redd counts. Thank you to Tom Weaver and John Fraley for advising me on study reach location selection and providing other background information. Thank you to Dan Kotter for helping me get started. Thank you to the Glacier National Park staff, especially Chris Downs, Tara Carolin, and Scott Emmerich, for allowing me to work in such an incredible field area. Thank you to the UM Geosciences Department faculty and staff, especially Aaron Deskins, Christine Foster, Loreene Skeel, and Wendy Wollett for all that you do. Thank you to Marco Maneta and Heiko Langner for helping with data analyses. This work was financially supported by grants from the USGS, the Cooperative Ecosystems Studies Unit (CESU), the National Park Service, the Montana Institute on Ecosystems (NSF EPSCoR program grant EPS-1101342), and the Montana Water Center. Any opinions, findings and conclusions or recommendations expressed in this material are those of the author(s) and do not necessarily reflect the views of the funding agencies.

Bean, Jared, M.S., Fall 2012 Geosciences

Multi-scale hydrogeomorphic influences on bull trout spawning habitat in snowmelt-dominated headwater streams

Committee Chairpersons: William Woessner and Andrew Wilcox
External Committee Member: Clint Muhlfeld

Abstract

I investigated relationships between geomorphology, hydrogeology, and bull trout (*Salvelinus confluentus*) redd occurrence and density at multiple spatial scales in gravel-bed, pool-riffle, snowmelt dominated headwater streams of northwestern Montana. Subreach redd occurrence tended to be associated with the finest available textural facies. In subreach streambed sections hosting bull trout redds, redd density was significantly (at α=0.05) positively related to bankfull Shields stress (τ^*_{bf}, p=0.04) and bankfull Shields stress adjusted for grain stress only (τ^{**}_{bf}, p=0.02). In stream reaches hosting bull trout redds, reach-average redd density was significantly positively related to reach-average τ^{**}_{bf} (p=0.02) and reach-average streambed grain size (D_{16}, p=0.01; D_{50}, p=0.02, D_{84}, p=0.02). Spawning reaches exhibited high streambed horizontal and vertical hydraulic conductivities, and streambed temperatures were dominated by stream water diurnal cycles to a depth of at least 25 cm. Groundwater provided substantial thermal moderation of stream water for multiple high density spawning reaches. At the valley-scale, redd occurrence tended to be associated with unconfined alluvial valleys. Many previous studies highlight the thermal sensitivity of bull trout. My spawning gravel competence results indicate that a shift in the timing of high flows could increase the likelihood of redd scour during the bull trout egg incubation period.

Table of Contents

List of Figures

List of Tables

INTRODUCTION

Research at the intersection of fluvial geomorphology, hydrology, and ecology has expanded in recent years (e.g. Poole, 2010), but an improved understanding of physical and associated ecological processes is needed to develop effective conservation and management practices for aquatic ecosystems. Preserving and improving spawning habitat requires defining key physical and ecological processes controlling spawning site selection and successful fry emergence (e.g. Kondolf 2000; Montgomery et al., 1996; Moir et al., 2002; Kondolf et al., 2008; Tonina and Buffington, 2009b). Species-specific spawning habitat suitability questions remain, especially for bull trout (*Salvelinus confluentus*) whose native range includes the northern Rocky Mountains and Pacific Northwest.

The purpose of this study was to determine primary micro-, subreach-, reach-, and valley-scale physical factors influencing bull trout spawning occurrence in snowmelt-dominated systems. I hypothesized:

1. At the subreach- and reach-scales, spawning locations are associated with channel sections of
   A) low spawning sediment mobility at bankfull flows; and
   B) extensive local streambed hyporheic exchange.
2. At the valley-scale, spawning locations are associated with alluvial valley segments where
   A) the stream valley narrows; and
   B) hyporheic water and groundwater discharges to the stream.

I review what is known about these topics below, explain the basis of these hypotheses, and, in the subsequent analysis and discussion of my data, reinterpret and broaden current understanding of physical process controls on bull trout spawning habitat.

Background

Large-scale connectivity of cold, clean, complex habitats is directly associated with robust bull trout populations (e.g. Rieman and McIntyre, 1993; Muhlfeld et al., 2003; Muhlfeld and Marotz, 2005; Dunham et al., 2008; Al-Chokhachy et al., 2010). Bull trout spawn in cold-water, gravel-bedded, headwater streams (e.g. Fraley and Shepard, 1989). Habitat destruction, fragmentation, invasive species, overharvest, and climate warming have led to a decline in bull trout populations throughout much of their native range (Rieman et al., 1997). Bull trout have been listed as a threatened species since 1998 (U.S. Office of the Federal Register, 1998). Critical habitat designations for bull trout in the United States include areas in Montana, Idaho, Washington, Oregon, and Nevada (US Office of the Federal Register, 2010); bull trout also inhabit parts of Western Canada (e.g. Rieman and McIntyre, 1993).

Bull trout exhibit two distinct life history forms, migratory and resident. Migratory forms often exceed 60 cm in length; they spend much of their adult life in large lake and river systems and migrate to small headwater streams to spawn (e.g. Goetz, 1989; Fraley and Shepard, 1989; Rieman and McIntyre, 1993). In contrast, resident bull trout range in length from 15 to 30 cm and spend their entire life in headwater streams (e.g. Goetz, 1989; Rieman and McIntyre, 1993). Adult bull trout typically spawn annually or biennially from late August to October (Fraley and Shepard, 1989; McPhail and Murray, 1979; Baxter and Hauer, 2000; Dunham et al., 2001) and fry emerge from the streambed gravels in February through April (Baxter and Hauer, 2000).

The bull trout is a member of the Salmonidae family and the Salmoninae subfamily. Whereas all fish species of the Salmonidae family are commonly referred to as “salmonids”, the use of the term “salmonid” in this paper refers only to salmonids in the Salmoninae subfamily (e.g. trout, salmon, and char). The literature describing bull trout spawning habitat characteristics (e.g. Fraley and Shepard, 1989; Rieman and McIntyre, 1993; Baxter and Hauer, 2000) is small in comparison to the collective body of literature on related salmonid species (e.g. Kondolf, 2000; Buffington et al., 2004; Moir et al., 2009; Montgomery et al., 1996; Montgomery et al., 1999; Tonina and Buffington, 2009b). I therefore draw on

the findings of studies on related salmonids to build a conceptual model of the physical conditions and processes that may influence bull trout spawning habitat suitability.

At various spatial scales, geomorphic and hydrogeologic conditions are commonly cited as important factors in salmonid spawning site selection and successful fry emergence (Figure 1, Table 1). At the micro- or patch-scale, streambed grain size constrains the abundance of potential salmonid spawning habitat (e.g. Kondolf and Wolman, 1993; Buffington et al., 2004) (Figure 1a, Table 1a). Optimal spawning substrate for bull trout is unembedded, well-sorted gravel-cobble deposits (Fraley and Shepard, 1989; Baxter and Hauer, 2000; Al-Chokhachy et al., 2010). Suitable median surface grain sizes (D_{50}) for bull trout spawning range from 8 mm to 64 mm (Baxter and McPhail, 1996; Dunham et al., 2001). Bull trout redd tailspill thicknesses have been observed in the range of about 15-25 cm (e.g. Weaver and Fraley, 1991). Migratory bull trout in western Washington reportedly bury their eggs at an average depth of 10-15 cm (DeVries, 1997; Shellberg, 2002).

The pit and tailspill of a salmonid redd functions to create a micro-scale concave-up streambed curvature within a given bedform and theoretically induces stream water flow through the tailspill hosting the eggs (e.g. Tonina and Buffington, 2009b). This modification of the streambed increases the hydraulic conductivity of the tailspill hosting the eggs by winnowing fines from the substrate matrix and therefore increasing intragravel flow velocities and dissolved oxygen concentrations within the redd (e.g. Tonina and Buffington, 2009b). High hydraulic conductivity and intragravel flow rates in redds are necessary for supplying oxygenated water to incubating eggs and removing metabolic waste (Cordone and Kelley, 1961; Chevalier et al., 1984; Bjornn and Reiser, 1991). Embryo survival and fry emergence success is vulnerable to deposition of fine sediments within redd gravels, a process that reduces the rates of water exchange and waste removal (e.g. Fraley and Shepard, 1989; Kondolf, 2000). The survival of bull trout embryos is optimized at water temperatures ranging from 2-4°C (McPhail and Murray, 1979).

Scaling up from the patch-scale, relationships between spawning locations and physical conditions at the subreach-scale are also important (e.g. Moir et al., 2009; Figure 1b, Table 1b). Geomorphically, at the subreach-scale, salmonid spawning frequency has been linked to streambed sections of low spawning sediment mobility at bankfull flows (e.g. Moir et al., 2009). Additionally, salmonids have evolved life history strategies including fall spawning and late-winter fry emergence that are adapted to avoid peak spring flows associated with snowmelt-dominated hydrographs (e.g. Tonina and McKean, 2010). Furthermore, large salmonids in gravel-bed, pool-riffle streams tend to bury their eggs below bankfull discharge scour depths to avoid scour of incubating eggs (Montgomery et al., 1996). In alluvial rivers, bankfull discharges are considered to be geomorphically significant in that they control channel morphology and streambed mobilization (e.g. Wolman and Miller, 1960; Moir et al., 2009); these flows tend to occur about every 1.5 to 2 years (e.g. Williams, 1978). In gravel-bed streams, streambed disturbance depths during bedload transport are typically less than 2 times surface D_{90} (DeVries, 2002). Large woody debris and side channels increase hydraulic roughness and spawning habitat complexity and help protect incubating salmonid eggs from scour (e.g. Shellberg et al., 2010; Buffington and Montgomery, 1999b).

At the subreach-scale, salmonids tend to spawn in concave-up bedforms (e.g. pool tail-outs) where streambed pressure gradients induce stream water flow through the bedform and back into the stream (e.g. Keller et al., 1990; Kondolf, 2000; Baxter and Hauer, 2000). This mixing zone of surface and shallow subsurface water beneath and adjacent to the stream channel is known as the hyporheic zone (e.g. White, 1993; Woessner, 2000; Tonina and Buffington, 2009a). Whereas groundwater can be thought of as subsurface water of considerable residence time, hyporheic water can be classified as the water that originates in the stream channel, travels through the subsurface, and returns to the stream channel within a timeframe that preserves surface water characteristics (e.g. temperature, dissolved oxygen, etc.) (e.g. Kazezyilmaz-Alhan and Medina, 2006; Tonina and Buffington, 2009a). Hyporheic flow

is driven by spatial changes in 1) total streambed pressure gradients (energy head gradients), 2) cross-sectional alluvial area, and/or 3) streambed hydraulic conductivity (Tonina and Buffington, 2009a). Hyporheic mixing underpins stream ecosystems (e.g. Stanford and Ward, 1993; Tonina and Buffington, 2011), and salmonid spawning habitat specifically (e.g. Baxter and Hauer, 2000, Tonina and Buffington, 2009b) because it impacts stream temperature and enhances the exchange of water and solutes between the stream, streambed, and banks (e.g. Arrigoni et al., 2008; Tonina and Buffington, 2011).

Streambed flux direction also influences spawning site selection for many salmonid species (e.g. Kondolf, 2000); and the preferred direction and magnitude can vary among different species. For example, bull trout and Chinook salmon (*Oncorhynchus tshawytscha)* have been observed to preferentially spawn in streambed gravel where stream water infiltrates (influent or losing stream sections, areas of downwelling stream water) (e.g. respectively Baxter and Hauer, 2000; Vronskiy, 1972). In contrast, chum salmon (*O. keta*) and brook trout (*S. fontinalis*) have been observed selecting upwelling streambed sections (effluent or gaining stream sections, areas of upwelling hyporheic and/or groundwater) (e.g. respectively Tautz and Groot, 1975; Van Grinsven et al., 2012).

Many researchers have observed that some salmonid species – including bull trout – typically do not spawn in streambed patches with seemingly acceptable substrate and bedform conditions (e.g. Burner, 1951; Baxter and Hauer, 2000). Several researchers propose that the lack of a preferred streambed flux magnitude and direction may explain this phenomenon (e.g. Healey, 1991; Baxter and Hauer, 2000; Hansen, 1975; Van Grinsven et al., 2012). Stream temperature also influences bull trout spawning behavior; bull trout tend to spawn in the fall as daily average water temperatures decline below 9˚C (Fraley and Shepard, 1989; Muhlfeld et al., 2006).

At the reach- and valley-scale, in headwater catchments, bull trout tend to spawn in pool-riffle channels (<1.5% slope: Fraley and Shepard, 1989; Montgomery et al, 1999), usually within alluvial valley sections (e.g. Baxter and Hauer, 2000; Figure 1c,d; Table 1c,d). Hydraulic roughness (e.g. wood, bank, and bar roughness; flow diversions or side channels) influences the distribution of streambed gravel textural facies and therefore, the location and abundance of potentially suitable spawning gravels (e.g. Buffington and Montgomery, 1999b; Buffington et al., 2004).

Also at the reach- and valley-scale, stream channel sections that receive groundwater discharge are often linked to bull trout spawning habitat (e.g. Weaver and White, 1985; Fraley and Shepard, 1989; Baxter and Hauer, 2000) and other salmonid spawning habitat (e.g. Benson, 1953; Latta, 1964; Hansen, 1975, Curry and Noakes, 1995; Van Grinsven et al., 2012). Changes in alluvial depth and valley width influence surface water – groundwater exchange. An increase in alluvial depth and width (e.g. transition from confined to unconfined valley) causes movement of water from the channel to the alluvium (e.g. hyporheic flow and groundwater recharge) whereas a decrease in depth and width (e.g. transition from unconfined to confined valley) causes movement of water from the alluvium to the channel (e.g. hyporheic and groundwater discharge) (e.g. Standford and Ward, 1993; Baxter and Hauer, 2000; Malcolm et al., 2005). Upwelling groundwater is often nutrient-rich and can promote patches of increased primary productivity within stream reaches (e.g. Boulton et al., 2010). Groundwater temperature is relatively constant at depths of 10-25 m and can be estimated as 1-2˚C warmer than mean annual air temperature (e.g. Kasenow, 2001). Stream sections receiving groundwater discharge are often considered thermal refugias for fish (e.g. McCullough et al., 2009). In summer, groundwater discharge can provide cold water refugia; in winter, it can provide warm water refugia (Gibson, 1966; Cunjak and Power, 1986; Nielsen et al., 1994). Upwelling groundwater can also prevent anchor ice formation in winter, a condition viewed as potentially adverse to embryo and fry survival (e.g. Benson, 1955; Baxter and Hauer, 2000). In addition, redd temperature regimes impact salmonid egg incubation time (e.g. Hansen, 1975; Weaver and White, 1985). Variations in streambed temperature can provide population resilience through variable emergence timing (Hansen, 1975).

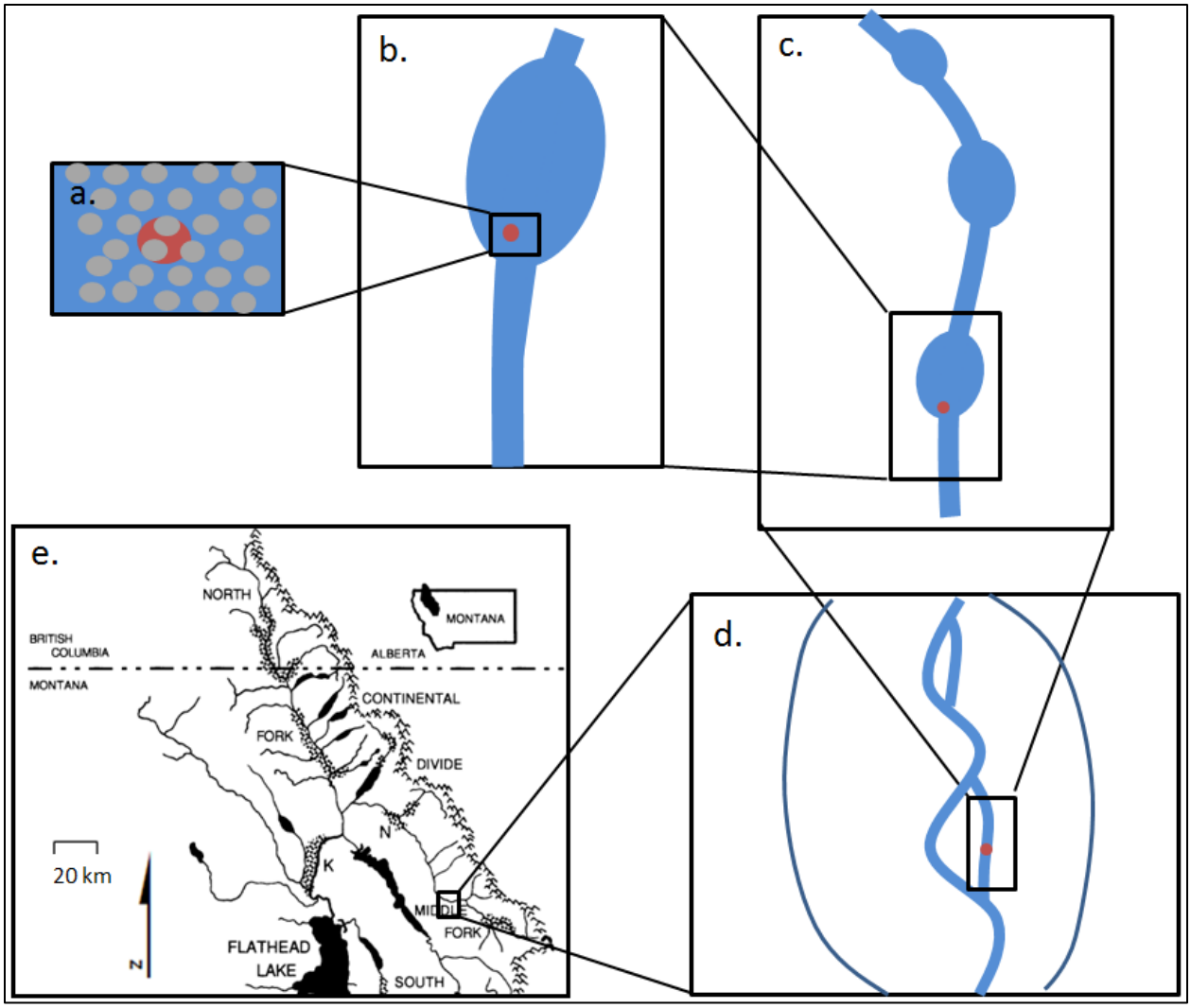

Figure 1. Spatial scales referenced in my conceptual model: (a) micro- or patch-scale; (b) subreach scale; (c) reach-scale; (d) valley-scale; (e) basin-scale (the inset basin-scale image is modified from Stanford and Ward, 1993).

Table 1. Multi-scale physical factors that influence bull trout and other salmonid species' spawning site selection. Literature examples are listed as pertaining specifically to bull trout, or another salmonid species, or to salmonids in general. See Figure 1 for illustrations of the spatial scales.

SPATIAL SCALE	CONCEPTUAL MODEL FACTORS
a. Micro- or patch-scale (centimeters to meters)	• mobile, well-sorted gravels to cobbles (e.g. bull trout: e.g. Fraley and Shepard, 1989; Baxter and Hauer, 2000; Al-Chokhachy et al., 2010; salmonids: e.g. Kondolf and Wolman, 1993) • redd construction that winnows fines, increases hydraulic conductivity, induces or increases downward hyporheic flow through the redd's tailspill, and increases dissolved oxygen supply around the redd (salmonids: e.g. Tonina and Buffington, 2009b)
b. Subreach-scale (tens of meters)	• concave-up bedforms (e.g. pool tail-outs) that induce downward hyporheic flow (bull trout: e.g. Baxter and Hauer, 2000; salmonids: e.g. Keller and Kondolf, 1990; Tonina and Buffington, 2009b) • streambed sections with a specific (preferred) streambed flux direction and magnitude (e.g. bull trout: e.g. Baxter and Hauer, 2000; salmonids: e.g. Healey, 1991) • low mobility of spawning sediment at bankfull flows (salmonids: e.g. Moir et al., 2009)
c. Reach-scale (tens to hundreds of meters)	• channel slopes < 1.5% (bull trout: e.g. Fraley and Shepard, 1989) • pool-riffle channels (bull trout: e.g. Baxter and Hauer, 2000; salmonids: e.g. Montgomery et al., 1999). • reaches with stream temperatures moderated by groundwater input (bull trout: e.g. Baxter and McPhail, 1999; Baxter and Hauer, 2000; brown trout: e.g. Hansen et al., 1975; coaster brook trout: e.g. Van Grinsven et al., 2012) • avoidance of streambed patches of direct groundwater upwelling (brown trout: e.g. Hansen et al., 1975; Atlantic salmon: e.g. Malcolm et al., 2005)
d. Valley-scale (hundreds of meters to kilometers)	• alluvial valley segments in sections of alluvial valley narrowing (bull trout: e.g. Baxter and Hauer, 2000; Atlantic salmon: e.g. Malcolm et al., 2005) • the distribution of spawning appropriate gravels (salmonids: e.g. Buffington et al., 2004; Buffington and Montgomery, 1999b)
e. Basin-scale (kilometers to hundreds of kilometers)	• large-scale connectivity (e.g. minimal anthropogenic migration barriers and streamflow regime alteration: Muhlfeld et al., 2011; low road density: Baxter et al., 1999) of complex local habitat (bull trout: e.g. Muhlfeld et al., 2003; Muhlfeld and Marotz, 2005; Dunham et al., 2008; Al-Chokhachy, et at., 2010)

Hypotheses justification

Hypothesis 1A is based on the premise that redds are created where spawning-appropriate gravels have a low potential for scour in high flow events (e.g. Moir et al., 2009). Hypothesis 1B is based on the premise that stream water cycling through the stream, banks, floodplain, and regional groundwater system influences bull trout spawning site selection because it enhances the delivery of dissolved oxygen and other nutrients to and removes waste products from eggs incubating in streambed gravels (e.g. Baxter and Hauer, 2000; Tonina and Buffington, 2011). Hypotheses 2A and 2B are based on the premise that bull trout redd occurrence is commonly associated with unconfined alluvial valleys and groundwater discharge to the stream channel (e.g. Baxter and Hauer, 2000). Valley narrowing is incorporated in hypothesis 2A because a decrease in valley width can decrease cross-sectional alluvial

area and can result in hyporheic and groundwater discharge to the stream channel (e.g. Stanford and Ward, 1993; Baxter and Hauer, 2000; Tonina and Buffington, 2009a).

I address the subreach-scale hypotheses through field measurements of physical variables in historical high-density spawning reaches of gravel-bed, pool-riffle, mountain headwater streams. I address the valley-scale hypotheses by using remotely sensed delineations of unconfined valleys as well as catchment-scale stream, streambed, and floodplain water temperature measurements. My findings are applicable to salmonid spawning habitat conservation, fisheries management, and stream restoration.

METHODS

Study area

The Flathead River Basin is a snowmelt-dominated headwater drainage of the Columbia River and encompasses 18,400 km^2 of northwestern Montana and southeastern British Columbia (Figure 2). The North and Middle Forks of the Flathead River, in which the study sites described below are located, converge upstream of Flathead Lake and are considered strongholds for native bull trout populations (Fraley and Shepard, 1989; Muhlfeld et al., 2009). Mean annual precipitation in the North and Middle Fork drainages ranges from 55 cm in the valleys to over 215 cm in the highest elevations (Daly and Taylor, 1998). Flow data from 1940 to 2010 indicate that peak annual flows in the North and Middle Fork drainages typically occur in late-May to mid-June (USGS stream gage data, Appendix 1A). Peak annual flows (95^{th} percentiles) occasionally occur while bull trout eggs are incubating in streambed gravels (e.g. in 2007 on November 8; USGS stream gage data, Appendix A). Additionally, the likelihood of fall and winter flood events is increasing (Isaak et al., 2012).

The North and Middle Fork basins are underlain by Precambrian Belt Supergroup metasediments (Vuke et al., 2007). Hydrologically, northwestern Montana is characterized by semiarid mountains with permeable soils and low permeability bedrock (Wolock et al., 2004). Shallow hyporheic and groundwater typically transports ~57% of the total catchment outflow whereas overland flow transports ~43% (Santhi et al., 2008).

For this study, I selected four tributary streams—Ole Creek, Quartz Creek, Trail Creek, and Whale Creek—for field characterization of high-density spawning reaches based on the following criteria: 1) availability of historical bull trout spawning records and active fisheries research and 2) inter-catchment geomorphic variability (Figure 2). Ole and Quartz are within Glacier National Park. Ole is a tributary of the Middle Fork of the Flathead River; Quartz is a tributary of the North Fork and is within the drainage basin of Rainbow Glacier. Draining from the Flathead National Forest, Trail and Whale are also tributaries of the North Fork. Adfluvial bull trout from Flathead Lake spawn in Ole, Trail, and Whale creeks, whereas those spawning in Quartz Creek represent an adfluvial population from Quartz Lake. Bull trout populations in the upper Flathead Lake and River system declined in the early 1990s as a result of community changes related to the invasion of the opossum shrimp (*Mysis diluviana*) in the 1980s into Flathead Lake and the subsequent boom in the non-native lake trout population (Ellis et al., 2011; Muhlfeld et al., 2012). Quartz Lake also hosts a resident lake trout population. Mature, spawning bull trout in the North and Middle Fork drainages are most commonly 6 years old (range 5-8 years old) (Fraley and Shepard, 1989). Focusing my research on headwater snowmelt-dominated streams in the Crown of the Continent ecosystem provided a model to identify natural factors and physical processes influencing bull trout spawning habitat.

In evaluating potential study reaches, I first reviewed historical spawning location data and consulted fisheries biologists familiar with the study streams. Secondly, I selected what I estimated to be consistent high density spawning reaches of each study stream for field characterization. All field

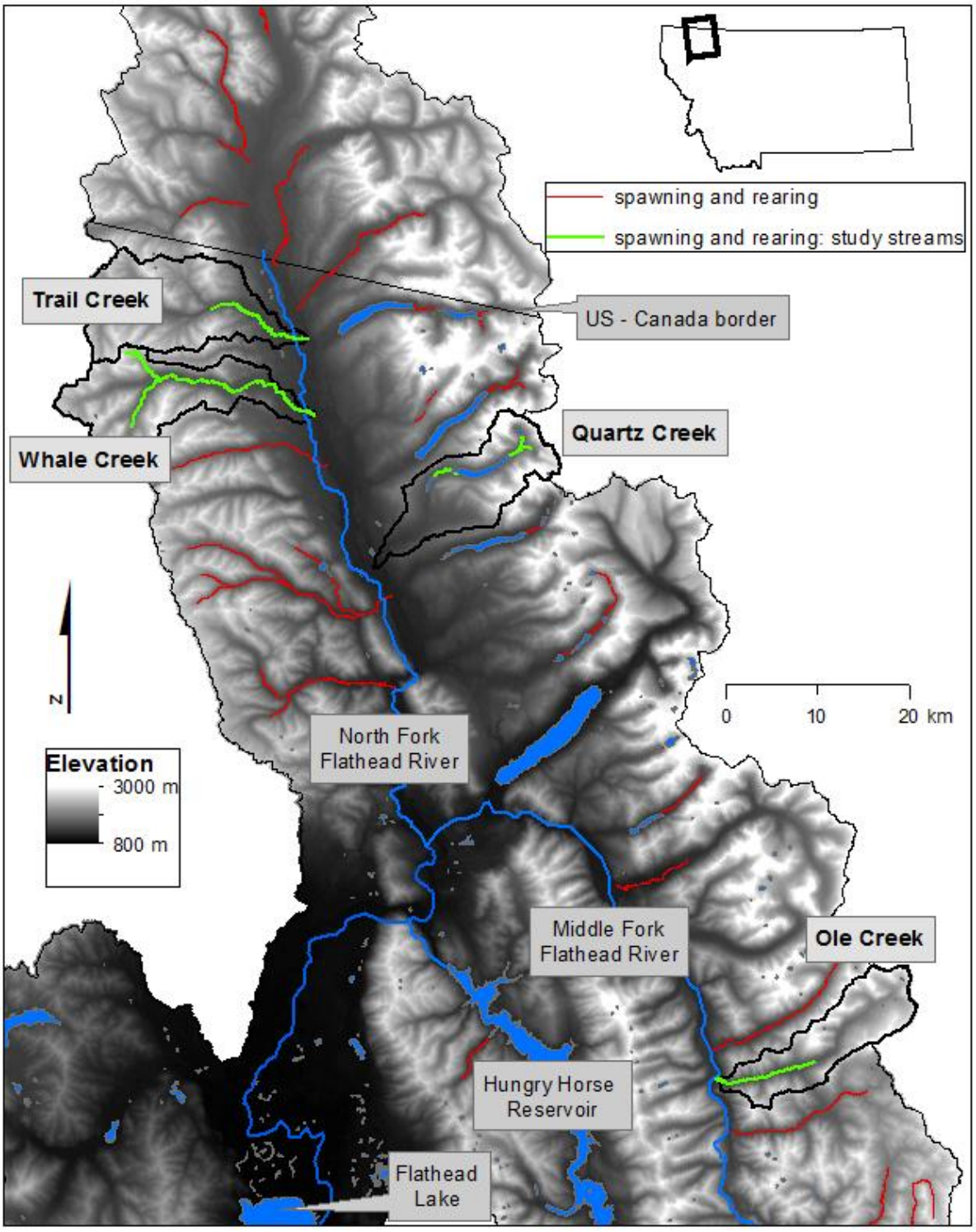

Figure 2. The study area is part of the Flathead River Basin in northwestern Montana. Stream reaches used by bull trout for spawning and rearing are highlighted in red and green (USFWS, 2008); green lines indicate the spawning and rearing reaches of the streams selected for this study. The study catchments are outlined and labeled with bold text.

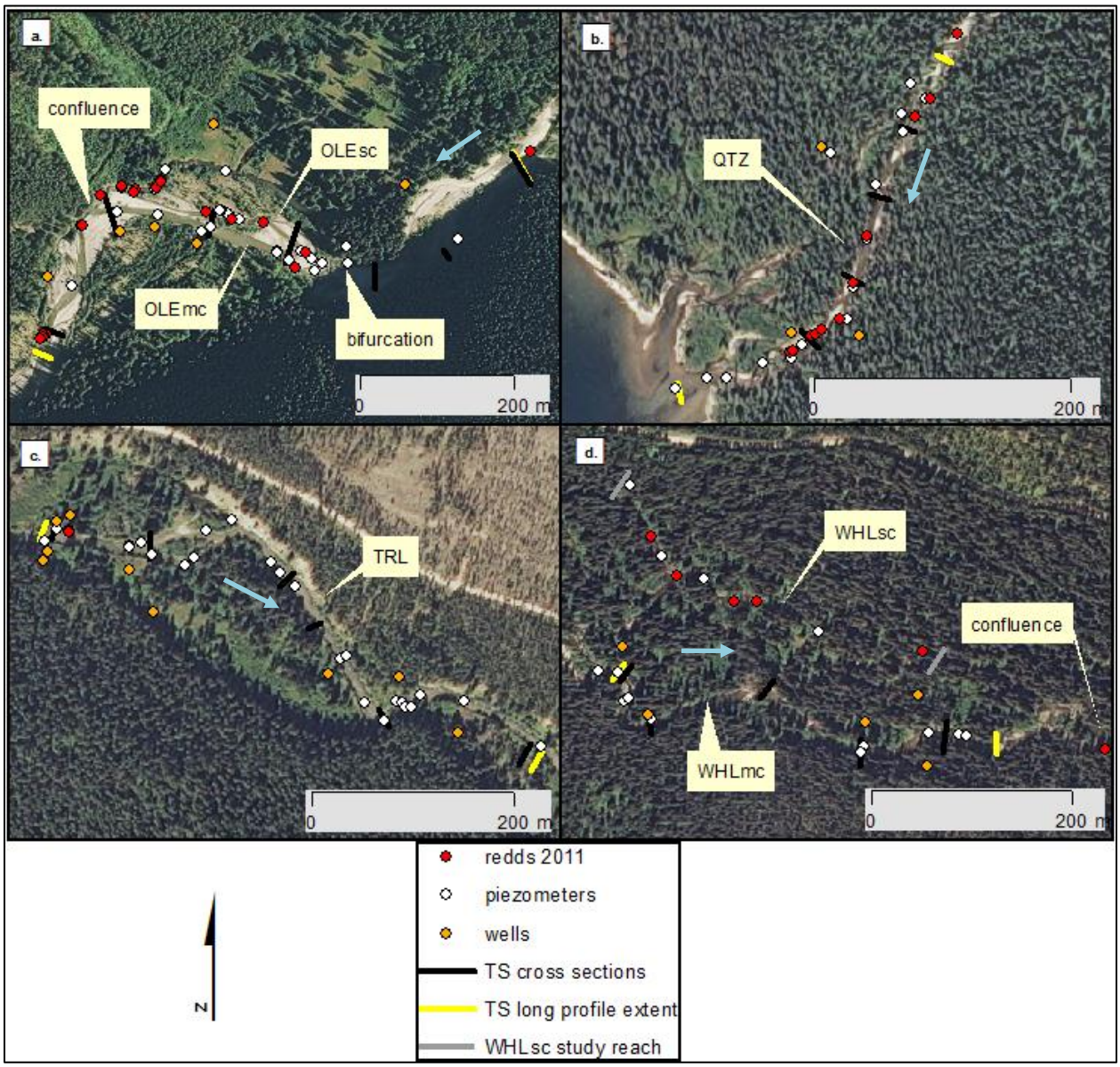

Figure 3. Aerial photographs of the 4 study streams and 6 study reaches. Bull trout redds observed in 2011 are also shown. Blue arrows show stream flow direction. In the legend, TS means "topographic survey"; WHL_{sc} is the only study reach not included in the topographic survey. (NAIP (2011) photos)

instrumentation and site characterization were completed prior to 2011 spawning because regulatory constraints prevented direct instrumentation of newly created redds (Figure 3).

The selected study reaches in Quartz and Trail contained one primary channel, whereas study reaches in Ole and Whale contained a main channel and a secondary channel. The secondary channels of the Ole and Whale study reaches were not connected to the main channels at bankfull discharge. I treat the secondary channels as separate study reaches. Therefore, there are 4 study streams and 6 study reaches. The 6 study reaches are hereafter referred to as: Ole main channel study reach = OLE_{mc}; Ole secondary channel study reach = OLE_{sc}; Quartz study reach = QTZ; Trail study reach = TRL; Whale main channel study reach = WHL_{mc}; Whale secondary channel study reach = WHL_{sc} (Figure 3). US Forest Service roads provided access to the Trail and Whale study sites. The Ole and Quartz sites were

accessible only by foot (and boat for Quartz), and site visits required remaining in the backcountry multiple days at a time. Few hydrogeomorphic datasets exist from remote study sites like OLE_{mc}, OLE_{sc}, and QTZ.

In early October 2011, I assisted fisheries professionals with bull trout redd counts in each of the study streams. In Ole, Quartz, and Trail creeks, I recorded the location of all redds with a handheld Trimble GeoXH 6000 GPS unit. I recorded redd locations in the WHL_{sc} with the same GPS unit; redd locations in WHL_{mc} and throughout the rest of Whale Creek were recorded in paces by fisheries biologists with Montana Fish, Wildlife and Parks.

1A&B) Reach-scale physical characterization

To characterize the geomorphic conditions of the study reaches, I surveyed channel topography, recorded changes in stream stage, measured stream discharge, mapped textural facies, and completed pebble counts (Table 2). I conducted channel topographic surveys with a Leica model TS06 total station (Figure 3). To prepare for the topographic survey, cross section endpoints were staked and their positions recorded with a Trimble GeoXH 6000. Accuracy of these positions was improved by consulting local base station files with the Differential Correction Wizard in GPS Pathfinder Office. These corrected positions were uploaded to the total station to facilitate spatial referencing of the topographic survey. I recorded changes in stream stage in each study stream with Solinst Levelogger Gold Model 3001 dataloggers.

I used stream discharge measurements and estimations to model the driving forces of stream competence—or the capacity of a flow to mobilize streambed particles. I measured stream discharge in late August (hereafter referred to as the "spawning discharge" or Q_{spawn}) using float test methods (3 timed floats over a 20 m distance; velocity correction factor of 0.8) in OLE_{mc}, OLE_{sc}, QTZ, and WHL_{mc} (e.g. Embody, 1927). I did not estimate Q_{spawn} for WHL_{sc}. I estimated Q_{spawn} for TRL as

$$Q_{spawn\,TRL} = Q_{spawn\,WHL_{mc}} * \frac{Q_{2\,TRL}}{Q_{2\,WHL_{mc}}} \quad (1)$$

where Q_2 is a 2-year recurrence interval flood discharge estimate (Equations 2 and 3) (Parrett and Johnson, 2004) (Appendix 1A). Different elements of my analysis required drawing linkages between the Q_2, for which empirical regional relations are available (Parrett and Johnson, 2004) and which are simulated in the HEC-RAS modeling described below, and field measurements of the bankfull level in the study streams. I adopted a simplifying assumption that Q_2 approximates bankfull discharge (Q_{bf}) (e.g. Woman and Miller, 1960). An assessment of ungaged streams in Montana found that the median ratio of Q_{bf} to Q_2 is 0.84, with considerable variability, across 41 sites (Lawlor, 2004). To estimate Q_2 (Q_{bf}) of the main channels of the study streams, I used the USGS Montana ungaged basin flood-frequency calculator which uses basin and climate characteristics and regression equations to estimate various recurrence interval flood discharges (Parrett and Johnson, 2004; Equations 2 and 3; Table 3). For OLE_{mc}, in the Northwest region of Montana, I estimated

$$Q_2 = 0.128A^{0.918}P^{1.33} \quad (2)$$

and for QTZ, TRL, and WHL_{mc}, in the West region of Montana, I estimated

$$Q_2 = 0.268A^{0.927}P^{1.60}(F+1)^{-0.508} \quad (3)$$

where A is drainage area (in mi^2), P is mean annual precipitation (in inches), and F is percentage of basin covered by forest (Parrett and Johnson, 2004) (Table 3).

Table 2. Summary of study reach geomorphic field measurements. X's indicate data was collected; -'s indicate data was not collected.

Study reach	Long profile	Cross sections	Stream stage change	Stream discharge (Q_{spawn})	Textural facies	Pebble counts
OLE_{mc}	x	7	-	x[a]	x	4
OLE_{sc}	x	3	x	x	x	2
QTZ	x	4	x	x	x	4
TRL	x	6	x	x	x	4
WHL_{mc}	x	5	x	x	x	5
WHL_{sc}	-	-	-	-	x	2

[a] I conducted the OLE_{mc} float test discharge measurement adjacent to the OLE_{sc} float test discharge measurement. Therefore, I estimated the OLE_{mc} discharge upstream of the OLE_{sc} bifurcation (and downstream of the OLE_{sc} confluence) to be the sum of the OLE_{mc} and OLE_{sc} float test discharge measurements.

Table 3. Study reach bankfull discharge (Q_{bf}) estimate input data to the "Basin and climate characteristics model" of the USGS Montana Ungaged Basin Flood-Frequency Calculator (Parrett and Johnson, 2004).

Stream	Region	Drainage area[a] (km^2)	Mean annual precipitation[b] (cm)	Basin forest cover[c] (%)	Flood recurrence interval[d] (yrs)
Ole	Northwest	100	102	NA[e]	2
Quartz	West	30	122	80%	2
Trail	West	140	122	80%	2
Whale	West	130	122	80%	2

[a] Calculated at the center of each study reach from 30 m digital elevation models (DEMs).
[b] Estimated from mean annual precipitation map provided by the Montana flood frequency calculator; mean annual precipitation data from the US Soil and Conservation Service (1981).
[c] Estimate based on visual field observations.
[d] The 2 yr recurrence interval (RI) flood (Q_2) is the lowest RI flood discharge value output by the calculator and is used as my estimate of bankfull discharge (Q_{bf}) for the study reaches.
[e] % basin cover is not included in the Northwest (MT) region flood-frequency regression equation (Equation 2).

Textural facies are defined herein as streambed surface patches of distinct grain size (e.g. Pettijohn, 1975; Kondolf et al., 2003). I created textural facies patch maps (Appendix 1A) from narrated field video recordings of each study reach in which I walked the study reach and described streambed grain size and wood distributions. I assigned descriptive grain size codes to each textural facies using the terminology described by Buffington and Montgomery (1999a). Random-walk pebble counts of the b-axis of 100 particles (Wolman, 1954) were conducted in the dominant textural facies of each study reach to estimate the D_{16} (the size for which 16% are finer), D_{50} (median grain size), and D_{84} (the size for which 84% are finer) of each textural facies in each study reach (Kondolf et al., 2003). Particles <2 mm were recorded as 1 mm (Buffington and Montgomery, 1999b). I did not truncate grain size data collection at 4 or 8 mm as is sometimes recommended (e.g. Wolman, 1954; Kellerhals and Bray 1971; Church et al., 1987; Bundt and Abt, 2001; Kondolf et al., 2003) because such truncation can distort the size distribution (Buffington and Montgomery, 1999b). Inclusion of fine particles in pebble count data should

not be problematic for characterizing the framework gravel sizes (e.g. Bundt and Abt, 2001; Kondolf et al., 2003).

I assess subreach- and reach-scale streambed mobility of the study reaches at bankfull flows with calculations of Shields stress (τ*), a dimensionless measure of stream competence (e.g. Shields, 1936; Church, 2006). The use of a dimensionless parameter allows direct comparisons of stream competence within and between stream systems. The critical, or threshold Shields stress (τ^*_c) for streambed particle entrainment in alluvial rivers varies; Buffington and Montgomery (1997) report a range from 0.03 to 0.086. For this study, I adopt a commonly used τ^*_c value of 0.045 (e.g. Yalin and Karahan, 1979; Buffington and Montgomery, 1997; Church, 2006; Dingman, 2009). Shields stress (τ*) is the ratio of the flow force per unit area (τ_o) to the submerged weight of sediments per unit area (Church, 2006):

(4) $$\tau^* = \frac{\tau_o}{(\rho_s - \rho_w) g D_{50}}$$

where

(5) $$\tau_o = \rho_w g R S$$

and τ_o is total boundary shear stress (in N/m^2), ρ_s is the density of the streambed sediment (estimated as the density of quartz, 2650 kg/m^3), ρ_w is the density of water (estimated as 1000 kg/m^3), g is the force of gravity (9.8 m/s^2), D_{50} is median surface grain size (in m), R is hydraulic radius (in m), and S is slope. Total boundary shear stress (τ_o) is commonly used in the calculation of streambed mobility, although sediment transport is driven only by the portion of τ_o applied to the streambed – known as bed or grain shear stress (τ') (e.g. Buffington and Montgomery, 1997). Bed shear stress (τ') is defined as total boundary shear stress (τ_o) corrected for momentum losses due to hydraulic roughness caused by banks, bars, and wood debris (e.g. Einstein and Banks, 1950; Einstein and Barbarossa, 1952; Buffington and Montgomery, 1999b). In gravel-bed rivers, hydraulic roughness due to bedforms alone (e.g. "form drag") can cause grain shear stress (τ') to be 10-75% less than total boundary shear stress (τ_o) (e.g. Parker and Peterson, 1980). Therefore, in order to more accurately calculate streambed mobility in the study reaches, I calculated an adjusted Shields stress (τ**):

(6) $$\tau^{**} = \frac{\tau'}{(\rho_s - \rho_w) g D_{50}}.$$

I calculate the grain shear stress (τ') using a modified form of an equation suggested by Wilcock et al. (2009) based on the Strickler relation for grain roughness:

(7) $$\tau' = 0.018 (S D_{50})^{1/4} U^{3/2}$$

where 0.018 represents the density of water, the force of gravity, and the Strickler relation for grain roughness; and U represents streamflow velocity (in m/s) (Wilcox, 2011).

For the Shields stress calculations, I obtained D_{50} values from my textural facies maps and pebble count data (e.g. Kondolf et al., 2003). Based on visual observations, I grouped the subreaches of each study reach into textural facies using the classification system of Buffington and Montgomery (1999a) (Appendix 1). I then conducted pebble counts in each textural facies and used the D_{50} values in my Shields stress calculations. Additionally, I input channel topography and stream discharge measurements into the Hydrologic Engineering Center's River Analysis System (HEC-RAS: Brunner, 2010) to calculate total boundary shear stress (τ_o), channel slope (S), and streamflow velocity (U) at the subreach-scale for bankfull conditions (see Appendix 1A for details on HEC-RAS input data and assumptions). I calculated bankfull Shields stress (τ^*_{bf}) and bankfull adjusted Shields stress (τ^{**}_{bf}) for 20 m long subreach-scale sections in OLE_{mc}, OLE_{sc}, QTZ, TRL, and WHL_{mc}.

To characterize the hydrogeologic properties of the study reaches, I installed in-stream mini-piezometers (hereafter referred to as "piezometers") and measured vertical hydraulic gradients (VHG), horizontal hydraulic conductivity (K_h), vertical specific discharge (q_v), vertical hydraulic conductivity (K_v), and hydraulic conductivity anisotropy ratios (K_h/K_v). Networks of in-stream piezometers were installed

by hand throughout each study reach using standard methods at various spatial densities depending on the geomorphic complexity of the reach (Figure 3; Table 4) (Lee and Cherry, 1978; Baxter et al., 2003).

Table 4. Number of in-stream piezometers per study reach.

Study reach	In-stream piezometers
OLE_{mc}	14
OLE_{sc}	11
QTZ	15
TRL	22
WHL_{mc}	10
WHL_{sc}	4

All piezometers were 2.54 cm diameter and 152 cm long polyvinyl chloride (PVC) tubes. Piezometers used to characterize streambed horizontal hydraulic conductivity ("slug test piezometers") had a 20 cm long perforated interval of ~14 drilled holes (~6 mm diameter); this screen section was wrapped with paint strainer nylon mesh. Piezometers not used for horizontal hydraulic conductivity (K_h) characterization had 5-7 cm long perforated intervals of 4 drilled holes (~2 mm diameter). I drove piezometers into the streambed using a similar method to that described by Baxter et al. (2003) (Appendix 1B). Piezometers were installed to an approximate total depth in the streambed of 45 cm, which is below the maximum depth of observed bull trout redd excavation (~25 cm; e.g. Weaver and Fraley, 1991). Characterization of hyporheic flows in spawning reaches allows inferences about the ease, magnitude, and direction of water flows through the streambed prior to redd construction. I made an effort to install piezometers in each textural facies identified in the subreach geomorphic characterization; however some textural facies were too coarse for piezometer installation. Because of literature-supported correlations of spawning with concave-up bedforms (e.g. pool tail-outs: Kondolf, 2000; Baxter and Hauer, 2000), I instrumented concave-up bedforms with piezometers more frequently than other bedform types (e.g. mid-riffle). Vertical hydraulic gradient (VHG) measurements were made monthly by hand using a tape measure and water soluble marker. VHG is calculated from the equation

$$VHG = \frac{\Delta h}{\Delta l} \quad (8)$$

where Δh is the length difference between the water level inside the piezometer to water level of the stream surface, and Δl is the length from the streambed surface to the center of the piezometer perforations at depth.

To estimate streambed horizontal hydraulic conductivity (K_h) in OLE_{mc}, QTZ, TRL, and WHL_{mc}, I conducted multiple falling-head slug tests in 4-5 piezometers per study reach by introducing a slug of 100 ml of water and measuring head change at 0.5 s or 1 s intervals with a Solinst Levelogger Gold Model 3001. Efforts were made to introduce the slug as instantaneously as possible as recommended by Butler (1998). I attempted to create a streambed surface seal to prevent vertical leakage by stomping and tamping sediment around the piezometer with my wading boots immediately after piezometer installation (e.g. Kondolf et al., 2008). In analyzing my slug test data, I followed the pre-analysis processing guidelines of Butler (1998). Because of non-instantaneous slug introduction, I used the translation method (Pandit and Miner, 1986). I normalized water level deviations from static and then used the AquiferTest software package (Schlumberger, 2011) to curve-match the head response data and estimate horizontal hydraulic conductivity (Appendix 1B).

To estimate streambed vertical specific discharge (q_v), I installed vertical arrays of Maxim iButton thermochrons (Part # DS1921Z-F5) inside piezometers (OLE_{mc} n=7; OLE_{sc} n=3; QTZ n=2; TRL n=9; WHL_{mc} n=5; WHL_{sc} n=2). iButton calibration and vertical array installation procedures were similar to methods described by Johnson et al. (2005); expected error in the calibrated temperature datasets is <0.25˚C (Johnson et al., 2005). I tested various waterproofing techniques and witnessed occasional failures of both "waterproofed" and "non-waterproofed" (unaltered) iButtons. To reduce the possibility of data loss, I deployed all iButtons as pairs. In an attempt to "waterproof" the iButtons, I wrapped each with parafilm and then covered each with liquid electrical tape. I employed two different vertical array designs (Figure 4). To analyze the vertical streambed temperature datasets, I first qualitatively described

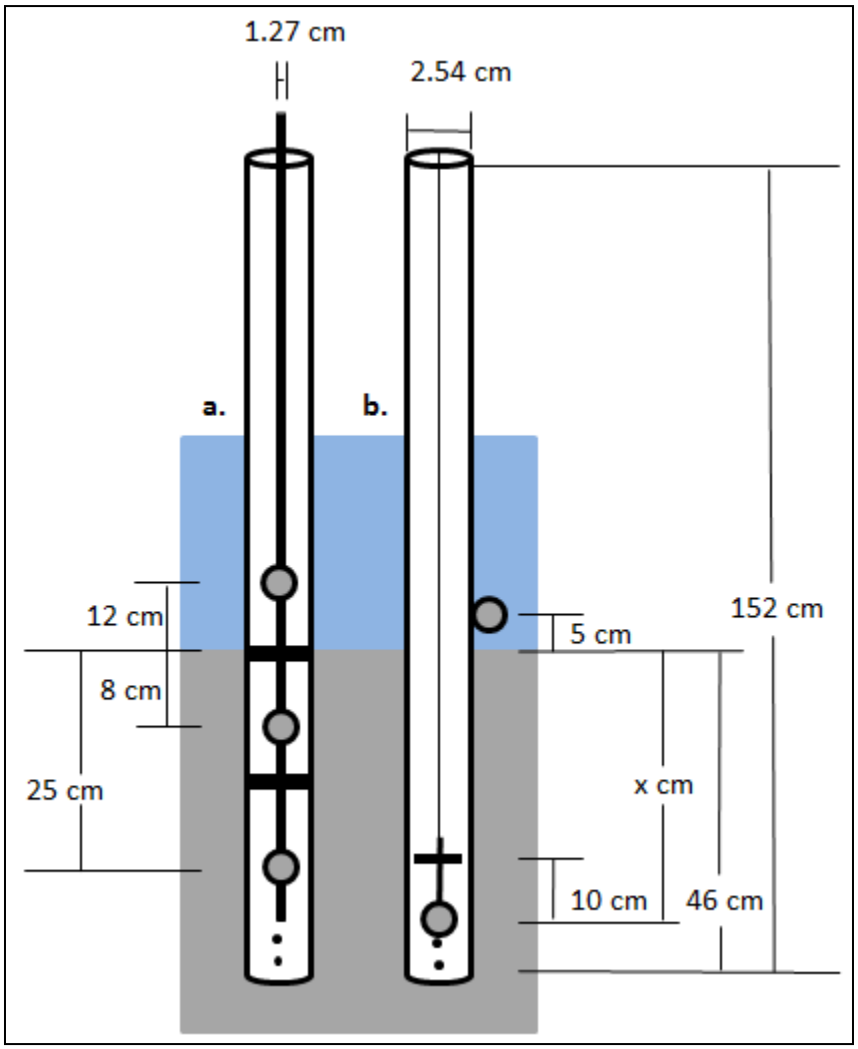

Figure 4. Illustrations of the vertical iButton array designs. iButtons were installed as pairs to reduce the possibility of data loss if one instrument failed. As stream stage lowered during the field season, I lowered the stream temperature iButton in design (a) to 6 cm above the streambed. The center rod hosting the iButton pairs in design (a) was a 1.27 cm diameter PVC tube. The baffles consisted of closed cell foam that was duct taped in place. In design (b), the stream iButton pair was duct taped to the outside edge of the piezometer on the north side to minimize solar exposure and potential artificial heat signatures. The inside iButton pair was taped near the bottom of a 14 cm long bolt that was hung from the top of the piezometer with fishing line. The hanging length varied from piezometer to piezometer but the iButton pair was intended to be positioned about 10 cm above the bottom of the piezometer. About 10 cm up from the hanging iButton pair, two 2.5 cm diameter galvanized washers separated by a nut acted as a baffle to isolate the iButtons.

differences between the stream water temperature signal and subsurface water temperature signals using any combination of the metrics coined by Arrigoni et al. (2008): buffered (decrease in amplitude), lagged (difference in phase), or cooled/warmed (difference in mean). Next, for vertical temperature datasets with the most substantial differences, I calculated daily averaged q_v with the MATLAB program Ex-Stream primarily employing the Keery et al. (2007) amplitude ratio method (Swanson and Cardenas, 2011). For all designs, I assumed the temperature recorded by the in-stream iButtons to be representative of the water temperature at the stream – streambed interface.

At locations where q_v was estimated, I used vertical hydraulic gradient (VHG) measurements from the same piezometer (obtained directly before, during, or after vertical array emplacement) and Darcy's Law to estimate vertical hydraulic conductivity (K_v) (Darcy, 1856):

$$K_v = \frac{q_v}{VHG} \quad (9)$$

where K_v is in (m/d), q_v is in ($m^3/(m^2d)$), and VHG is dimensionless ($\Delta h/\Delta l$). At sites where both K_h and K_v were determined I calculated the hydraulic conductivity anisotropy ratio (K_h/K_v). Where possible, I compare and contrast conditions within a study reach; however, much of my analysis focused on inter-study reach comparisons of reach-averaged hydrogeologic variables.

2A&B) Valley-scale physical characterization

At the valley-scale (Figure 1d), I evaluated the influence of valley confinement on spawning occurrence. Delineations of unconfined and confined valleys were conducted for all tributary catchments of the Flathead River Basin by Wenger et al. (2011) using ground slope and convolution filtering methods of 30 m digital elevation models (DEMs) and NHDPlus streamlines (Wenger et al., 2011). Unconfined valley inclusion criteria included maximum ground slope of 8%, maximum valley width of 500 m, minimum stream length of 1500 m, and minimum valley area of 3700 m^2 (Nagel et al., *in press*). Field validation by Wenger et al. (2011) indicated that the valley confinement algorithm successfully distinguished unconfined and confined valley segments in the interior Columbia River Basin. Occasionally, the Wenger et al. (2011) valley confinement algorithm mistakes terraces for valley bottoms (David Nagel, 2012, personal communication). A new version of the algorithm (Nagel et al., *in press*) fixes this problem with a flooding routine (David Nagel, 2012, personal communication)) but was not applied here. I edited unconfined valley delineations of each study catchment in ArcMap 10.0 based on field and DEM observations (Appendix 2A).

I characterized valley confinement of the study reaches using the valley confinement ratio (VCR)

$$VCR = \frac{unconfined\ valley\ width}{active\ channel\ width}. \quad (10)$$

I estimated unconfined valley width (in m) of each study reach from the Wenger et al. (2011) unconfined valley polygons as the average valley width at the upstream end, center, and downstream end of each study reach. I estimated valley width of confined valley sections as 30 m (because 30 m DEMs were used to create the unconfined valley polygons). I estimated study reach active channel width (in m) as reach-average bankfull channel width. I obtained reach-average bankfull channel widths for OLE_{mc}, OLE_{sc}, QTZ, TRL, and WHL_{mc} from the channel cross sections surveys. I visually estimated reach-average bankfull channel width for WHL_{sc}. Unconfined valleys are generally described by VCRs > 2.5-5.0; VCRs < 2.5-5.0 indicate confined valleys (e.g. Hall et al., 2007; Nagel et al., in press).

To characterize valley confinement characteristics near bull trout redds observed throughout the study catchments in the 2011 count, I first recorded whether or not each redd was located in an unconfined valley using the edited Wenger et al. (2011) unconfined valley delineations. For redds located in unconfined valleys, I made general observations of valley narrowing, broadening, or remaining constant in the downstream direction. Representations of these qualitative assessments of rate of change in valley width are presented in the results. Due to the coarse scale of the unconfined valley delineations and the error associated with their creation, broad qualitative observations were

more appropriate than quantitative measurements of change in valley width at redd locations. Quantitative measurements of change in valley width at redd clusters were attempted, but the differences in spatial resolution of the unconfined valley delineations (coarse) and redd clusters (fine) limited the utility of these assessments.

To characterize the valley-scale (Figure 1d) hydrogeology and surface water – groundwater interactions, I installed a limited network of shallow floodplain wells adjacent to each study reach to determine floodplain water table elevations and floodplain water temperatures (Figure 3). These wells were the same dimensions and material as the in-stream piezometers and were installed to a maximum depth of 140 cm. Each floodplain well was paired with an in-stream piezometer positioned on the same perpendicular line from the stream channel to act as a staff gage. I surveyed the elevations of the tops of the wells and staff gage piezometers to compare water level elevations between the floodplain and stream. I measured water table elevations monthly by hand per stream section on the same day that I measured VHGs of the in-stream piezometers. Using monthly water table and stream stage measurements in August, September, and October, I created potentiometric surface maps by plotting the floodplain wells and in-stream staff gages spatially in ArcMap 10.0 and hand drawing contour lines of water table elevation. Taking into account the valley confinement polygons, I drew floodplain alluvial subsurface water flow lines perpendicular to the water table contour lines (Appendix 2B) (Fetter, 2001).

I assessed the influence of hyporheic exchange and valley-scale groundwater system discharges associated with spawning reaches using shallow floodplain water temperature datasets from the study reaches and catchment-wide stream temperature datasets. I instrumented at least one floodplain well in each study reach with a pair of iButton thermochrons to measure floodplain water temperature through time. I obtained the stream temperature datasets from upstream and downstream of my study reaches from the USGS and the Flathead National Forest (Appendix 2B). I compared floodplain water temperature data to stream water temperature in the study reaches to evaluate hyporheic mixing processes and rates. I also estimated the temperature of theoretical regional groundwater at 10-25 m depth as 1-2˚C higher than average annual air temperature (Kasenow, 2001). I estimated average annual air temperature of the study area as the average air temperature from 2007-2011 recorded by the 3 most proximal SNOTEL stations (Appendix 2B). The SNOTEL station elevations are within 150 m of the study reach elevations (Appendix 2B).

Water temperature metrics calculated for various durations included average, standard deviation, rate of change (dT/dt), and coefficient of variation (C_v). Coefficient of variation (C_v) is a dimensionless measure of the extent of variability in relation to the average of a sample population:

$$C_V = \frac{\sigma}{\bar{T}} \quad (11)$$

where σ is the standard deviation in water temperature (in Kelvin), and $\overline{T}$ is the average water temperature (in Kelvin). Kelvin temperatures must be used because C_v is computed from a ratio scale rather than an interval scale, such as Celsius. In analyzing the stream temperature datasets, I considered sensor distribution in relation to the valley confinement delineations.

Statistical analyses

I statistically tested relationships between physical factors and redd density of the study reaches using linear, exponential, and power function regressions (using SigmaPlot 12.3). For each pair of independent and dependent variables, I present the regression with the strongest explanatory power. At the subreach-scale, I tested the dependence of redd density on subreach bankfull and adjusted bankfull Shields stress (τ^*_{bf}, τ^{**}_{bf}) within and among the study reaches. To satisfy statistical test assumptions of normal distribution (Shapiro and Wilk, 1965) and constant variance, I log transform subreach-scale redd density. For subreach channel sections, I calculate redd density as

$$subreach\ redd\ density = \frac{redds}{(20\ m)*(\overline{w})} \quad (12)$$

where 20 m represents the longitudinal subreach section length and $\overline{w}$ represents average channel width (in m) per study reach at the time of spawning.

At the reach-scale, I tested the dependence of reach-average redd density on reach-averaged physical variables (D_{16}, D_{50}, D_{84}, τ^*_{bf}, τ^{**}_{bf}, slope, VCR, VHG, K_h, q_v, K_v, average stream temperature during spawning, standard deviation in stream temperature, and stream temperature C_v). I calculated reach-average redd density as:

$$(13) \qquad reach\ average\ redd\ density = \frac{redds}{(L_{sr})*(\overline{w})}$$

where L_{sr} was study reach length (in m).

I also tested statistical relationships among reach-average physical variables, including the dependence of (1) reach-average D_{50} on reach-average slope and reach-average VCR, (2) reach-average slope on VCR, and (3) various reach-averaged hydrogeologic variables (VHG, K_h, q_v, and K_v) on reach-averaged geomorphic variables (D_{50}, τ^{**}_{bf}, and VCR). Multiple regression analyses of reach-average redd density dependence on physical variables were attempted but were limited by collinearity of physical variables and dataset size.

RESULTS

Flow data from gages on the North Fork and Middle Fork Flathead Rivers, which were used to infer flow conditions in the study reaches, show that in the spring runoff period preceding my data collection (i.e., spring 2011), peak flow magnitudes were above average, with a 3 year recurrence interval (RI) on the North Fork and a 5 year RI on the Middle Fork (USGS gage data; Figure 5; Appendix 1A). Peak flows occurred on June 8 at these gages, within the normal May to June time range of peak discharges in these rivers. Baseflow conditions characterized the majority of the 2011-2012 spawning and incubation period (Figure 5). September (spawning) stream stage in each of study reaches fluctuated less than +/-0.15 m (Appendix 1A).

In October 2011, the number of redds observed in the Ole, Quartz, and Whale drainages, 40, 35, and 42, respectively, was in the range of redds observed over the previous decade (Table 5). In Trail, the 8 redds counted in 2011 was the lowest since 1996 (also 8 redds; Fraley, 2010). Redd densities in the study reaches in 2011 ranged from 0 redds/m^2 in WHL_{mc} to 0.004 redds/m^2 in OLE_{sc} (Table 6).

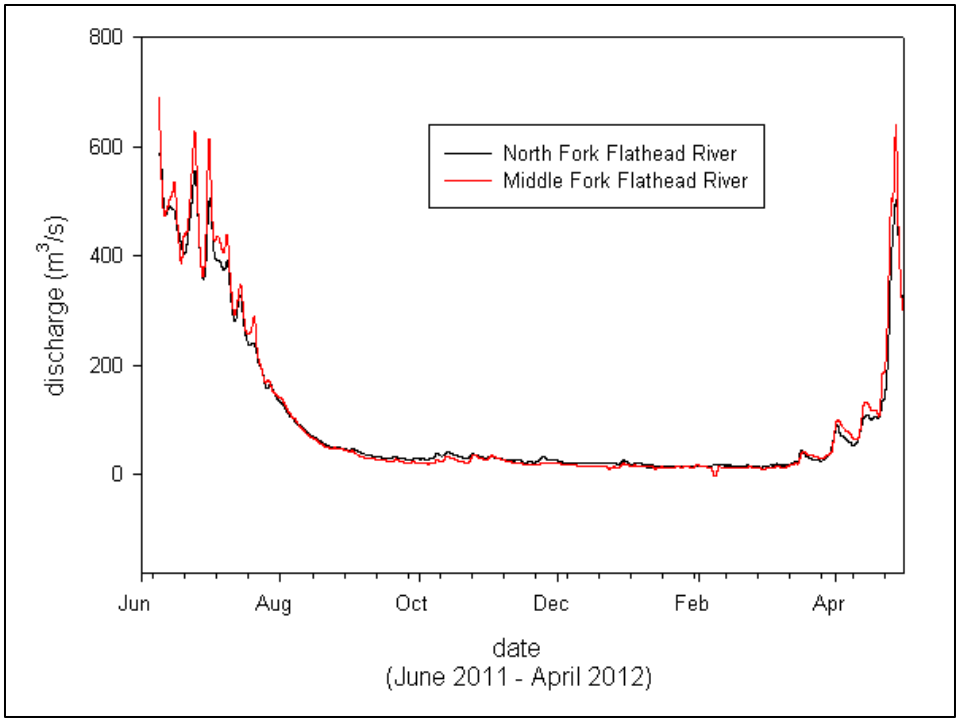

Figure 5. USGS stream gage data for the North and Middle Forks of the Flathead River (USGS gage numbers: North Fork 12355500; Middle Fork 12358500) from the 2011 peak flow (June 8) through spawning (August through October; e.g. Fraley and Shepard, 1989) and emergence (February through April; e.g. Baxter and Hauer, 2000).

Table 5. Historical redd numbers in the index sections of the study streams.

Year	Ole[a]	Quartz[a]	Trail[b]	Whale[b]
2000	33		42	68
2001	29		27	77
2002	21		26	71
2003	21	31	14	34
2004	14	46	34	41
2005	16[c]	4[c]	30	39
2006	31	36	34	56
2007	29	14[d]	51	27
2008	42	51	49	34
2009	34	34	19	43
2010	32	27	11	31
2000-2010 Avg.	27	30	31	47
2011	40[e]	35[f]	8[g]	42[h]
2011 % of 2000-2010 Avg.	148%	117%	25%	89%

[a] Data from Downs et al. (2011). The Quartz index section does not include Rainbow Creek (from the mouth of Cerulean Lake downstream to the confluence with Quartz Creek).
[b] Data from Fraley (2010).
[c] High flows may have obliterated some redds – minimum count (Downs et al., 2011).
[d] Weir at mouth of Quartz Creek likely inhibited spawning activity (Tennant, 2010; Downs et al., 2011).
[e] Redd count by John Fraley, Chris Downs, and Jared Bean.

[f] Redd count by Clint Muhlfeld and Jared Bean. Does not include the 8 additional redds observed in Rainbow Creek near the Mouth of Cerulean Lake.
[g] Redd count by Mark Deleray, Clint Muhlfeld, and Jared Bean.
[h] Redd count by Mark Deleray and Gary Michael.

Table 6. Study reach geomorphic characteristics and 2011 redd numbers per study reach.

Study reach	Channel length (m)	W_{spawn} [b] (m)	Slope	Reach-avg. D_{50} (mm)	2011 Q_{spawn} (m^3/s)	2011 Q_{bf} (m^3/s)	Redds in study reach (2011)	Reach-avg. redd density (redds/m^2)
OLE_{mc}	890	11	1.1%	49	3.4[c]	14	7	0.0007
OLE_{sc}	360	7	1.2%	18	1.6	-	9	0.004
QTZ	400	8	0.74%	22	2.4	4.1	10	0.003
TRL	620	16	1.0%	76	3.9	16	1	0.0001
WHL_{mc}	490	13	0.36%	45	3.5	15	0	0
WHL_{sc}	390[a]	6	-	16	-	-	5	0.002

[a] All study reaches were topographically surveyed except WHL_{sc}; 390 m is the observed channel length for WHL_{sc}.
[b] Reach-average channel width at Q_{spawn}.
[d] Discharge of OLE_{mc} upstream of OLE_{sc} bifurcation.

1A) Reach-scale fluvial geomorphology

Redds in the study reaches tended to be located in concave-up bedforms (Figure 6, Figure 7) and the finest textural facies of the study reaches (Figure 6, Figure 8, Appendix 1A). At the subreach-scale, considering all study reaches, redd density was significantly (α=0.05) positively correlated with subreach bankfull Shields stress (τ^*_{bf}, p=0.04) and bankfull adjusted Shields stress (τ^{**}_{bf}, p=0.02) (Figure 9a,b). Within individual study reaches, subreach-scale redd density was not significantly related to subreach bankfull or bankfull adjusted Shields stress (Figure 9c).

At the reach-scale, study reach redd density was significantly negatively correlated with reach-averaged D_{16} (p=0.01), D_{50} (p=0.02), and D_{84} (p=0.02) (Figure 10, Table 7). Reach-average redd density was significantly positively correlated with τ^{**}_{bf} (p=0.02) (Figure 11, Table 7). There was no relationship between reach-average slope and D_{50} (R^2=0.00; p=1.0; Figure 12. Modeled bankfull adjusted Shields stresses (τ^{**}_{bf}) in the majority of subreach streambed sections in OLE_{sc}, the study reach with the highest redd density, are above the 0.045 value of critical Shields stress (τ^*_c) that is often considered the threshold for particle entrainment (Figure 13). Based on visual observations and patch maps, median surface grain size (D_{50}) of spawning sites in OLE_{sc}, QTZ, and WHL_{sc} were ~16-18 mm; in OLE_{mc}, D_{50} of spawning sites was ~35 mm. Variation in D_{50} of dominant textural facies is most prominent in OLE_{mc}, TRL, and WHL_{mc} (Figure 6, Figure 8). Streambed grain size distributions in OLE_{sc}, QTZ, and WHL_{sc} are relatively consistent (Figure 5, Figure 8). Based on qualitative visual assessment, I rank the study reaches in terms of relative hydraulic roughness (e.g. bar, bank, and wood roughness) from highest to lowest as WHL_{sc}, QTZ, WHL_{mc}, OLE_{sc}, OLE_{mc}, and TRL.

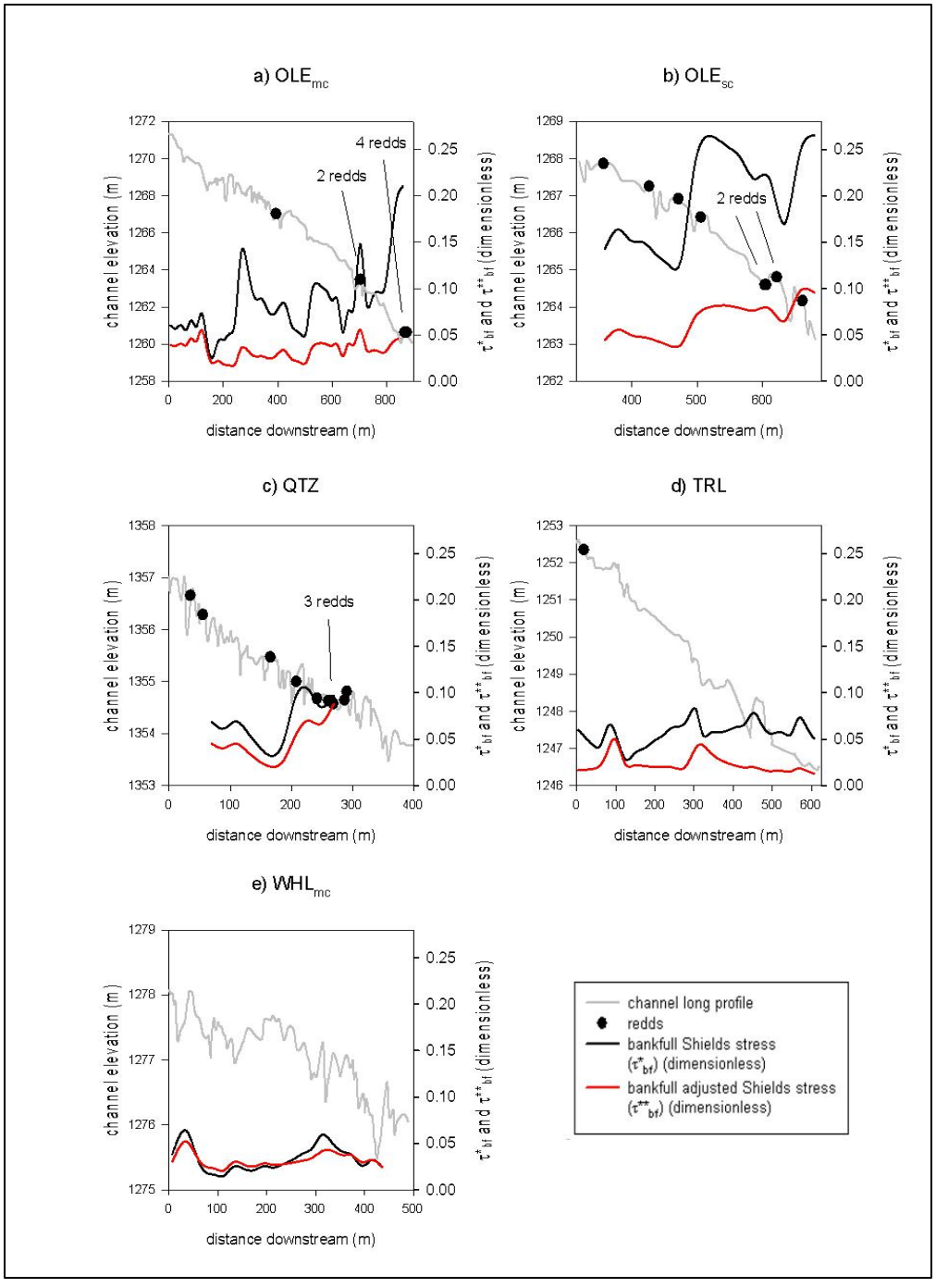

Figure 6. Redd locations in relation to study reach channel long profile, bankfull Shields stress, and bankfull adjusted Shields stress. WHL$_{sc}$ is not included in these plots because it was not topographically surveyed. Finer-scale examples of redd location in relation to bedform curvature are presented in Figure 7.

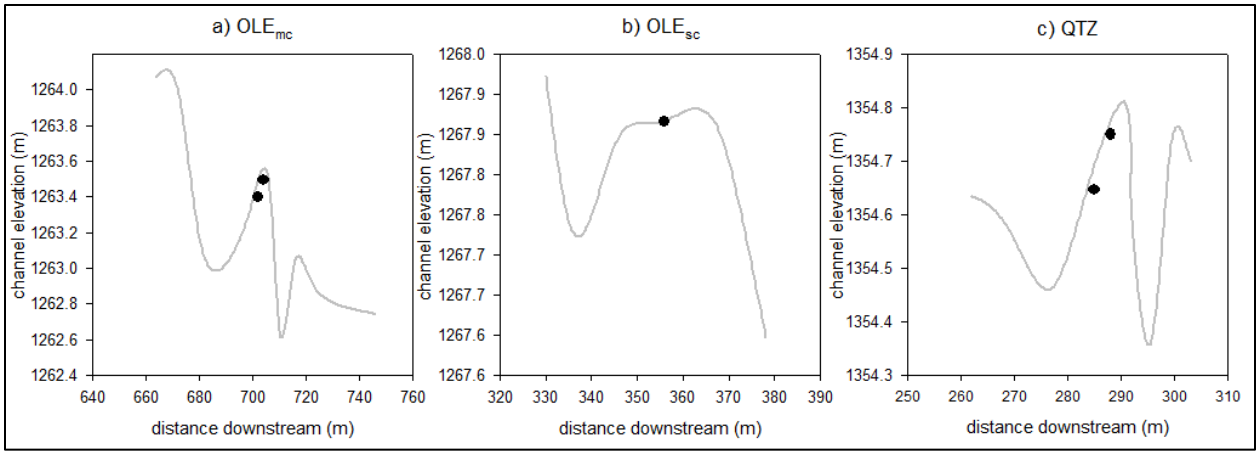

Figure 7. Examples of redds (black dots) in concave-up bedforms. Gray lines represent streambed long profile.

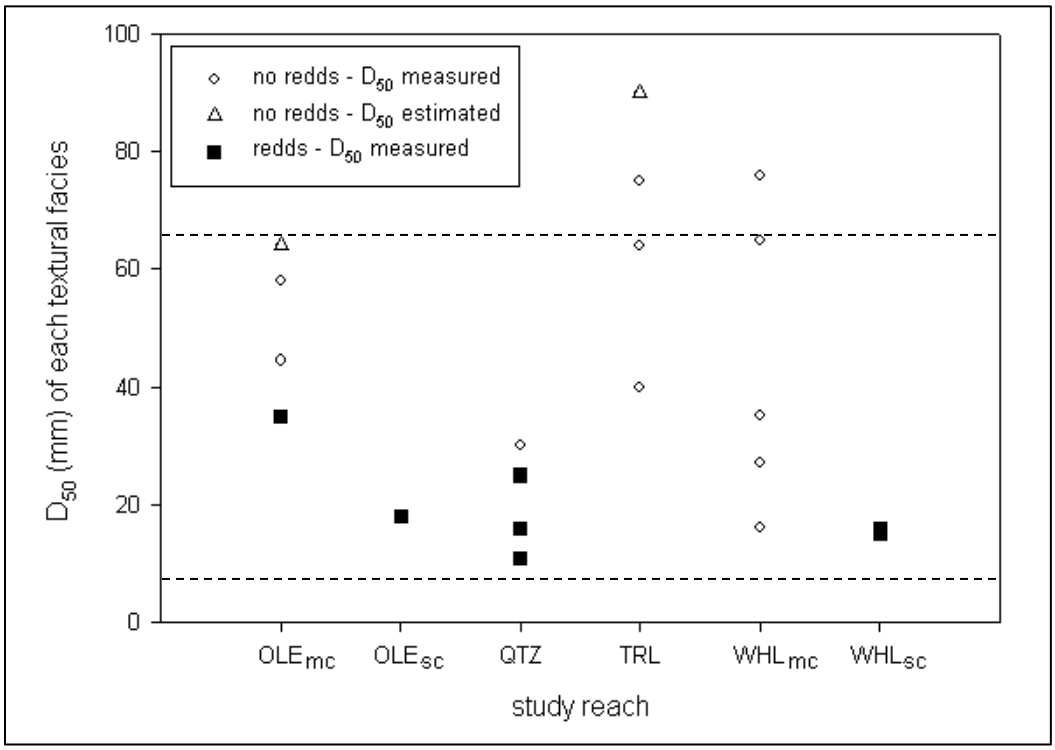

Figure 8. Median surface grain size (D_{50}) of the primary textural facies of each study reach, based on pebble counts that were used to characterize the textural facies. D_{50} values of the coarsest textural facies in Ole and Trail were visually estimated (Appendix 1A). Textural facies observed hosting 2011 redds are indicated with black boxes. The dashed lines indicate the lower (8 mm) and upper (64 mm) bounds of the reported range of suitable spawning gravel D_{50} for bull trout (Baxter and McPhail, 1996; Dunham et al., 2001).

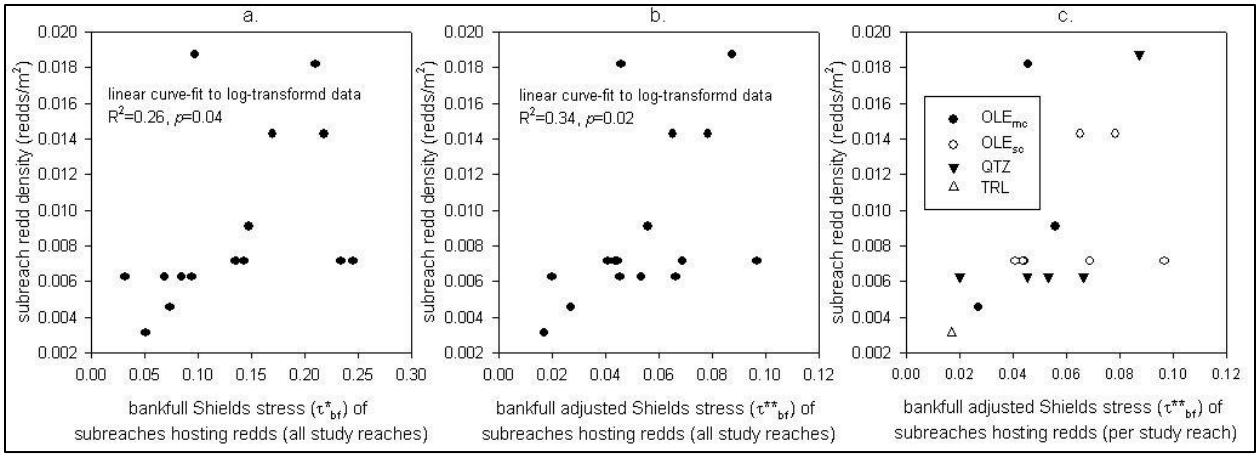

Figure 9. Subreach-scale bankfull and bankfull adjusted Shields stress (τ^*_{bf}, τ^{**}_{bf}) versus redd density: (a) and (b) show subreach sections hosting redds from all study reaches, and (c) shows subreach sections hosting redds per study reach. Linear curve-fits to log transformed data in (a) and (b) satisfy statistical assumptions (normality and constant variance) and describe statistically significant relationships. Regression equations: (a) y=-2.3169+1.6254x; (b) y=-2.3893+5.4154x; (c) OLE_{mc}: y=-2.6050+13.158x (R^2=0.41, *p*=0.6, failed constant variance test); OLE_{sc}: y=-2.1921+2.1086x (R^2=0.09, *p*=0.5, failed constant variance test); QTZ: y=-2.4513+6.2901x (R^2=0.54, *p*=0.2).

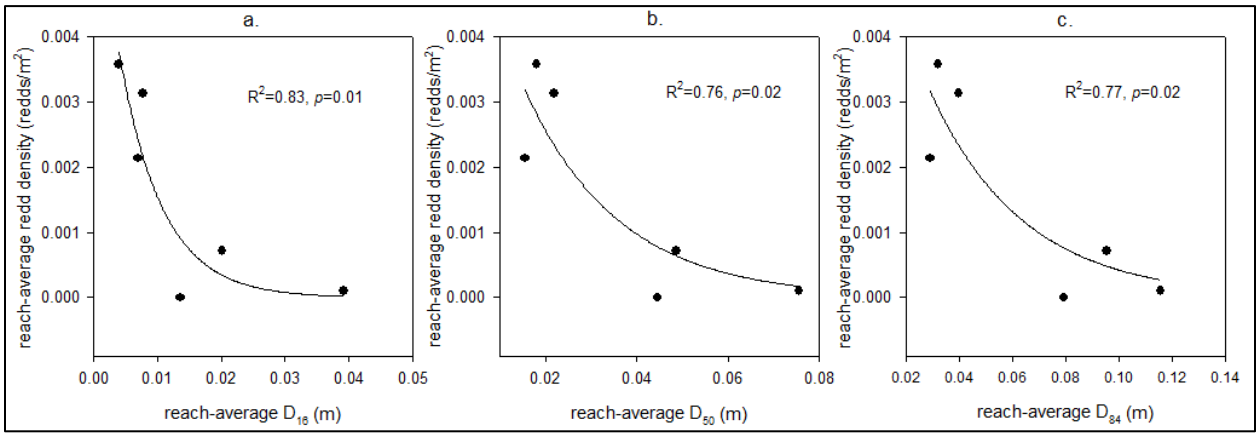

Figure 10. Reach-averaged grain size metrics (D_{16}, D_{50}, D_{84}) versus reach-averaged redd density. Regression equations: (a) y=0.0068*exp(-148.2543x); (b) y=0.0068*exp(-48.4346x); (c) y=0.0072*exp(-28.3850x).

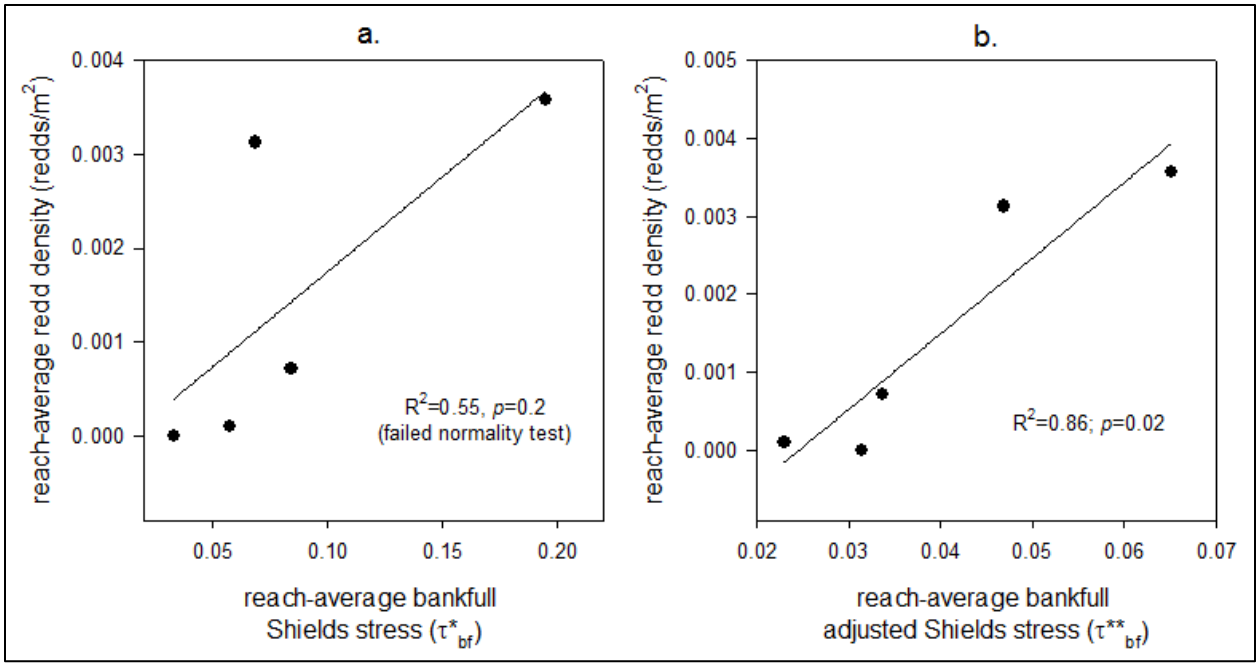

Figure 11. Reach-averaged (a) bankfull and (b) bankfull adjusted Shields stress (τ^*_{bf}, τ^{**}_{bf}) versus reach-averaged redd density (for all study reaches except WHL_{sc}). Regression equations: (a) y=-0.0003+0.0202x; b) (y=-0.0024+0.0969x.

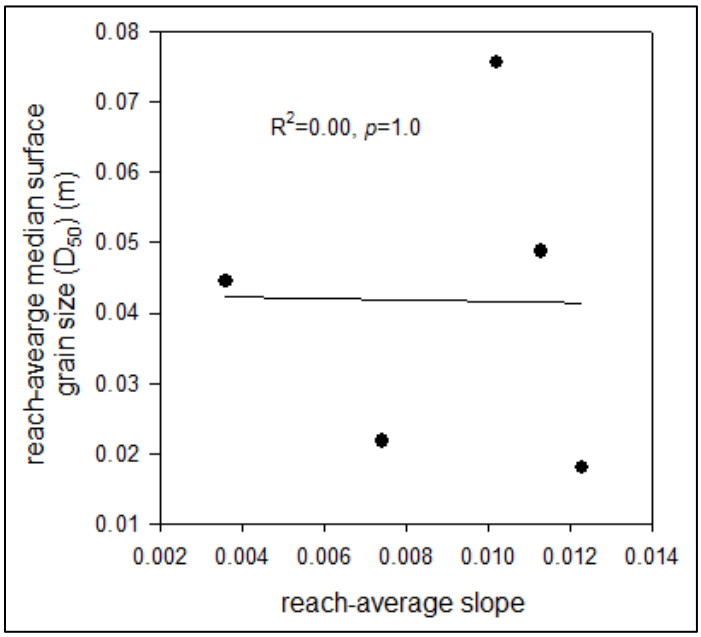

Figure 12. Study reach streambed slope versus reach-average median surface grain size (D_{50}).

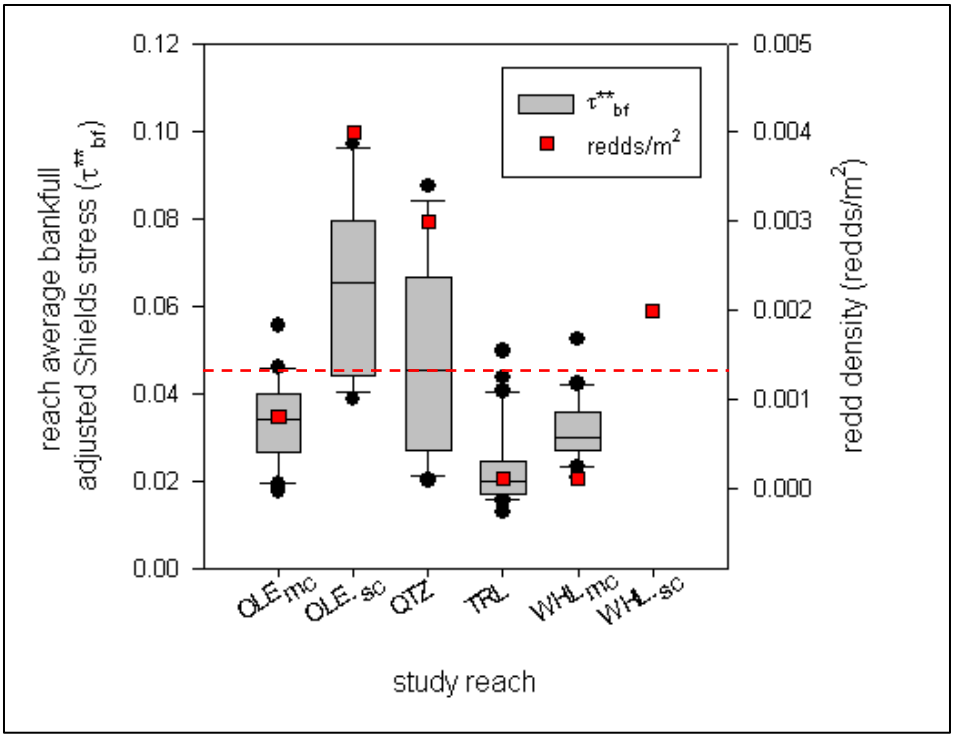

Figure 13. Distribution of subreach-scale bankfull adjusted Shields stress (τ^{**}_{bf}) in each study reach. Study reach-average redd density is also plotted. WHL_{sc} was not topographically surveyed, therefore I did not model shear stress distributions in that study reach. The dashed red line represents critical Shields stress (τ^{*}_{c}=0.045), an often-cited threshold for streambed particle entrainment in alluvial rivers (e.g. Yalin and Karahan, 1979). Solid lines within the box plots represent medians; boxes bound the upper and lower quartiles; whiskers illustrate upper and lower tenths; solid dots represent extrema. (OLE_{mc} n=42; OLE_{sc} n=17; QTZ n=11; TRL n=30; WHL_{mc} n=21.)

Table 7. Reach-average correlations between measured physical variables and redd density. Reach-average redd density is the y variable for all regressions. Statistically significant relations are bold (p<0.05).

x variable	n	R^2	*p*	Equation
D_{16}	**6**	**0.83**	**0.01**	**y=0.0068*exp(-148.2543*x)**
D_{50}	**6**	**0.76**	**0.02**	**y=0.0068*exp(-48.4346*x)**
D_{84}	**6**	**0.77**	**0.02**	**y=0.0072*exp(-28.3850*x)**
τ^*_{bf}	5	0.55	0.2[a]	y=-0.0003+0.0202*x
τ^{**}_{bf}	**5**	**0.86**	**0.02**	**y=-0.0024+0.0969*x**
slope	5	0.14	0.5	y=-0.0001+0.1794*x
VCR	6	0.08	0.6	y=0.0009+0.0000356*x
VHG	6	0.00	0.9	y=0.0017+0.0006*x
K_h	4	0.02	0.8[b]	y=0.0015-0.0000035156*x
q_v	5	0.00	1.0	y=0.0012-0.00003555*x
K_v	5	0.14	0.5	y=0.0004+0.00004953*x
Stream temperature (9/27/11-10/10/11)				
Avg.	6	0.38	0.2	y=-0.0064+0.0012*x
σ	6	0.02	0.8	y=0.0008+0.0015*x
C_v	6	0.02	0.8	y=0.0026-0.0119*x

[a] Shapiro-Wilks normality test failed.
[b] Constant variance test failed.

1B) Reach-scale hydrogeology

Of the subreach-scale physical hydrogeologic variables measured (VHG, K_h, q_v, and K_v), reach-averaged values were not significantly related to reach-average redd density between the streams (Table 7, Figure 16). Streambed water temperature data in the study reaches tended to mimic stream water diurnal cycles. In late September, during the spawning period, average streambed temperatures at ~25 cm depth were <2% different from stream temperatures (Table 8). Stream and streambed temperatures in OLE_{mc} and QTZ were warmer than the reported 7°C threshold of spawning appropriate water temperature, whereas water temperatures in TRL and WHL_{mc} were below the threshold (Table 8) (streambed temperatures for WHL_{sc} were not measured in this time window) (e.g. Goetz, 1989; Fraley and Shepard, 1989; Sauter et al., 2000). Additional water temperature data are presented in Results section 2B.

In September and October, during the spawning and early incubation period, streambed vertical hydraulic gradients (VHG) for all study reaches were dominantly downward indicating overall movement of stream water into the streambed (Figure 14). Vertical hydraulic gradients (VHGs) within the study reaches exhibited little change from September to October (Figure 14).

Horizontal hydraulic conductivity (K_h) measurements in the study reaches ranged from 35-660 m/d (Figure 15a). Reach-average K_h showed no correlation with redd density (R^2=0.02, p=0.8; Table 7; Figure 16a). The falling-head slug test responses ranged from over-damped to critically-damped to under-damped and tended to equilibrate within 5-10 seconds (Appendix 1B). Horizontal hydraulic conductivity (K_h) values reported here have substantial uncertainty as differences in estimated K_h values where the datalogger was measuring head change at the 1 s intervals ranged from 0%-160%; at 0.5 s intervals, differences in K_h derived from repeat slug tests ranged from 0%-90% (Appendix 1B).

Comparing K_h values derived from 1 s and 0.5 s curves at a single piezometer, differences ranged from 0%-440% (Appendix 1B). However, 0.5 s interval tests did not consistently compute higher or lower K_h values than 1 s interval tests. Considering error margins and sample sizes, there is no distinguishable difference in K_h between the study reaches.

In agreement with the VHG data, vertical streambed temperature arrays in each study reach indicate streambed water vertical flux (q_v) is dominantly downward throughout the study period (Figure 15b). Vertical thermochron datasets analyzed in Ex-Stream indicated q_v ranged from +1.6 $m^3/(m^2d)$ (upward) to -2.5 $m^3/(m^2d)$ (downward) with median values per study reach varying between -2.0 to -0.5 $m^3/(m^2d)$ (Figure 15b). Reach-average q_v showed no correlation with redd density (R^2=0.02, *p*=0.8; Table 7; Figure 16b). Due to uncertainty and error in the q_v estimates as well as the low sample numbers in each study reach, comparisons of inter-stream q_v beyond the general range of values are not presented. Athough downward streambed flux dominated the study reaches, spawning preference for downward or upward streambed flux was not detected as redds were observed <2 m from piezometers of both downwelling and upwelling flux signatures. Vertical steambed streambed flux (q_v) datasets typically ranged in extent from 36-40 days; total rate of change in flux over this time period ranged from 0.02% - 7% with an average of 3% (Appendix 1B). Vertical hydraulic conductivity (K_v) values in the study reaches ranged from 3 m/d to 58 m/d and cluster in the range of 3 m/d to 15 m/d (Figure 15c). Reach-averaged K_v exhibited the strongest correlation (positive) to reach-average redd density of all streambed hydrogeologic properties measured (Table 7, Figure 16). Again, due to the low sample numbers in each study reach, comparisons of inter-study reach K_v beyond the general range of values is not warranted. Hydraulic conductivty anisotropy ratios (K_h/K_v) in the study reaches ranged from 3-150 (Figure 15d).

Table 8. Average channel and streambed water temperature from 9/19/11-9/30/11 (during the spawning period). (The number of temperature dataloggers contributing to these average values are: OLE_{mc} n=4; OLE_{sc} n=1; QTZ n=1; TRL n=4; WHL_{mc} n=4.)

Average spawning water temperature (°C) (9/19/11-9/30/11)			
study reach	**channel**	**subsurface (~25cm)**	**% difference**
OLE_{mc}	7.6	7.6	0.0%
OLE_{sc}	7.7	7.7	0.0%
QTZ	8.1	8.2	1.2%
TRL	6.1	6.1	0.0%
WHL_{mc}	6.3	6.4	1.6%

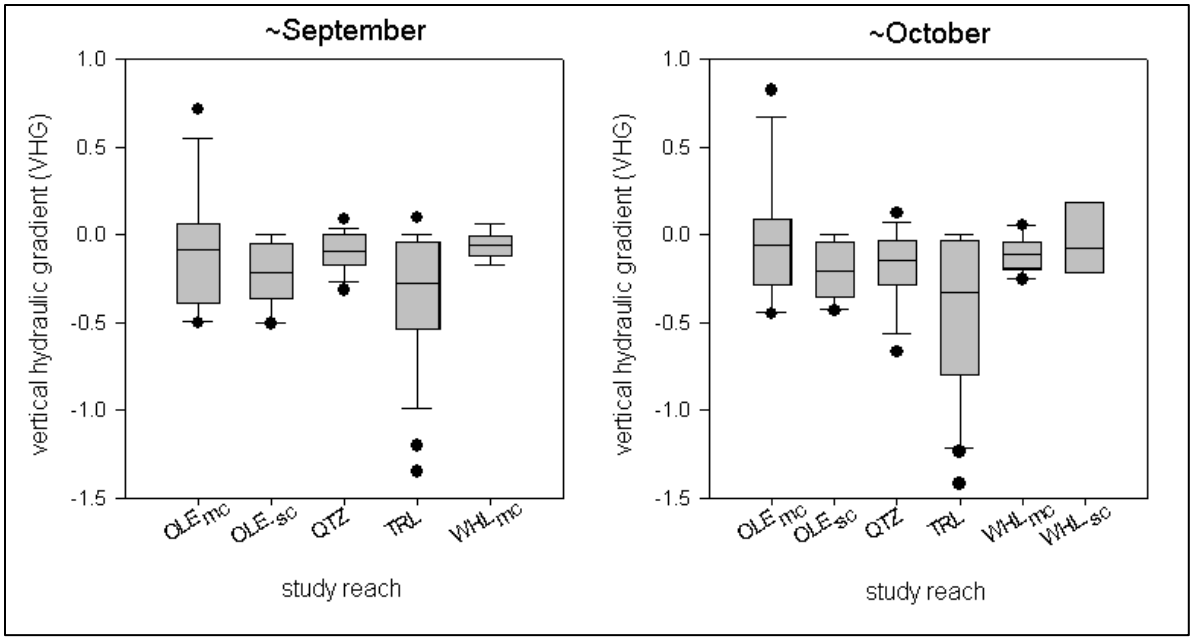

Figure 14. Range of vertical hydraulic gradient (VHG) measurements in each study reach for September and October. Piezometers in WHL_{sc} were installed on 10/12/11, therefore there is no WHL_{sc} VHG data for September. (September plots: OLE_{mc} n=14; OLE_{sc} n=14; QTZ n=15; TRL n=25; WHL_{mc} n=9.) (October plots: OLE_{mc} n=13; OLE_{sc} n=13; QTZ n = 13; TRL n=21; WHL_{mc} n=10; WHL_{sc} n=4.)

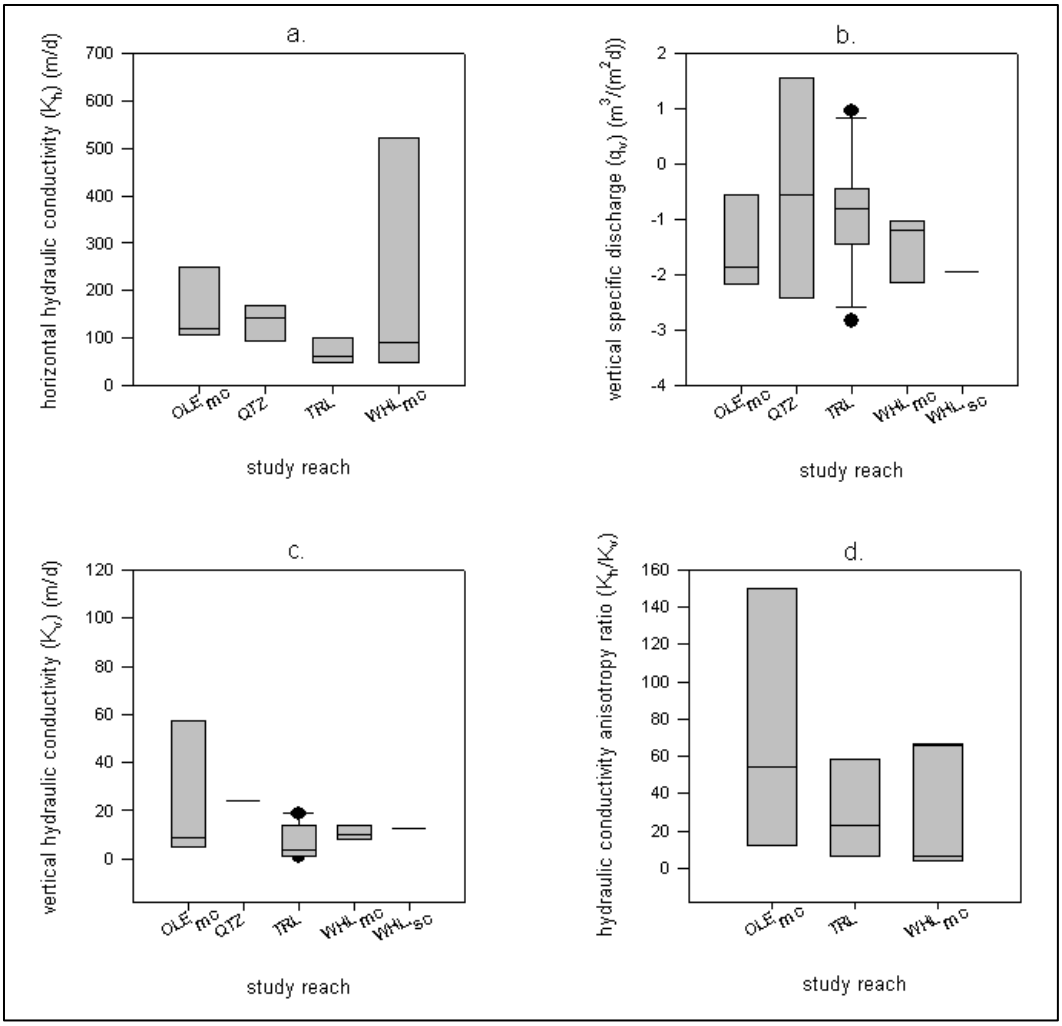

Figure 15. Summary plots of hydrogeologic variables measured in the study reaches. (a) Horizontal hydraulic conductivity (K_h) of streambed sediments at ~40 cm depth measured in each of the study stream sections. Input for each K_h box plot is the average K_h value derived from each slug test piezometer in a given study reach (OLE_{mc} n = 6; QTZ n = 5; TRL n = 5; WHL_{mc} n = 4). (b) Ex-Stream estimated vertical specific discharge (q_v) magnitude and direction. Negative values represent downward flow; positive values represent upward flow. Input values for the plot are the average value of the daily averaged q_v computed for each thermochron instrumented piezometer (OLE_{mc} n=5; QTZ n=3; TRL n=11; WHL_{mc} n=5; WHL_{sc} n=1). (c) Vertical hydraulic conductivity (K_v) estimates in each study reach (OLE_{mc} n=5; QTZ n=1; TRL n=10; WHL_{mc} n=5; WHL_{sc} n=1). (d) Hydraulic conductivity anisotropy ratio ranges in the streambed sediments (OLE_{mc} n=3; TRL n=7; WHL_{mc} n=3).

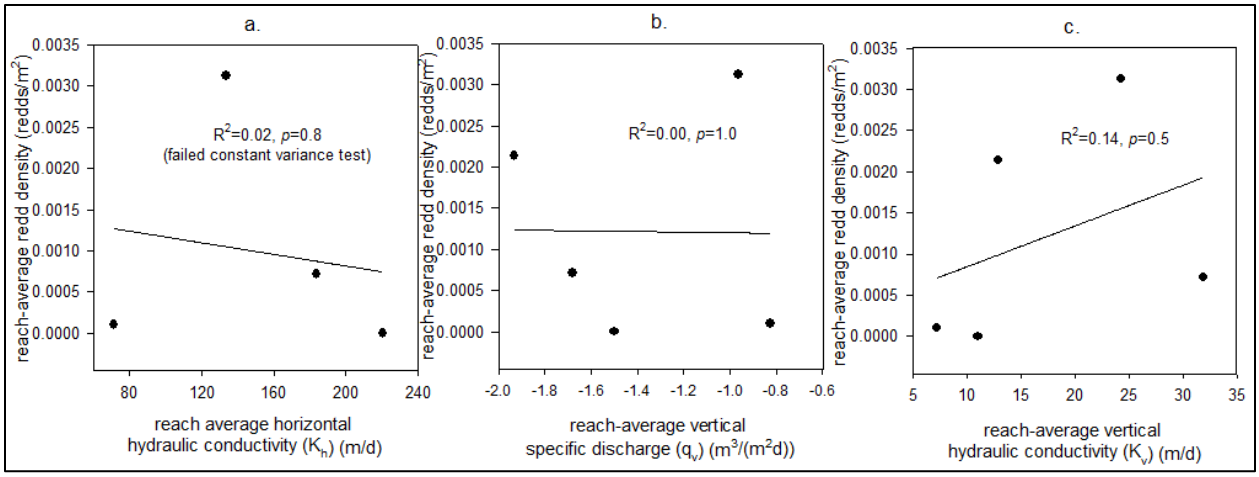

Figure 16. Reach-average hydrogeologic variables versus reach-average redd density. Regression equations are presented in Table 7.

No relationships between reach-average geomorphic and hydrogeologic variables were significant, although weak trends were evident (Figure 17, Figure 18; Table 9). Reach-average D_{50} was negatively correlated with K_h and K_v (Figure 17; Table 9). Reach-average τ^{**}_{bf} was positively correlated with K_h and K_v (Figure 18, Table 9).

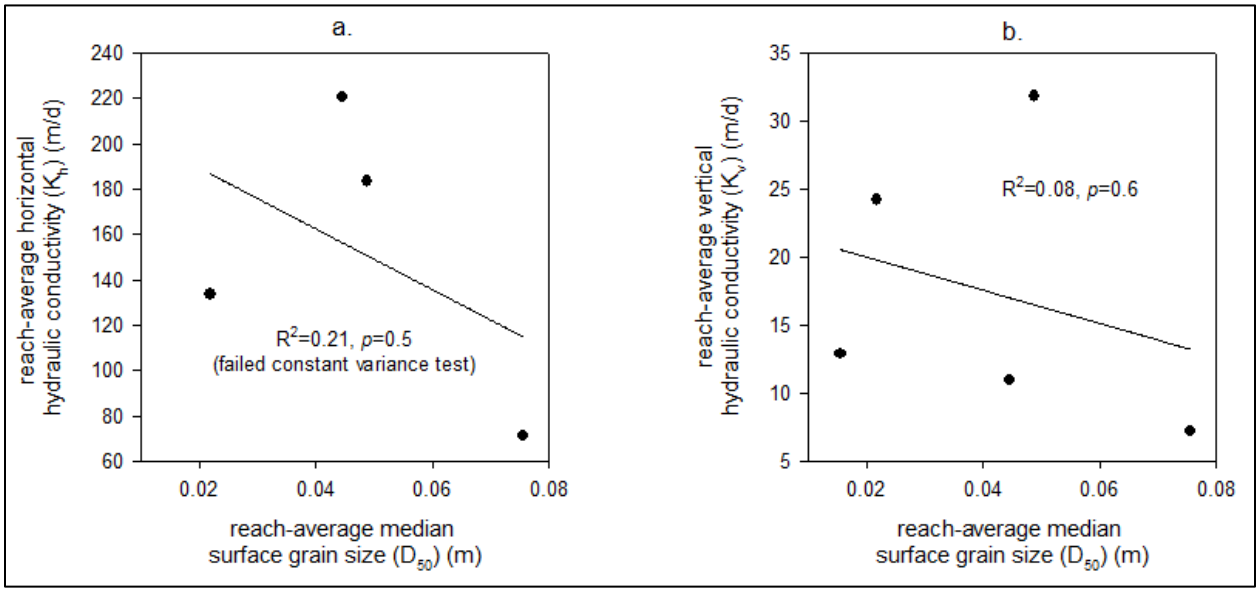

Figure 17. Reach-average median surface grain size (D_{50}) versus reach-average (a) horizontal hydraulic conductivity (K_h) and (b) vertical hydraulic conductivity (K_v). Regression equations are presented in Table 9.

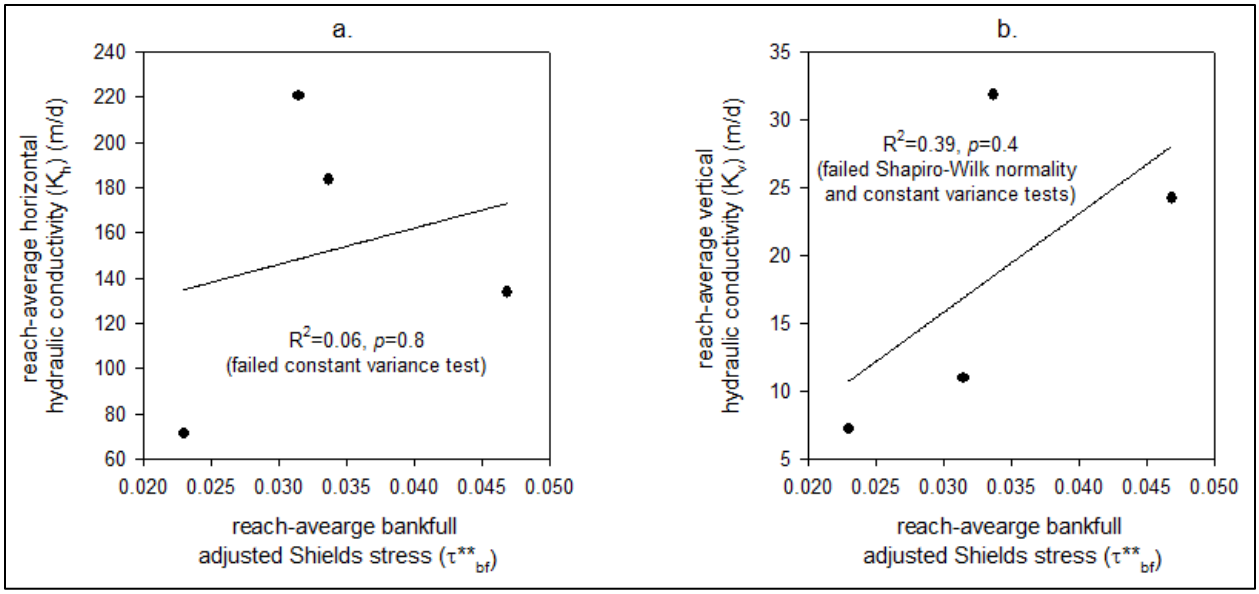

Figure 18. Reach-average bankfull adjusted Shields stress (τ^{**}_{bf}) versus reach-average (a) horizontal hydraulic conductivity (K_h) and (b) vertical hydraulic conductivity (K_v). Regression equations are presented in Table 9.

Table 9. Dependency of reach-average hydrogeologic variables on reach-average geomorphic variables.

(x) v (y)	n	R^2	*p*	Equation
D_{50} v VHG	6	0.25	0.3	y=-0.0522-2.9293x
D_{50} v K_h	4	0.21	0.5[b]	y=216.0898-1339.6806x
D_{50} v q_v	5	0.25	0.4	y=-1.7848+9.7963x
D_{50} v K_v	5	0.08	0.6	y=22.4603-121.9581x
τ^{**}_{bf} v VHG	5	0.01	0.9	y=-0.2101+0.6016x
τ^{**}_{bf} v K_h	4	0.06	0.8[b]	y=98.2559+1597.4226x
τ^{**}_{bf} v q_v	4	0.00	1.0[b]	y=-1.2225-0.5994x
τ^{**}_{bf} v K_v	4	0.39	0.4[a,b]	y=-5.954+726.3009x
VCR v VHG	6	0.47	0.1	y=-0.3012+0.0074x
VCR v K_h	4	0.61	0.2[b]	y=81.5863+4.8356x
VCR v q_v	5	0.48	0.2	y=-0.9270-0.0234x
VCR v K_v	5	0.01	0.9	y=18.8972-0.0759x

[a] Shapiro-Wilks normality test failed.
[b] Constant variance test failed.

2A) Valley-scale geomorphology

At the valley-scale, according to the edited unconfined valley delineations of Wenger et al. (2011), 74% of the 133 redds observed in the 4 study catchments were within unconfined valleys and 26% were within confined valleys (Figure 19, Table 10). The Ole and Quartz catchment unconfined valley delineations of Wenger et al. (2011) appropriately represented landscape conditions (Figure 19a,b). In the Trail and Whale Creek catchments (Figure 19c,d), I removed unconfined valley polygon sections that I deemed to include terraces above the active valley bottom (Appendix 2A). According to my unconfined

valley delineations, rate of change in valley width is not related to redd density, except for in the Ole drainage. Of the 40 redds observed in Ole in 2011, 53% were clustered in the downstream extent of a narrowing unconfined valley (Figure 19a). All other redds in the study catchments were located either in unconfined valley segments of relatively constant width or in confined valley segments.

In the Ole catchment, the furthest downstream 3 km of Ole Creek is coarser and steeper and has narrower valley walls than the rest of the drainage of the highlighted spawning and rearing area (Figure 19a). Redds are rarely observed in this section (John Fraley, 2011, personal communication). In the Quartz catchment, the base level created by Quartz Lake is a confining factor of the valley-scale geomorphic and hydrogeologic processes.

In the Trail catchment, migratory spawning bull trout are unable to access much of the drainage because of an intermittent stream section that acts as a migration barrier during late summer and fall baseflow conditions (the downstream extent of the intermittent stream section is indicated by the yellow star in Figure 19c). In the Whale catchment, Whale Creek Falls (indicated by the yellow star in Figure 19d) is a migration barrier. However, bull trout can and do migrate up the adjacent tributaries near the upstream extent of the large alluvial valley in Whale (Figure 19d). These adjacent tributaries are not included in the annual "index stream" redd count surveys (Table 5). However, the southern tributary, Shorty Creek, which hosts a ~2 km long unconfined valley, is known to annually host spawning bull trout (Tom Weaver, 2012, personal communication) (Figure 19d).

Reach-average VCRs of the study reaches range from 38 in WHL_{sc} to 2 in TRL (Table 11).Reach-average VCR was negatively correlated with reach-average D_{50} and S (Figure 20a,b) and positively correlated with reach-average τ^{**}_{bf} but the relationships were not significant (Figure 20c). Reach-average VHG trended towards zero as VCR increased; VCR and K_h were positively correlated; q_v trended towards larger negative values as VCR increased; and K_v exhibited no correlation with VCR; all of these relationships were non-significant (Figure 21).

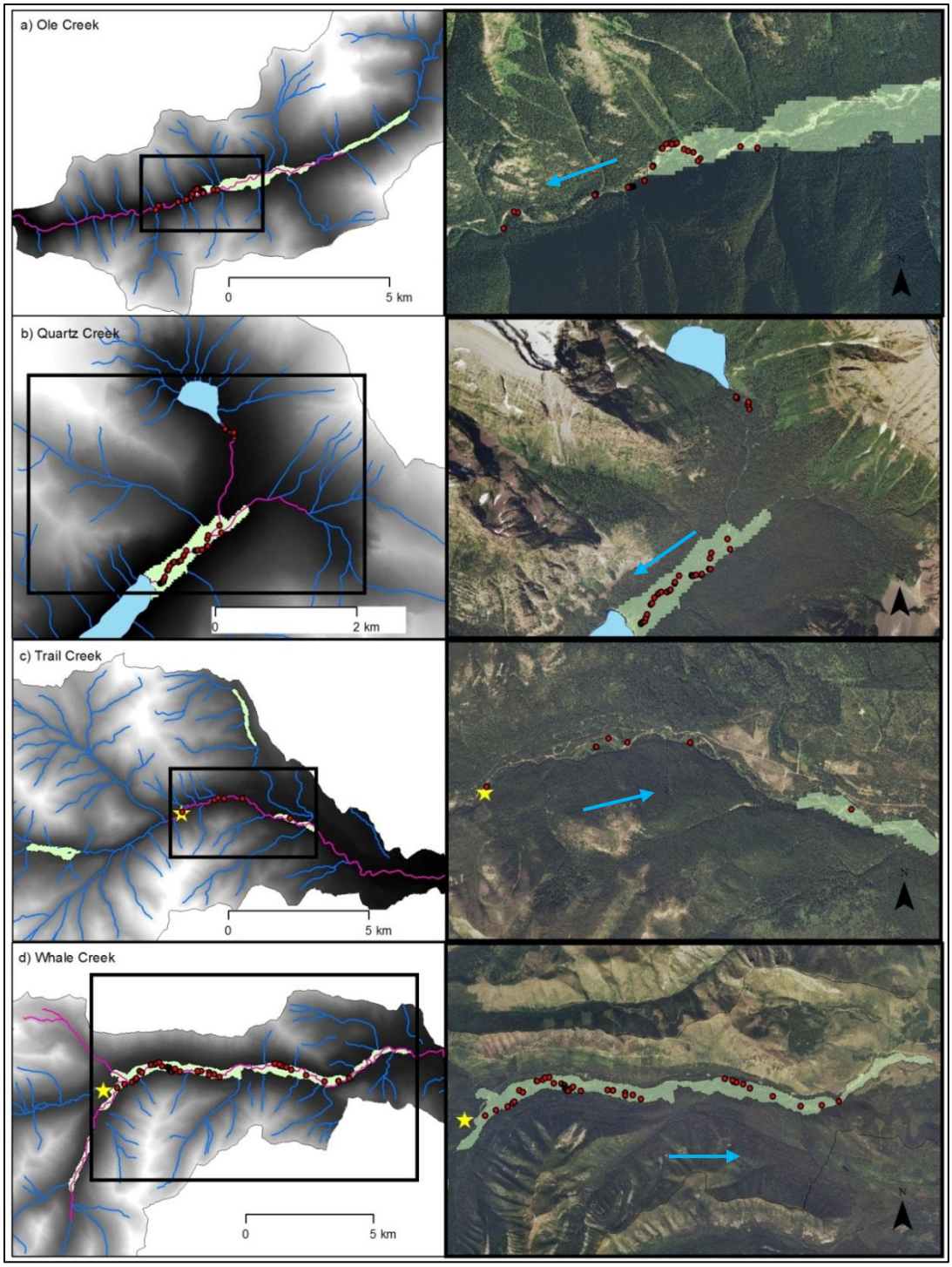

Figure 19. Valley confinement and 2011 bull trout redd occurrence in each study stream. Left panel maps are digital elevation models (DEMs) of the study catchments, and right panel maps are air photos of the 2011 bull trout spawning sections in each study catchment. Blue arrows indicate streamflow direction. Redd dots indicate 2011 redds. Green polygons indicate the edited unconfined valley delineations (originals created by Wenger et al., 2011)). In the left panel maps, blue lines are NHDPlus streamlines; pink lines are spawning and rearing reaches (USFWS, 2008). The southernmost lake in b) is Quartz Lake and the northernmost is Cerulean Lake. Rainbow Creek connects Cerulean Lake to Quartz Creek and Quartz Lake. Yellow stars in c) and d) maps indicate barriers to upstream fish migration. (NAIP (2011) air photos)

Table 10. Bull trout 2011 redd distribution in relation to valley type per study catchment.

Study stream	**Unconfined valley redds** (n=99) (74%)	**Confined valley redds** (n=34) (26%)
Ole	21 (52.5%)	19 (47.5%)
Quartz	35 (81%)	8 (19%)
Trail	1 (12.5%)	7 (87.5%)
Whale	42 (100%)	0 (0%)

Table 11. Valley confinement ratios (VCR) per study reach.

Study reach	**Average valley width (m)**	**Bankfull channel width (m)**	**Valley confinement ratio -**
OLE_{mc}	190	17	11
OLE_{sc}	190	12	16
QTZ	340	17	20
TRL	30	18	2
WHL_{mc}	460	18	26
WHL_{sc}	460	12	38

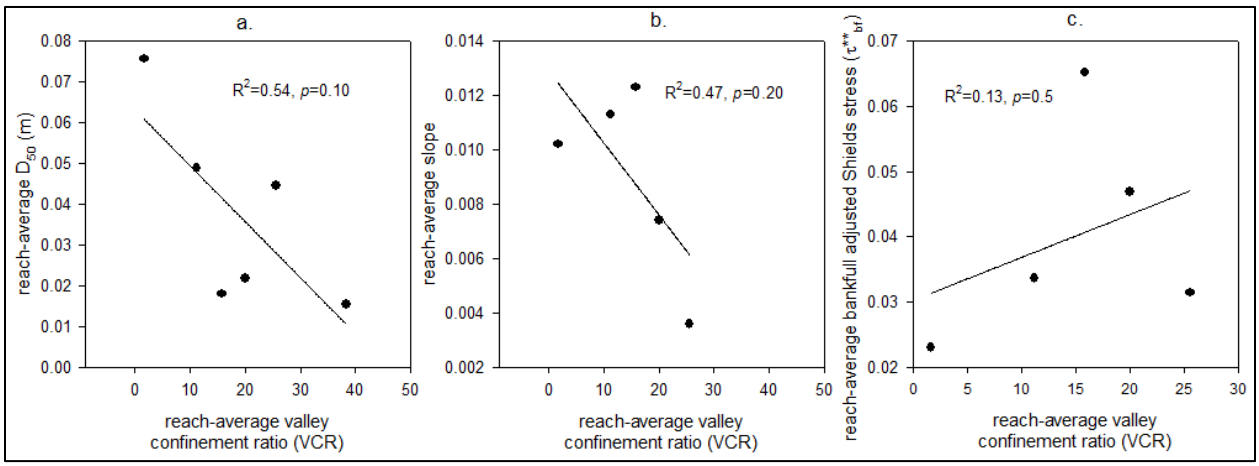

Figure 20. Reach-average valley confinement ratio (VCR) versus other reach-average geomorphic variables. Regression equations: (a) y=0.0129-0.0003x; (b) y=0.0631-0.0014x; (c) y=0.0303+0.0007x.

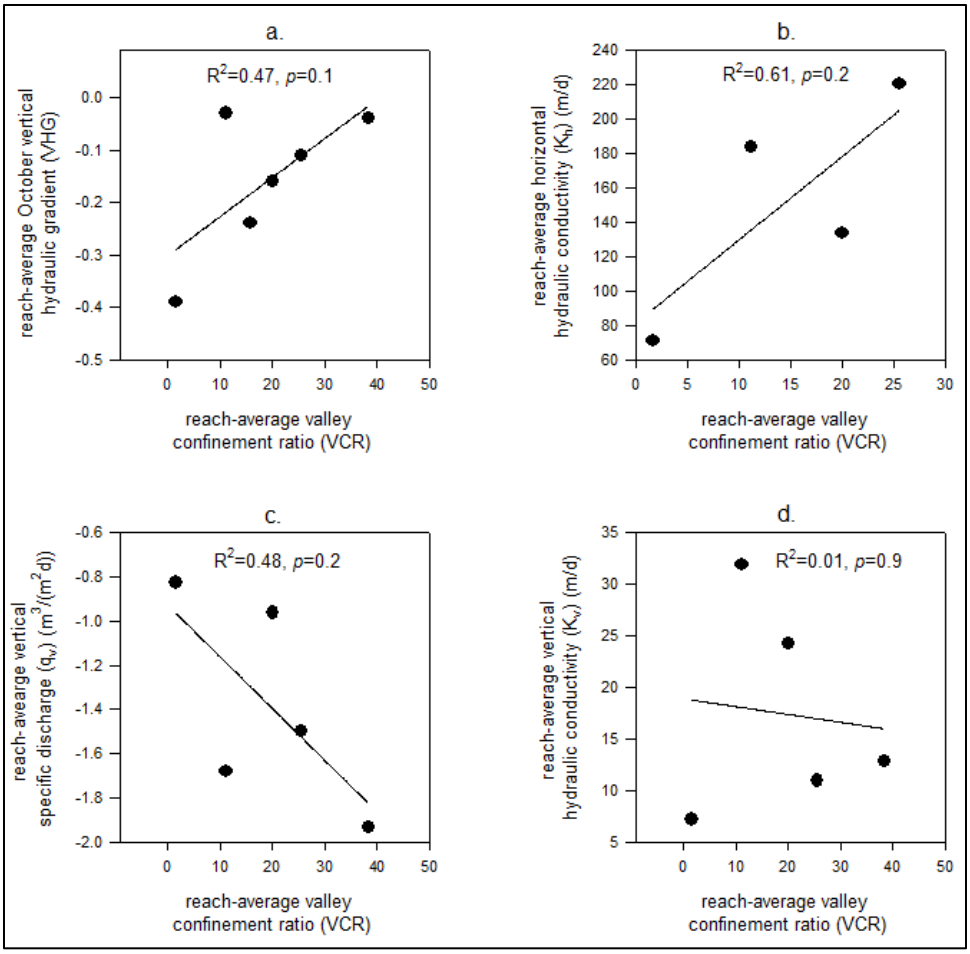

Figure 21. Reach-average valley confinement ratio (VCR) versus reach-average hydrogeologic variables. Regression equations: (a) y=-0.3012+0.0074x; (b) y=81.5863+4.8356x; (c) y=-0.9270-0.0234x; (d) y=18.8972-0.0759x.

2B) Valley-scale hydrogeology

Flownets based on floodplain water level and stream stage data indicate a general down-valley flow direction of floodplain subsurface water in all study reaches (Appendix 2B). Water table maps of the Ole study reaches indicated apparent flow line convergence where the unconfined valley narrows, suggesting valley-scale groundwater was discharging to the stream channel during the study period (Figure 22).

Mean annual air temperature recorded by the 3 most proximal SNOTEL stations was 4.3˚C (Appendix 2B). Therefore, I estimated groundwater temperature at 10-25 m depth in all of the study catchments to be ~5.3-6.3˚C (Kasenow, 2001). Although streambed water temperatures tended to mimic stream water diurnal cycles, one Ole upward flux (VHG measurements were positive or 0) piezometer recorded constant streambed water temperatures of 5.3˚C in August at 8 and 25 cm depth below the streambed. During this time, the stream water temperature sensor varied diurnally from ~6-9.5°C (Figure 26: subsurface temperature signal representative of groundwater = O-gw; stream temperature signal = O-5sc).

September shallow floodplain water temperatures in Ole, Trail, and Whale also exhibit near constant temperature signals (Figure 24, Figure 26). In Ole, the shallow floodplain water temperature (~8˚C, sensor O-2fp) plotted near the average of the stream water diurnal cycle (~2˚C warmer than computed groundwater temperate) (Figure 24, Figure 26). In Trail and Whale, the shallow floodplain

water temperature was ~7˚C (~1˚C+ warmer than average stream water temperature and expected groundwater temperature) (Figure 24).

The catchment-wide stream water temperature sensors in each study catchment (Figure 23) show Trail and Whale average September stream temperatures (~5.6-6.5°C) approximately within the range of expected groundwater temperature (~5.3-6.3°C), whereas average stream temperatures in Ole and Quartz (~7.1-8.6°C) are warmer (Figure 24). Spawning reaches in all streams were characterized by stream temperatures with coefficients of variation (C_v) of ≤0.004 that decreased during the spawning and early incubation period (September and October) (Figure 25); spawning was not observed where stream temperature C_v was >0.004 and increased during the spawning and early incubation period (Figure 25a).

In the Ole drainage, during the spawning and early incubation period (September and October), stream temperature in the spawning area was colder and less variable (sensors O-4mc and O-5sc) than stream temperature upstream and downstream of the spawning area (sensors O-1mc and O-6mc) (Figure 24, Figure 25, Figure 26). Furthermore, variation of the spawning area water temperature (O-4mc and O-5sc) decreased over time whereas variation upstream and downstream (O-1mc and O-6mc) increased over time (Figure 25).

In the Quartz drainage, spawning (September) stream temperature 200 m upstream of Quartz Lake (Q-2mc) warmed ~0.4°C but was not buffered compared to Rainbow Creek stream temperature 200 m downstream of Cerulean Lake (Q-1mc) (Figure 24, Figure 25). Both stream temperature sensors indicate decreasing variability in stream water temperature over the spawning and early incubation period (September through October) (Figure 25).

In Trail, stream temperature above the intermittent section (T-1mc) was colder and more variable than stream temperature below the intermittent section (T-2mc, T-3mc) (Figure 24, Figure 25). In Whale, stream temperatures are coldest at the upstream extent of the ~20 km long alluvial valley, but stream temperatures appear to exhibit similar diurnal variations throughout the valley (Figure 24, Figure 25). All Trail and Whale stream temperatures dataloggers indicated a decrease in variation in stream temperature through the spawning and early incubation period (Figure 25). Average September air temperature in the study reaches ranged from 12°C in Ole to 8°C Whale (Figure 27). Daily diurnal fluctuations in air temperature between the study catchments were similar in trend and phase (Figure 27).

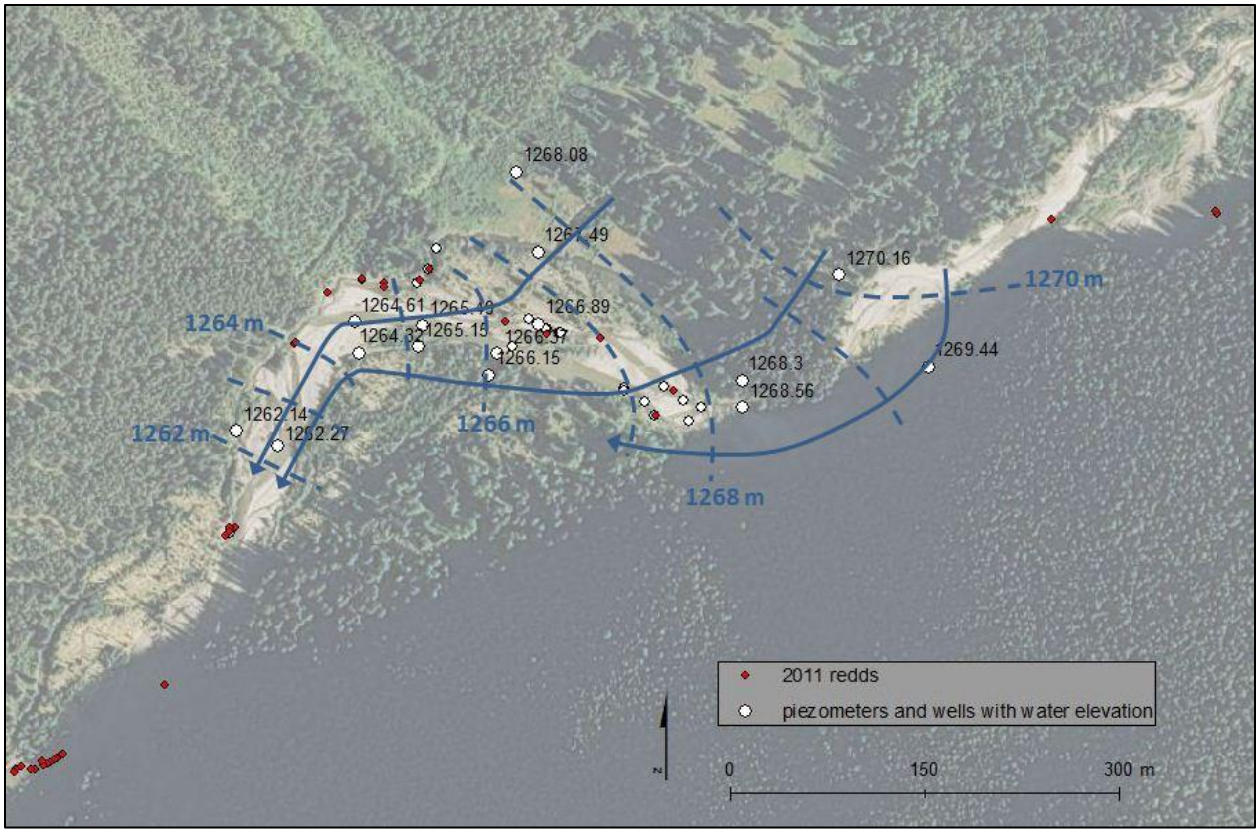

Figure 22. Ole Creek water table contour map encompassing OLE_{mc} and OLE_{sc} on 9/11/11. Dashed blue lines are water table contours with blue elevation numerical labels. Solid blue lines are inferred subsurface flow direction lines. (NAIP (2011) photos)

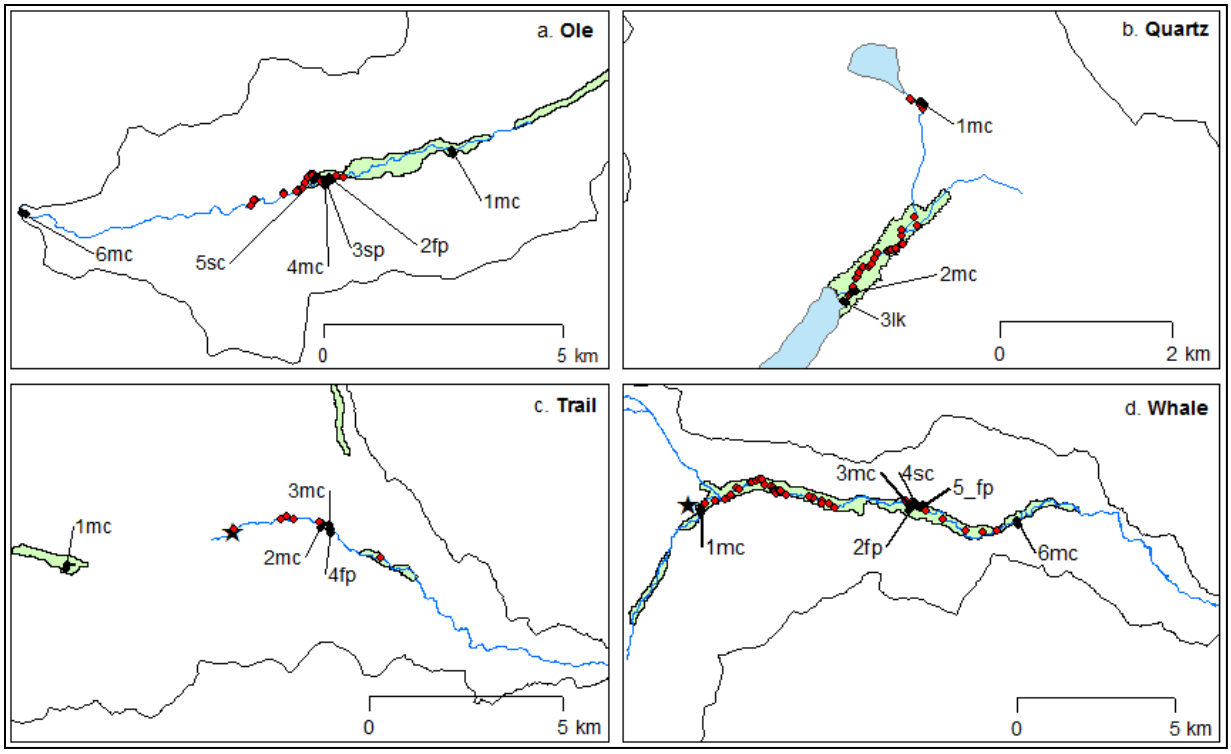

Figure 23. Location of catchment-scale water temperature dataloggers (black dots) and 2011 bull trout redds (redd dots). Numerically, prefixes of the sensor names in each drainage increase in the downstream direction (e.g. 1 = furthest up stream). Suffixes indicate the lateral location of the sensor in relation to the stream channel: mc = main channel stream water temperature sensor; sc = secondary channel stream water temperature sensor; sp = spring channel stream water temperature sensor; fp = floodplain well water temperature sensor.

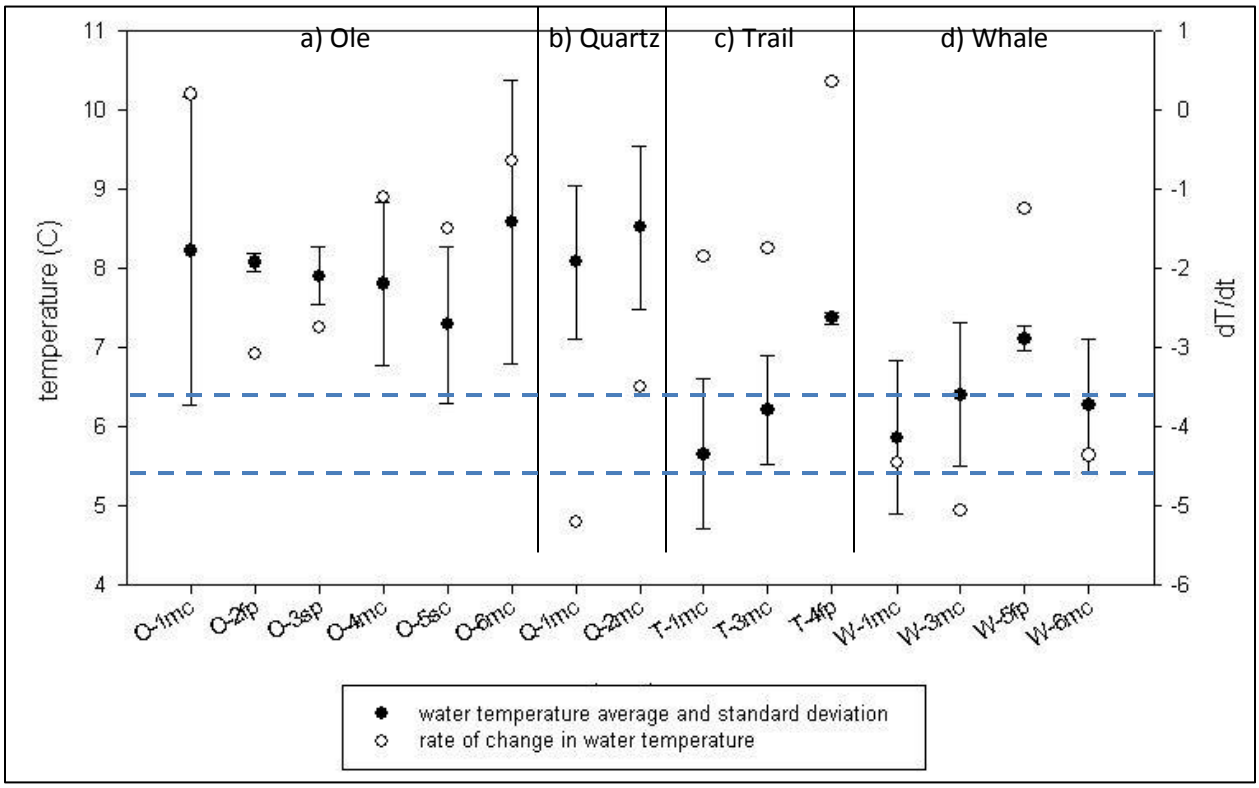

Figure 24. Comparison of the average (dark dots), standard deviation (whiskers), and rate of change in stream temperature (white dots) in September for various longitudinal locations in each study stream. The x-axis indicates datalogger names and locations: label prefixes indicate the stream (e.g. O = Ole); suffixes indicate the longitudinal stream location as shown in Figure 23. Sensor naming codes are further explained in the Figure 23 caption. The blue dashed lines encompasses the estimated temperature of long residence time groundwater at 10-25 m depth for the study area latitude and elevation.

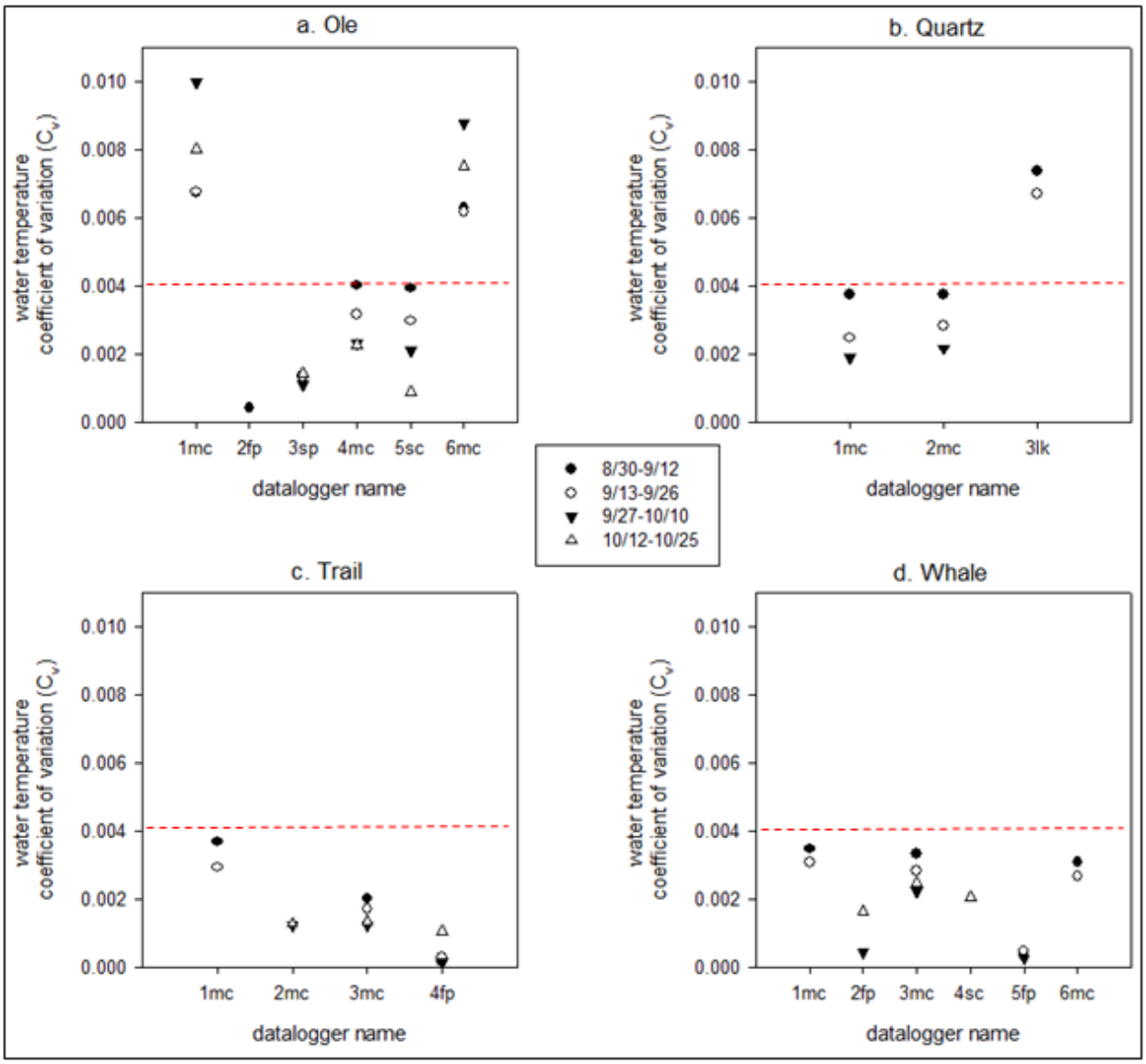

Figure 25. Coefficient of variation (C_v) in water temperature of the catchment-wide temperature sensors for the time windows indicated. Stream temperature sensors in spawning reaches plot below the red dashed line at C_v=0.004.Sensor locations are shown in Figure 17. Sensor naming codes are further explained in the Figure 23 caption.

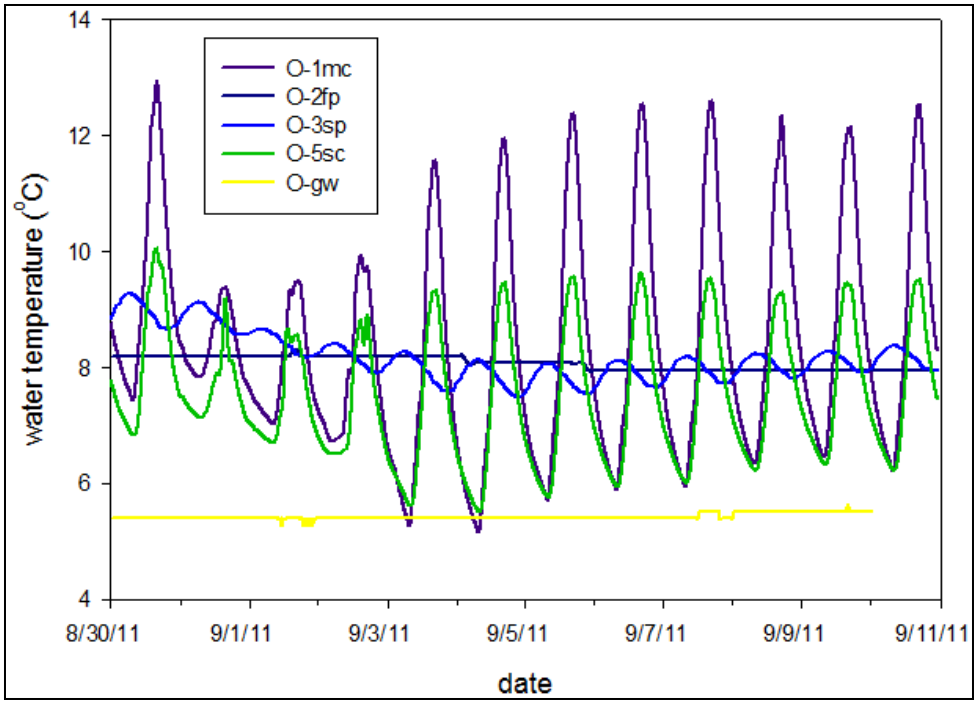

Figure 26. Spatial comparison of diurnal water temperature oscillations in the Ole Creek catchment. Temperature sensor locations are shown in Figure 18a-d. All sensors in this plot measured surface water temperatures except O-gw, which was located 8 cm below the streambed in OLE_{sc} – about 100 m downstream from O-5sc.

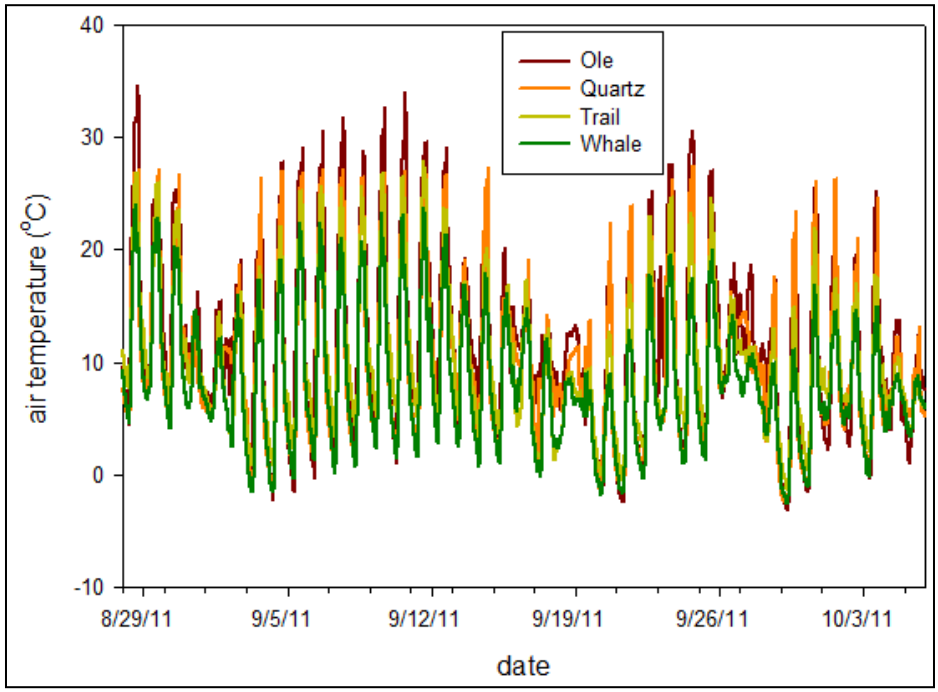

Figure 27. Air temperature in each of the study reaches ~1-2 m above the ground or water surface. From 8/28/11 – 10/6/11, the average air temperature in the study reaches was: Ole 12°C, Quartz 10°C, Trail 10°C, and Whale 8°C.

DISCUSSION

Whereas 2011 redd counts in Ole, Quartz, and Whale are within the annual range of 2000-2010 redd counts, the Trail redd count was lower than any recorded in the previous decade. Some of the year

to year variability in redd counts is attributable to observer error (e.g. Muhlfeld et al., 2006). All of the redd counts reported here may be low compared to historical levels as a result of the change in community dynamics of the Flathead Lake and river system related to the opossum shrimp invasion and the lake trout population surge of the 1980s and 1990s (e.g. Ellis et al., 2011; Muhlfeld et al., 2012).

1A) Reach-scale fluvial geomorphology

Hypothesis 1A, which related spawning occurrence at the subreach- and reach-scales to areas of low mobility of spawning appropriate sediment at bankfull flows, was not supported (e.g. Figure 9, Figure 11). This hypothesis was based on the premise that because high flows (e.g. bankfull) can occur while eggs are incubating in the streambed, salmonids may select redd sites with low streambed mobility at high flows (e.g. Moir et al., 2009). In my highest redd density study reach, OLE_{sc}, bankfull Shields stress and bankfull adjusted Shields stress typically exceeded 0.045, a commonly cited threshold for streambed particle entrainment (e.g. Buffington and Montgomery, 1997) (Figure 6a,b, Figure 9, Figure 11, Figure 13). Furthermore, subreach and reach-average redd density of all study reaches was positively correlated with bankfull adjusted Shields stress (τ^{**}_{bf}) and the relationships were significant (p=0.02) (Figure 9b; Figure 11b). Bull trout may choose to spawn in subreach- and reach-scale channel sections of higher Shields stresses and sediment mobility because these sediments should be easiest to move and excavate a redd. Additionally, high Shield stresses may be indicative of dynamic stream sections in which reworking of the shallow streambed sediments by bankfull flows decreases the amount of fine sediment accumulation in the streambed, thus allowing hyporheic water to more freely circulate. The positive (albeit non-significant) correlation between reach-average τ^{**}_{bf} and K_v (R^2=0.39, p=0.4; Figure 18b) supports this notion.

Subreach- and reach-average Shields stress results in the study reaches (e.g. Figure 13) indicate that bankfull flows likely mobilize and sort the dominant textural facies of OLE_{sc} and QTZ as well as certain portions of OLE_{mc} (the study reaches with the highest redd density in 2011). The dominant textural facies of TRL and WHL_{mc} (the study reaches with the lowest redd density in 2011) are likely not mobilized by bankfull flows (Figure 13).

In contrast to my findings, Moir et al. (2009) found the spawning frequency of Atlantic salmon at the subreach-scale in a gravel-bed Scottish mountain stream to be negatively correlated with streambed mobility. These conflicting results are likely due to several factors. First, my study has the potential for including redds in the analyses that were constructed in isolated, seasonally transient patches of sediment that are not accurately described by subreach-scale physical characteristics (e.g. subreach-scale τ^{**}), because my study used only 1 year of direct redd location observations. In contrast, Moir et al. (2009) assessed spawning subreaches consistently used by spawning salmon over a 5 year period. Secondly, Moir et al. (2009) only consider mobility of a single D_{50}, whereas I used the observed dominant D50 of each subreach channel section. Because the competence of a given flow is dependent on streambed grain size (e.g. Montgomery et al., 2009), and salmonid species are known to spawn in a range of D_{50} (e.g. bull trout 8 mm – 64 mm: Baxter and McPhail, 1996), interpretations of spawning sediment mobility are dependent on choices about the representative grain size in calculations, including whether true grain size or a constant, average grain size is used. Finally, Moir et al. (2009) used total boundary shear stress (τ_o), whereas I used grain stress (τ') in an effort to account for form drag from bank, bar, and wood roughness, which can be substantial in my study reaches.

My work on streambed mobility is anchored to the recognition that availability of appropriate spawning gravels is a primary control on the spatial distribution of salmonid spawning habitat (e.g. Buffington et al., 2004; Moir et al., 2006). Similarly, my results indicate that the spatial distribution of spawning appropriate gravels in the study reaches plays a major role in bull trout redd distributions and densities. In all of my study reaches, bull trout spawned only the finest of the dominant textural facies (Figure 6, Figure 8, Figure 10).

Salmonids can spawn in substrate with a D_{50} up to 10% of their body length (Kondolf and Wolman, 1993). The D_{50} values of textural facies used by spawning bull trout in my study tend to be smaller than those reported by others (e.g. Baxter and McPhail, 1996; Dunham et al., 2001). Because Flathead River bull trout are among the largest in their native range (Clint Muhlfeld, 2012, personal communication), it appears that the bull trout in my study reaches were large enough to excavate redds in larger substrate, but they preferentially chose to spawn in the finer textual facies. Because fish length can be approximated from redd dimensions (e.g. Crisp and Carling, 2006), these speculations could be tested from redd dimension measurements.

Potential error in my Shields stress values arise from many sources. Streambed grain size distributions relied on simplified visual observations of dominant textural facies. HEC-RAS flow modeling used measured cross sections of approximately 100 m spacing and therefore involve substantial interpolation, simplification, and uncertainty. Furthermore, there are additional physical factors reported to influence bull trout spawning site selection, such as proximity to cover, that are not incorporated in my study.

Additional statistical analyses would help describe the relationship between streambed competence and redd occurrence and density. For example, a logistic regression model describing trends in presence or absence of redds may further explain the degree to which bull trout select or avoid streambed sections of high competence. Additionally, due to my low sample sizes, the use of simple, non-parametric correlations may be more appropriate than the regression analyses I performed as part of this study.

1B) Reach-scale hydrogeology

Hypothesis 1B, which related spawning occurrence at the subreach- and reach-scale to extensive vertical and lateral hyporheic exchange, was supported. Streambed water temperature data indicated rapid hyporheic mixing of stream water into the streambed for all study reaches. Other researchers have observed similar streambed conditions in potential salmon spawning areas (e.g. Alexander and Cassie, 2003). Additionally, reach-average redd density was positively correlated with streambed K_v (Figure 16c). In salmonid spawning habitat studies, measurements of streambed hydraulic conductivity often include only the measurement of the horizontal component (K_h) (e.g. Baxter and Hauer, 2000). Sediment sorting processes often produce stratified beds (e.g. Marion et al., 2008b), and vertical hydraulic conductivity (K_v) values are generally one or two orders of magnitude less than K_h (Chen, 2000). All of the study reaches exhibited K_h values representative of a mix of well-sorted gravel and sand and glacial outwash (Fetter, 2001).

Whereas vertical hydraulic gradients (VHG) in all study reaches were dominantly negative, most piezometers were installed in concave-up bedforms where negative VHG was to be expected (e.g. Keller and Kondolf, 1990; Tonina and Buffington, 2011; Bhaskar et al., 2012). Hydrogeologic conditions during the spawning period appeared stable because stream stage, VHG, and q_v were relatively constant (Janssen et al., 2012; Tonina and Buffington, 2009a). Use of streambed temperature signals to compute q_v values in site conditions similar to mine (lack of buffering, lagging, or cooling/warming of shallow (<25 cm deep) streambed temperatures) should be done with caution. I recommend, as a first order check on specific discharge direction estimation by an analytical heat and fluid flow model, VHG should be measured periodically along with the vertical temperature time series (Figure 28). This provides a second set of flow direction data. Conceptually, using only temperature data, it appears that certain temperature signals can be calculated as downward when they are in fact parallel to the streambed or even upward (Figure 28). For this study, I assumed temperature signals indicated upward or downward flow; I did not account for horizontal streambed flow conditions.

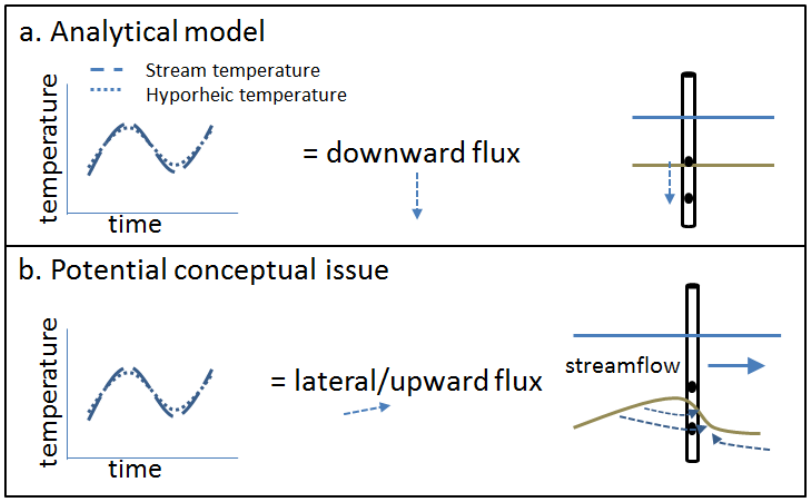

Figure 28. Illustration of potentially inaccurate heat and fluid flow analytical model calculation of specific discharge magnitude and direction from vertically spaced streambed temperature time series data. (a) represents potential input and output from the analytical model; (b) represents a physical conditions creating the same temperature curves but with an entirely different flux direction and magnitude.

Streambed temperature data indicated one distinct zone of groundwater upwelling (sensor O-gw in Figure 26), located in OLE_{sc}. Distinct zones of groundwater upwelling have been observed by many researchers (e.g. Hansen, 1975; Bhaskar et al., 2012); potential conceptual models explaining why groundwater discharge is focused to sections of the streambed have been proposed (e.g. Bhaskar et al., 2012) (Figure 29). Additionally, channel depositional processes and structures facilitate preferential subsurface flow paths and may help explain the presence of distinct zones of groundwater discharge to the stream (e.g. inter-connected open framework gravels: Lunt and Bridge, 2007).

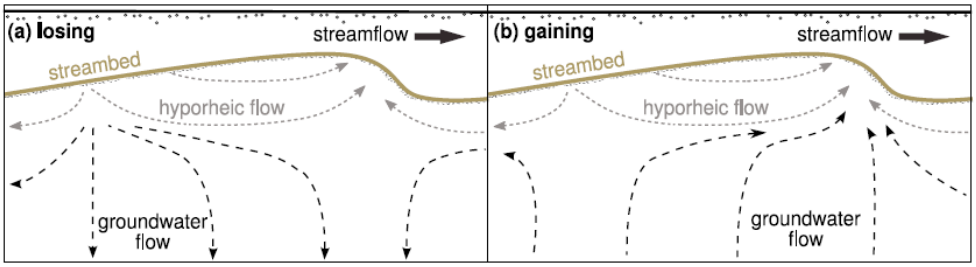

Figure 29. Conceptual models illustrating the interaction of hyporheic and groundwater flow paths in relation to bedforms. In (b) notice the localized zone of groundwater discharge to the stream. (Figure copied from Bhaskar et al. (2012).)

Errors and uncertainties associated with the measurement of hydrogeological parameters determined in this study arise from a number of sources. For example, VHG data, though relatively easy to measure, can be misrepresented by vertical leakage ("short circuiting") along the outside of the piezometer casing (related issues in similar physical settings are extensively discussed by Kondolf et al. (2008) and others). In coarse-grained bed sediments, short circuiting is difficult to quantify; I attempted to minimize vertical leakage by packing sediment near the piezometers with my wading boots after installations. A second concern related to slug tests and streambed hydraulic property characterization was the influence of frictional losses in the piezometer may inhibit my ability to obtain high resolution datasets for K_h determination (e.g. McElwee and Butler, 1996; Butler, 1998). These concerns were alleviated by laboratory tests of the field piezometer design (Woessner and Rambo, 2012, unpublished

data). Larger errors came from fitting graphical solutions to the observed slug response datasets. Because of the rapid response of piezometer water levels and the 0.5 to 1 second measurement interval available in the transducers used, it was not always clear that a detailed enough dataset was collected. Future work in similar settings should not only use an instantaneous slug removal (e.g. Butler, 1998) but also transducers that can record at 0.1 second measurement intervals. In spite of the issues listed above, curve matching of head response data generally provided K_h values within the range of expected values (Figure 15a).

2A) Valley-scale geomorphology

My hypothesis 2A, which related spawning occurrence to areas of alluvial valley narrowing, was not supported. This hypothesis was based on the premise that bull trout spawning is commonly associated with alluvial valley sections where hyporheic water and groundwater discharge to the stream to create favorable spawning and incubation temperature regimes (e.g. Stanford and Ward, 1993; Baxter and Hauer, 2000). It is also based on the premise that as valleys narrow, the cross sectional alluvial area transmitting down-valley flowing groundwater decreases causing a rise in the water table and thus there is an increase in groundwater discharge to the stream channel (e.g. Stanford and Ward, 1993; Baxter and Hauer, 2000; Tonina and Buffington, 2009a).

Only in Ole did a high density spawning reach correlate with distinct valley wall narrowing (Figure 19). However, no data on the change in valley alluvial cross-sectional area was available for any of the study catchments. In Quartz and Whale, high density spawning reaches were continuously distributed throughout extensive unconfined valleys and appeared to have no correlation with valley narrowing. It is possible that the base level of Quartz Lake acts to confine the cross sectional alluvial area for down-valley transport in the Quartz drainage and causes upwelling of hyporheic water and valley groundwater. In Trail, there was no high density spawning reach, and only 1 of the 8 redds (13% of the 2011 Trail redd count) was located in an unconfined valley.

The high percentage (74%, this study) of redds in unconfined valleys suggests that unconfined (alluvial) valleys provide important spawning habitat for bull trout. Many studies corroborate this finding (e.g. Stanford and Ward, 1993; Baxter and Hauer, 2000). Physical characteristics of alluvial valleys cited as important for spawning and ecosystem health include a floodplain accessible by high flows and high channel roughness factors. Overbank flows and high hydraulic roughness (due to bar, bank, and wood roughness: e.g. Buffington and Montgomery, 1999b) act to decrease bed shear stress relative to total boundary shear stress of high flow events. Additionally, large woody debris and side channels contribute to spawning habitat complexity and help protect incubating salmonid eggs from scour (Shellberg et al., 2010). Furthermore, alluvial valleys are known to host extensive hyporheic and groundwater exchange with stream water (e.g. Woessner, 2000).

Baxter and Hauer (2000) observed a lack of bull trout redds in unconfined alluvial valleys at the mouth of their study streams. Similarly, I did not observe bull trout redds near the downstream extent of the Ole, Trail, or Whale catchments. From topographic map analyses, they termed these valley segments as “unbounded” alluvial valleys because they did not possess a constricting knickpoint at their downstream extent. Baxter and Hauer (2000) speculated that the lack of bull trout spawning in these unbounded alluvial valley sections may be attributed to the lack of a confining knickpoint that would decrease the alluvial valley cross-sectional area and theoretically provide thermally moderating hyporheic and groundwater discharge to the stream channel. I observed other likely factors contributing to the lack of spawning – namely incised channels and substrate too coarse for spawning. Coarse-scale DEM observations of the Trail and Whale catchment mouths show broad alluvial valleys that merge with the valley floor of the North Fork of the Flathead River. However, finer-scale DEM observations, as well as field observations, show an incised stream channel and an elevated, disconnected floodplain – indicating a likelihood of streambed coarsening (and high streambed shear stresses and high potential

for scour of spawning appropriate gravels). Pebble counts confirmed that the dominant textural facies in the sampled sections of these unbounded alluvial valleys were too coarse for spawning (Baxter and McPhail, 1996; Dunham et al., 2001). Another reason potentially contributing to the lack of spawning near the downstream extent of the Whale catchment may be that the downstream third of the catchment burned in the early 2000s, and no 2011 bull trout redds were observed in the burned area. Wildfire and loss of riparian vegetation can increase stream temperatures (e.g. Isaak et al., 2010; Boughton et al., 2012) and fine sediment delivery to streams; both factors are detrimental to bull trout spawning habitat (e.g. Isaak et al., 2010).

Whereas valley confinement ratio (VCR) did not correlate with redd density (R^2=0.08, p=0.6), relationships between VCR and field-measured geomorphic and hydrogeologic variables appear evident, but none were statistically significant. As theoretically expected, VCR influenced reach-average grain size distribution and channel slope. Surprisingly, channel slope exhibited no measureable control on grain size. The lack of control of channel slope on grain size distributions is likely attributable in part to hydraulic roughness factors (e.g. Buffington and Montgomery, 1999b).

Hydrogeologically, VCR exhibited the strongest apparent influence on reach-average VHG. Among the study reaches, as VCR increased, reach-average VHG trended from higher negative values towards zero. This trend may indicate that the higher VCR study reaches exhibited more variable (positive and negative) VHGs throughout the study reach than the study reaches with low VCR, which showed dominantly downward VHG.

2B) Valley-scale hydrogeology

My hypothesis 2B, which related spawning occurrence to areas of hyporheic water and groundwater discharge to the stream, was supported. This is most notable in the Ole catchment. The buffered and cooled stream temperature signals of OLE_{mc} (sensor O-4mc) and OLE_{sc} (sensor O-5sc) relative to the O-1mc (Figures 24, 25, 26) indicate substantial stream temperature moderation within the spawning reaches. I attribute this temperature moderation to valley-scale groundwater discharging to the stream channel; the groundwater temperature signal is represented by temperature sensor O-gw (Figure 26). Temperature moderation of unconfined valley portion of the Ole spawning reach is further substantiated by the decrease in variation in stream temperature with time whereas the stream temperature sensors 2 km upstream (O-1mc) and 5 km downstream (O-6mc) increase in variation with time (Figure 25). Conceptually, as stream flow decreases through the summer and fall, groundwater contribution to stream flow ("baseflow") becomes a greater percentage of total streamflow, and the thermally moderating effect of groundwater becomes more evident in reaches experiencing groundwater discharge (e.g. Figure 25a: sensors O-4mc, O-5mc).

The catchment-wide spatial scale of these water temperature measurements was essential to facilitate observations of the thermally moderated spawning reaches in OLE_{mc} and OLE_{sc}. Arrigoni et al. (2008) found hyporheic discharge temperatures in a section of the Umatilla River, Oregon (a gravel and cobble bedded system) to be primarily buffered and lagged (as opposed to cooled) relative to diurnal temperature cycles of the main channel. In the Ole catchment, only when considering stream temperatures kilometers upstream and downstream does the water temperature in the study reaches of Ole show evidence of substantial cooling. This highlights the importance of measuring and considering catchment-wide water temperatures in evaluating relative buffering, lagging, and cooling to interpret roles of hyporheic water and groundwater contribution to stream and floodplain water temperatures. Catchment-wide point measurements of specific electrical conductance may be an alternative way to delineate zones of long residence time groundwater contribution to the stream channel (e.g. Haria et al., 2013).

These groundwater moderated stream temperatures of OLE_{mc} and OLE_{sc} may continue downstream to the 19 redds (48% of total in Ole) in the confined valley section downstream of the Ole

study reaches. However, the moderated stream temperatures do not persist to the mouth of Ole Creek. At the mouth, the O-6mc temperature signal has a similar average, diurnal variation, and rate of change as O-1mc (Figure 24, Figure 25). Therefore, for the O-1mc and O-6mc sections of Ole Creek, stream temperatures are presumably dominated by air temperature and solar radiation.

Potential reasons why Ole temperature sensor O-1mc exhibits a relatively unmoderated stream water temperature signal despite being within an alluvial valley segment *and* proximally downstream of another unconfined valley segment include: 1) it is near the upstream extent of an unconfined valley so hyporheic and groundwater interaction are limited, 2) the unconfined valley upstream of O-1mc may be falsely delineated or may not possess adequately deep or conductive alluvial sediments to allow water temperature moderation.

In the Quartz drainage, Cerulean Lake is fed by melt water from Rainbow Glacier. Standard deviations in stream temperature downstream of Cerulean Lake (Q-1mc) and upstream of Quartz Lake (Q-2mc) were equal; however, Q-2mc average water temperature was warmed ~0.4°C relative to Q-1mc. Arrigoni et al. (2008) attributed warming of shallow hyporheic water (relative to main channel water) to either 1) solar heating of floodplain sediments, or 2) heating of channel water in stagnant sections by solar radiation prior to it entering the hyporheic zone. I have no floodplain water temperature data in Quartz, but I frequently observed calm eddies and backwater environments in the wood-forced, pool-riffle channel. I also commonly observed ponded floodplain depressions in the Quartz unconfined valley section. These still water bodies indicate potential for warming of hyporheic floodplain temperatures. Because hyporheic temperature differences tend to increase with flow path length, (Arrigoni et al., 2008), I interpret the lack of change in standard deviation and relatively small change in average temperature from between Q-1mc and Q-2mc to indicate hyporheic exchange in the unconfined alluvial valley upstream of Quartz Lake is dominated by short and fast hyporheic flow paths. Similarly, other researchers report that short hyporheic flow paths tend to dominate hyporheic exchange in streams (e.g. Arrigoni et al., 2008; Poole et al., 2008; Cardenas et al., 2004; Haggerty et al., 2002; Gooseff et al., 2003; Kasahara and Wondzell, 2003). Another potential reason for the lack of change in water temperature from Q-1mc to Q-2mc is that the Quartz drainage is heavily vegetated and riparian vegetation overhangs much of the stream channel. Riparian shading acts to cool stream water (Bhaskar et al., 2012); therefore, it is possible that the cooling effect of the dense riparian vegetation countered solar heating of calm waters and caused the temperature signals of Q-1mc and Q-2mc to remain similar.

Mellina et al. (2007) reported that mountain streams with headwater lakes tend to cool as they flow downstream due to relatively warm lake outlet temperatures and cold groundwater inflows. The apparent moderate warming and lack of buffering between Q-1mc and Q-2mc may indicate a lack of thermally moderating groundwater contribution to the stream channel in the unconfined alluvial valley portion of the Quartz drainage. This could mean that 1) groundwater does not discharge to the stream (i.e. the stream channel is dominantly losing or exhibits parallel flow conditions (Woessner, 2000) in the unconfined valley) or 2) there is not enough conductive alluvial sediment volume or depth to develop a water temperature regime representative of “groundwater”. Although groundwater does not play an obvious role in moderating stream temperature in the Quartz drainage, variation in stream temperature (and Quartz Lake temperature) decreases from September through October (Figure 25). The Q-1mc temperature sensor indicates that Cerulean Lake outlet stream temperatures also decrease over time. This is consistent with previously published literature: alpine lakes serve as thermal moderators of stream temperature (e.g. Mellina et al., 2002; Hieber et al., 2002). Compared to downstream stream segments, stream temperatures at alpine lake outlets tend to exhibit higher maximum water temperatures and lower daily temperature fluctuations (Hieber et al., 2002). Between Q-1mc and Q-2mc is the confluence of Rainbow and Quartz creeks. The mixing of stream temperature regimes at the confluence, combined with a potential lack of groundwater input in the unconfined alluvial valley, and

potential warming of hyporheic water in floodplain sediments (e.g. Arrigoni et al., 2008) appear to complicate the usual trend of downstream cooling reported by Mellina et al. (2007). Regardless, it is apparent that Cerulean Lake, supplied by glacial melt water, provides an aspect of thermal moderation to the stream water (which is usually attributed to groundwater input).

The Trail and Whale stream temperature data indicates that groundwater likely moderates of stream temperatures. Observations contributing to this conclusion include: 1) the stream temperatures decrease in variability over time (Figure 25); 2) all measured average stream temperatures in both drainages plot in the range of expected groundwater temperature (Figure 24); and standard deviations in stream temperature are similar to those in OLE_{mc} and OLE_{sc} (Figure 24), which were shown to be substantially thermally influenced by groundwater input. The cooler September water temperatures of Trail and Whale compared to Ole and Quartz could also be attributed to cooler air temperatures measured in the study reaches (Figure 27).

In Trail, the effect of the intermittent channel section (between sensors T-1mc and T-3mc) on water temperature moderation is unclear. Installation of stream temperature sensors above and below the intermittent section would inform this question. The shallow (~1-1.4 m below ground surface) floodplain water temperature signals in Trail and Whale exhibit almost no daily variation and are ~1°C+ warmer than the stream temperature and expected groundwater temperature at 10-25 m depth (Figure 24, Figure 25). Similar to Quartz, I attribute warming of shallow floodplain water to solar heating of floodplain sediments and/or solar warming of channel or floodplain ponded areas prior to entering the hyporheic zone (e.g. Arrigoni et al., 2008). Shallow floodplain water temperatures, such as those measured in my study areas, may not be representative of regional groundwater temperature or short residence-time hyporheic water. Future studies could clarify floodplain water thermal regimes and sources by installing deeper floodplain wells and temperature sensors at various depths.

The Big Picture

My results show that geophysical, thermal, and hydrological factors appear to influence bull trout spawning occurrence at multiple spatial scales. At the subreach and reach-scales, high density spawning tends to occur where dominant textural facies exhibit mobile spawning appropriate gravels where streambed hydraulic conductivities and rates of streambed hyporheic exchange are high. Specific local-scale pre-spawning streambed flux direction and magnitude may be less relevant because redd structure induces the necessary hyporheic flows through the redd gravels (e.g. Tonina and Buffington, 2011). In streams and reaches where dominant textural facies are not fine enough for redd construction, redd distribution is patchy, occurring in isolated gravel accumulations not represented by sub-reach scale characterization (e.g. behind boulders or large woody debris). Spawning bull trout in these study streams tended to select fine-grained textural facies easily mobilized and reworked by geomorphically significant flows in alluvial valleys, suggesting that bull trout are responsive to the most dynamic sections of catchments were flows, sediments, and nutrients are most actively cycled. Transport and reworking of these streambed sections also appears to result in higher vertical hydraulic conductivity (K_v) of the streambed. However, spawning preference for streambed sections of mobile sediment at bankfull flows indicates that redds may be susceptible to scour during late fall, winter, and early spring high flow events. Such high flow events can be caused by heavy rains, rain on snow events, or snowmelt.

At the valley scale, high density spawning reaches tend to occur in unconfined alluvial valley segments where stream temperatures are moderated (buffered and cooled or warmed – depending on the season) by hyporheic and groundwater discharge to the stream. Unconfined alluvial valley segments tend to host more spatially extensive suitable spawning gravels than confined valley segments because of increased hydraulic roughness factors (e.g. bars, banks, wood, riparian vegetation, and an accessible floodplain at high flows: Buffington and Montgomery, 1999b). Hydraulic roughness factors act to decrease the amount of total channel shear stress applied to the streambed and allows for more

extensive distributions of spawning appropriate gravels. Additionally, alluvial valley sediment depositional processes determine alluvial depth, structure, and horizontal and vertical hydraulic conductivities. Interrelations of these factors contribute to the development of various surface and subsurface temperature regimes, which are dependent on flow path residence time and depth. Discharge of hyporheic and groundwater to the stream channel can moderate (buffer, lag, warm or cool: Arrigoni et al., 2008) stream water temperatures and help support salmonid spawning habitat.

Implications and applications of this study and related research are many. My study shows that dimensionless variables such as Shields stress (or Shields stress adjusted for bed stress only) and the coefficient of variation in water temperature can be used to evaluate ecologically important physical conditions and processes within and between stream systems and to assess salmonid spawning habitat and other ecological topics in similar physical systems.

My study provides further evidence that alluvial valleys in snowmelt-dominated mountain streams are essential components of natural ecosystem function; as these features cannot be created, their preservation is important. Further, I illustrate how remote sensing of landscape features (e.g. confined and unconfined valley segments) can be used to relate physical processes to ecological responses, such as relating of bull trout spawning occurrence to alluvial valley presence and surface water – groundwater exchange.

To delineate and protect critical interior coho salmon spawning habitat, McRae et al. (2012) recommend intensive sampling of physical and chemical hyporheic zone characteristics**.** My study indicates that less resource intensive, broader-scale salmonid habitat assessments (of variables such as valley confinement, streambed mobility, stream temperature variability, and groundwater discharge zones) may be efficient and effective in delineating critical habitat zones and prioritizing conservation and management plans.

Changes in habitat suitability due to climate change is a topic of recent research (e.g. Rieman et al., 2007; Isaak et al., 2010; Wenger et al., 2011; Isaak et al., 2012; Jones et al., *in press*). Isaak et al. (2012) suggest that, for the period 1950-2009, flows have increased in winter months in the Flathead River Basin. My spawning gravel competence results suggest that a shift in timing of high flows could increase the likelihood of bull trout redd scour.

Thermal sensitivity has long been a focus of bull trout habitat studies. My data indicate that groundwater is a more dominant control on stream temperature than snow- or ice-melt during the fall bull trout spawning season in the Flathead River Basin. One reason for the diminished role of glacial melt on stream temperature cooling in the Quartz drainage and similar glacier drainages in Glacier National Park is the thermal moderation (warming) of headwater lakes that intercept the melt water prior to flowing downstream into bull trout spawning reaches (e.g. Mellina et al., 2002; Hieber et al., 2002). Supporting this, Jones et al. (*in press*) used empirical temperature data to model stream temperatures in the Flathead River Basin and found significant warming (+3˚C) of summer (August) stream temperatures downstream of lakes. Streams dominated by groundwater thermal moderation may be more buffered from habitat fragmentation due to climate warming. Therefore, to reduce existing and future stressors, an important conservation strategy is to protect and enhance the physical connectivity of existing high quality bull trout habitat (Jones et al., in press).

Salmonid habitat suitability studies can be particularly applicable to stream restoration. My study emphasizes the importance the physical and biological connection of the stream, hyporheic, and groundwater systems. Protection and improvement of spatially extensive suitable physical and thermal habitat is important for conserving threatened bull trout populations in the northern Rocky Mountains and Pacific Northwest.

CONCLUSIONS

My findings indicate that physical processes at multiple-spatial scales influence bull trout redd occurrence in snowmelt dominated systems. At the subreach- and reach-scale, redd occurrence tends to be associated with mobile surface gravels that have high horizontal and vertical hydraulic conductivities. At the valley-scale, redd occurrence tends to be associated with unconfined alluvial valleys where stream temperatures are thermally suitable. Groundwater appears to play a major role in providing favorable conditions for bull trout spawning reaches. In light of the spawning gravel competence results, shifts in timing of high flows associated with climate change (e.g. Isaak et al., 2012) could adversely affect bull trout spawning by increasing the likelihood of redd scour.

The difference between my findings and previous studies related to streambed mobility and salmonid spawning site selection merits further attention. In terms of using and expanding on the findings of this study, basin-wide grain size prediction models (e.g. Buffington et al., 2004) could be used to assess the broader-scale distribution of physically suitable spawning habitat. Basin-wide valley confinement delineations and stream temperature monitoring networks could be used to further assess stream thermal regimes and identify the role of groundwater in modifying the thermal regime of this system. Further clarification of the role of groundwater in patch and subreach-scale bull trout spawning site selection is also merited.

List of abbreviations and symbols used in text and their definitions

OLE_{mc}	Ole Creek main channel study reach
OLE_{sc}	Ole Creek secondary channel study reach
QTZ	Quartz Creek study reach
TRL	Trail Creek study reach
WHL_{mc}	Whale Creek main channel study reach
WHL_{sc}	Whale Creek secondary channel study reach
τ_o	total boundary shear stress
τ'	bed shear stress
τ^*	Shields stress (incorporates τ_o)
τ^{**}	adjusted Shields stress (incorporates τ')
ρ_w	water density
ρ_s	sediment density
VHG	vertical hydraulic gradient
K_h	horizontal hydraulic conductivity
K_v	vertical hydraulic conductivity
K_h/K_v	hydraulic conductivity anisotropy ratio
q_v	specific discharge
C_v	coefficient of variation in stream temperature

REFERENCES

Al-Chokhachy, R., B.B. Roper, T. Bowerman, and P. Budy. 2010. A review of bull trout habitat associations and exploratory analyses of patterns across the interior Columbia River Basin. North American Journal of Fisheries Management 30 (2): 464–480.

Alexander, M.D., and D. Caissie. 2003. Variability and comparison of hyporheic water temperatures and seepage fluxes in a small Atlantic salmon stream. Ground Water 41 (1): 72–82.

Arrigoni, A.S., G.C. Poole, L.A.K. Mertes, S.J. O'Daniel, W.W. Woessner, and S.A. Thomas. 2008. Buffered, lagged, or cooled? Disentangling hyporheic influences on temperature cycles in stream channels. Water Resources Research 44: W09418.

Barnes, H.H. 1967. Roughness characteristics of natural channels. USGS Water Supply Paper 1849.

Baxter, C., F.R. Hauer, and W.W. Woessner. 2003. Measuring groundwater-stream water exchange: new techniques for installing minipiezometers and estimating hydraulic conductivity. Transactions of the American Fisheries Society 132 (3): 493–502.

Baxter, C.V., and F.R. Hauer. 2000. Geomorphology, hyporheic exchange, and selection of spawning habitat by bull trout (*Salvelinus Confluentus*). Canadian Journal of Fisheries and Aquatic Sciences 57 (7): 1470–1481.

Baxter, C.V., C.A. Frissell, and F.R. Hauer. 1999. Geomorphology, logging roads, and the distribution of bull trout spawning in a forested river basin: implications for management and conservation. Transactions of the American Fisheries Society 128 (5): 854–867.

Baxter, J.S., and J.D. McPhail. 1999. The influence of redd site selection, groundwater upwelling, and over-winter incubation temperature on survival of bull trout (*Salvelinus Confluentus*) from egg to alevin. Canadian Journal of Zoology 77 (8): 1233–1239.

Baxter, J.S., and J.D. McPhail. 1996. A review of bull trout (*Salvelinus Confluentus)* life-history and habitat use in relation to compensation and improvement opportunities. Fisheries Management Report Number 104. Ministry of Environment, Lands and Parks.

Benson, N.G. 1953. The importance of groundwater to trout populations in the Pigeon River, Michigan. *In* Transactions of the North American Wildlife Conference (18): 260–281.

Benson, N.G. 1955. Observations on anchor ice in a Michigan trout stream. Ecology 36 (3): 529–530.

Bhaskar, A.S., J.W. Harvey, and E.J. Henry. 2012. Resolving hyporheic and groundwater components of streambed water flux using heat as a tracer. Water Resources Research 48: W08524.

Bjornn, T.C., and D.W. Reiser. 1991. Habitat requirements of salmonids in streams. American Fisheries Society Special Publication (19): 83–138.

Boulton, A.J., T. Datry, T. Kasahara, M. Mutz, and J.A. Stanford. 2010. Ecology and management of the hyporheic zone: stream-groundwater interactions of running waters and their floodplains. Journal of the North American Benthological Society 29 (1): 26–40.

Boughton, D.A., C. Hatch, and E. Mora. 2012. Identifying distinct thermal components of a creek. Water Resources Research 48: W09506.

Buffington, J.M., D.R. Montgomery, and H.M. Greenberg. 2004. Basin-scale availability of salmonid spawning gravel as influenced by channel type and hydraulic roughness in mountain catchments. Canadian Journal of Fisheries and Aquatic Sciences 61 (11): 2085–2096.

Buffington, J.M., and D.R. Montgomery. 1997. A systematic analysis of eight decades of incipient motion studies, with special reference to gravel-bedded rivers. Water Resources Research 33 (8): 1993–2029.

Buffington, J.M., and D.R. Montgomery. 1999a. A procedure for classifying textural facies in gravel-bed rivers. Water Resources Research 35 (6): 1903–1914.

Buffington, J.M., and D.R. Montgomery. 1999b. Effects of hydraulic roughness on surface textures of gravel-bed rivers. Water Resources Research 35 (11): 3507–3521.

Bunte, K. and S.R. Abt. 2001. Sampling surface and sub-surface particle size distributions in wadeable gravel- and cobble-bed streams for analysis in sediment transport, hydraulics, and streambed Monitoring. USDA Forest Service, General Technical Report, RMRS-GTR-74. 450 pp.

Burner, C.J. 1951. Characteristics of Spawning Nests of Columbia River Salmon. US Department of the Interior.

Butler, J.J. Jr. 1998. The design, performance, and analysis of slug tests. Lewis Publishers.

Brunner, G.W. 2010. HEC-RAS River Analysis System: user's manual. US Army Corps of Engineers, Hydrologic Engineering Center.

Cardenas, M.B., J.L. Wilson, and V.A. Zlotnik. 2004. Impact of heterogeneity, bed forms, and stream curvature on subchannel hyporheic exchange. Water Resources Research 40 (8): W08307.

Caissie, D. The thermal regime of rivers: a review. Freshwater Biology 51: 1389–1406.

Chen, X. 2000. Measurement of streambed hydraulic conductivity and its anisotropy. Environmental Geology 39 (12): 1317–1324.

Chevalier, B., C. Carson, and W.J. Miller. 1984. Report of Engineering and Biological Literature Pertaining to the Aquatic Environment: With Special Emphasis on Dissolved Oxygen and Sediment Effects on Salmonid Habitat. Colorado State University, Department of Agriculture and Chemical Engineering.

Church, M. 2006. Bed material transport and the morphology of alluvial river channels. Annual Review of Earth and Planetary Sciences 34: 325–354.

Church, M.A., D.G. McLean, and J.F. Wolcott. 1987. River bed gravels: sampling and analysis. Sediment transport in Gravel-Bed Rivers. John Wiley and Sons New York. 43-88.

Cordone, A.J., and D.W. Kelley. 1961. The influences of inorganic sediment on the aquatic life of streams. California Fish and Game 47.

Cunjak, R.A., and G. Power. 1986. Winter habitat utilization by stream resident brook trout (*Salvelinus fontinalis*) and brown trout (*Salmo trutta*). Canadian Journal of Fisheries and Aquatic Sciences 43 (10): 1970–1981.

Curry, R.A., and D.L. Noakes. 1995. Groundwater and the selection of spawning sites by brook trout (*Salvelinus fontinalis*). Canadian Journal of Fisheries and Aquatic Sciences 52 (8): 1733–1740.

Daly, D., and G. Taylor. 1998. Montana average annual precipitation (1961-1990). Oregon Climate Service at Oregon State University.

DeVries, P. 1997. Riverine salmonid egg burial depths: review of published data and implications for scour studies. Canadian Journal of Fisheries and Aquatic Sciences 54 (8): 1685-1698.

DeVries, P. 2002. Bedload layer thickness and disturbance depth in gravel bed streams. Journal of Hydraulic Engineering. 128 (11): 983-991.

Dingman, S. L. 2009. Fluvial Hydraulics. Oxford University Press.

Dunham, J., B. Rieman, and K. Davis. 2001. Sources and magnitude of sampling error in redd counts for bull trout. North American Journal of Fisheries Management 21 (2): 343–352.

Dunham, J., C. Baxter, K. Fausch, W. Fredenberg, S. Kitano, I. Koizumi, K. Morita, et al. 2008. Evolution, ecology, and conservation of dolly varden, white spotted char, and bull trout. Fisheries 33 (11): 537–550.

Embody, G. C. 1927. An outline of stream study and the development of a stocking policy. Aquicultural Laboratory, Cornell University: 1-21.

Einstein, H.A., and R.B. Banks. 1950. Fluid resistance of composite roughness, American Geophysical Union Eos Transactions 31: 603–610.

Einstein, H.A., and N.L. Barbarossa. 1952. River channel roughness. Transaction of the American Society of Civil Engineers 117: 1121–1146.

Ellis, B.K., J.A. Stanford, D. Goodman, C.P. Stafford, D.L. Gustafson, D.A. Beauchamp, D.W. Chess, J.A. Craft, M.A. Deleray, and B.S. Hansen. 2011. Long-term effects of a trophic cascade in a large lake ecosystem. Proceedings of the National Academy of Sciences 108 (3): 1070–1075.

Fetter, C. W. 2001. Applied Hydrogeology, 4th Ed. Prentice Hall.

Fraley, J. 2010. Bull trout counts steady in the Flathead, up in the South Fork, down in the Swan. Montana Fish, Wildlife, and Parks News Release.

Fraley, J.J., and B.B. Shepard. 1989. Life history, ecology and population status of migratory bull trout (*Salvelinus confluentus*) in the Flathead Lake and River system. Northwest Science 63 (4): 133–143.

Gibson, R.J. 1966. Some factors influencing the distributions of brook trout and young Atlantic salmon. Journal of the Fisheries Board of Canada 23 (12): 1977–1980.

Goetz, F. 1989. Biology of the Bull Trout, *Salvelinus Confluentus*: a Literature Review. Oregon State University, Department of Fisheries and Wildlife.

Gooseff, M.N., J.M. Wondzell, R. Haggerty, and J. Anderson. 2003. Comparing transient storage modeling and residence time distribution(RTD) analysis in geomorphically varied reaches in the Lookout CreekBasin, Oregon, USA. Advanced Water Resources. 26 (9): 925– 937.

Haggerty, R., S.M. Wondzell, and M.A. Johnson. 2002. Power-law residence time distribution in the hyporheic zone of a 2nd-order mountain stream. Geophysical Research Letters 29 (13): GL014743.

Hall, J.E., Holzer, D.M. and Beechie, T.J. 2007. Predicting river floodplain and lateral channel migration for salmon habitat conservation. Journal of the American Water Resources Association 43: 786–797.

Hansen, E.A. 1975. Some effects of groundwater on brown trout redds. Transactions of the American Fisheries Society 104 (1): 100–110.

Haria, A.H., P. Shand, C. Soulsby, and S. Noorduijn. 2013. Spatial delineation of groundwater-surface water (GW-SW) interactions through intensive in-stream profiling. Hydrological Processes 27: 628-634.

Hatch, C.E., A.T. Fisher, J.S. Revenaugh, J. Constantz, and C. Ruehl. 2006. Quantifying surface water-groundwater interactions using time series analysis of streambed thermal records: method development. Water Resources Research 42: W10410.

Healey, M. C. 1991. Life history of chinook salmon (*Oncorhynchus shawytscha*). Pacific Salmon Life Histories: 313–393.

Hieber, M., C.T. Robinson, U. Uehlinger, and J.V. Ward. 2002. Are alpine lake outlets less harsh than other alpine streams? Archiv fur Hydrobiologie 154: 199-223.

Isaak, D.J., C.C. Muhlfeld, A.S. Todd, R. Al-Chokhachy, J. Roberts, J.L. Kershner, K.D. Fausch, S.W. Hostetler. The past as prelude to the future for understanding 21st-Century climate effects on Rocky Mountain trout. Fisheries Management 37: 542-556.

Isaak, D.J., C. H. Luce, B.E. Rieman, D.E. Nagel, E.E. Peterson, D.L. Horan, S. Parkes, and G.L. Chandler. 2010. Effects of climate change and wildfire on stream temperatures and salmonid thermal habitat in a mountain river network. Ecological Applications 20 (5): 1350–1371.

Janssen, F., M.B. Cardenas, A.H. Sawyer, T. Dammrich, J. Krietsch, and D. de Beer. 2012. A comparative experimental and multiphysics computational fluid dynamics study of coupled surface–subsurface flow in bed forms. Water Resources Research 48: W08514.

Johnson, A.N., B.R. Boer, W.W. Woessner, J.A. Stanford, G.C. Poole, S.A. Thomas, and S.J. O'Daniel. 2005. Evaluation of an inexpensive small-diameter temperature logger for documenting ground water–river interactions. Ground Water Monitoring & Remediation 25 (4): 68–74.

Kasahara, T., and S.M. Wondzell. 2003. Geomorphic controls on hyporheic exchange flow in mountain streams. Water Resources Research 39.

Kasenow, M. 2001. Applied ground-water hydrology and well hydraulics. Water Resources Publication.

Keery, J., A. Binley, N. Crook, and J.W.N. Smith. 2007. Temporal and spatial variability of groundwater-surface water fluxes: development and application of an analytical method using temperature time series. Journal of Hydrology 336: 1–16.

Keller, E.A., and G.M. Kondolf. 1990. Groundwater and fluvial processes; selected observations. *In::* Groundwater Geomorphology: The role of subsurface water in earth-surface processes and landforms. Geological Society of America. 319-340.

Kellerhals, R., and D.I. Bray. 1971. Sampling procedures for coarse fluvial sediments, Journal Hydraulics Division American Society of Civil Engineers 97: 1165–1180.

Kondolf, G.M. 2000. Assessing salmonid spawning gravel quality. Transactions of the American Fisheries Society 129 (1): 262–281.

Kondolf, G.M., T.E. Lisle, and G.M. Wolman. 2003. Bed sediment measurement. *In*: Tools in Fluvial Geomorphology, edited by G.M. Kondolf and H. Piegay, 347-395.

Kondolf, G.M., and M.G. Wolman. 1993. The sizes of salmonid spawning gravels. Water Resources Research 29 (7): 2275–2285.

Kondolf, G.M., J.G. Williams, T.C. Horner, and D. Milan. 2008. Assessing physical quality of spawning habitat. *In*: , 65.

Latta, W.C. 1964. Relationship of young of-the-year trout to mature trout and groundwater. Transactions of the American Fisheries Society 94: 32-39.

Lawlor, S.M. 2004. Determination of channel-morphology characteristics, bankfull discharge, and various design-peak discharges in Western Montana. USGS Special Investigations Report 2004-5263: 1-26.

Lee, D.R., and J.A. Cherry. 1978. A field exercise on groundwater flow using seepage meters and mini-piezometers. Journal of Geological Education 27: 6–10.

Lunt, I.A., and J.S. Bridge. 2006. Formation and preservation of open-framework gravel strata in unidirectional flows. Sedimentology 54 (1): 71–87.

Malcolm, I.A., A.F. Youngson, and C. Soulsby. 2003. Survival of salmonid eggs in a degraded gravel-bed stream: effects of groundwater–surface water interactions. River Research and Applications 19 (4): 303–316.

Malcolm, I.A., C. Soulsby, A.F. Youngson, and D.M. Hannah. 2005. Catchment-scale controls on groundwater-surface water interactions in the hyporheic zone: implications for salmon embryo survival. River Research and Applications 21 (9): 977–989.

Marion, A., A.I. Packman, M. Zaramella, and A. Bottacin-Busolin. 2008. Hyporheic flows in stratified beds. Water Resources Research 44 (9).

McCullough, D.A., J.M. Bartholow, H.I. Jager, R.L. Beschta, E.F. Cheslak, M.L. Deas, J.L. Ebersole. 2009. Research in thermal biology: burning questions for coldwater wtream fishes. Reviews in Fisheries Science 17 (1): 90–115.

McElwee, C.D. and J. J. Butler, Jr. 1996. Experimental verification of a general model for slug tets. Kansas Geological Survey Open-File Report 96-47.

McPhail, J.D., and C.B. Murray. 1979. The early life-history and ecology of Dolly Varden (*Saluelinus malma*) in the upper Arrow Lakes. Department of Zoology and Institute of Animal Resources, University of British Columbia.

Mellina E., R.D. Moore, S.G. Hinch, J.S. Macdonald, and G. Pearson. 2002. Stream temperature responses to clearcut logging in British Columbia: the moderating influences of groundwater and headwater lakes. Canadian Journal of Fisheries and Aquatic Sciences 59, 1886-1900.

Moir, H.J., C.N. Gibbins, J.M. Buffington, J.H. Webb, C. Soulsby, M.J. Brewer, and others. 2009. A new method to identify the fluvial regimes used by spawning salmonids. Canadian Journal of Fisheries and Aquatic Sciences 66 (9): 1404–1408.

Moir, H.J., C. Soulsby, and A.F. Youngson. 2002. Hydraulic and sedimentary controls on the availability and use of Atlantic salmon (*Salmo Salar*) spawning habitat in the River Dee system, northeast Scotland. Geomorphology 45 (3): 291–308.

Moir, H.J., C.N. Gibbins, C. Soulsby, and J.H. Webb. 2006. Discharge and hydraulic interactions in contrasting channel morphologies and their influence on site utilization by spawning Atlantic salmon (*Salmo salar*). Canadian Journal of Fisheries and Aquatic Sciences 63 (11): 2567–2585.

Montgomery, D.R., E.M. Beamer, G.R. Pess, and T.P. Quinn. 1999. Channel type and salmonid spawning distribution and abundance. Canadian Journal of Fisheries and Aquatic Sciences 56 (3): 377–387.

Montgomery, D.R., and J.M. Buffington. 1997. Channel-reach morphology in mountain drainage basins. Geological Society of America Bulletin 109 (5): 596-611.

Montgomery, D.R., J.M. Buffington, N.P. Peterson, D. Schuett-Hames, and T.P. Quinn. 1996. Stream-bed scour, egg burial depths, and the influence of salmonid spawning on bed surface mobility and embryo survival. Canadian Journal of Fisheries and Aquatic Sciences 53 (5): 1061–1070.

Muhlfeld, C.C., M.L. Taper, D.F. Staples, and B.B. Shepard. 2006. Observer error structure in bull trout redd counts in Montana streams: implications for inference on true redd numbers. Transactions of the American Fisheries Society 135 (3): 643–654.

Muhlfeld, C.C., S. Glutting, R. Hunt, D. Daniels, and B. Marotz. 2003. Winter diel habitat use and movement by subadult bull trout in the Upper Flathead River, Montana. North American Journal of Fisheries Management 23 (1): 163–171.

Muhlfeld, C..C, S.T. Kalinowski, T.E. McMahon, M.L. Taper, S. Painter, R.F. Leary, and F.W. Allendorf. 2009. Hybridization rapidly reduces fitness of a native trout in the wild. Biology Letters 5 (3): 328-331.

Muhlfeld, C.C., L. Jones, D. Kotter, W.J. Miller, D. Geise, J. Tohtz, and B. Marotz. 2011. Assessing the impacts of river regulation on native bull trout (*Salvelinus Confluentus*) and western cutthroat trout (*Oncorhynchus Clarkii Lewisi*) habitats in the Upper Flathead River, Montana, USA. River Research and Applications: RRA.1494.

Muhlfeld, C.C., and B. Marotz. 2005. Seasonal movement and habitat use by subadult bull trout in the Upper Flathead River System, Montana. North American Journal of Fisheries Management 25 (3): 797–810.

Muhlfeld, C.C., J.J. Giersch, and B. Marotz. 2012. Seasonal movements of non-native lake trout in a connected lake and river system. Fisheries Management and Ecology 19: 224-232.

Nagel, D.E., J.M. Buffington, S.L. Parkes, S. Wenger, and J Goode. *In press*. A landscape scale valley confinement algorithm: delineating unconfined valley bottoms for geomorphic, aquatic, and riparian applications. USDA/USFS Rocky Mountain Research Station General Technical Report Draft.

NAIP. 2011. U.S. Farm Services Agency National Agricultural Imagery Program (NAIP): Natural-color aerial photos of Montana. http://nris.mt.gov/nsdi/orthophotos/naip_2011.asp

Nielsen, J.L., T.E. Lisle, and V. Ozaki. 1994. Thermally stratified pools and their use by steelhead in northern California streams. Transactions of the American Fisheries Society 123 (4): 613–626.

Pandit, N.S., and R.F. Miner. 1986. Interpretation of slug test data. Ground Water 24 (6): 743–749.

Parker, G., and A.W. Peterson. 1980. Bar resistance of gravel-bed streams. Journal Hydraulics Division of the American Society of Civil Engineers 106, 1559–1575.

Parrett, C., D.R. Johnson. 2004. Methods for Estimating Flood Frequency in Montana Based on Data Through Water Year 1998. US Department of the Interior, US Geological Survey.

Pettijohn, F.J. 1975. Sedimentary Rocks. 3rd Ed. Harper & Row, New York.

Poff, N. 1996. A hydrogeography of unregulated streams in the United States and an examination of scale-dependence in some hydrological descriptors. Freshwater Biology 36 (1): 71–79.

Poole, G.C., S.J. O'Daniel, K.L. Jones, W.W. Woessner, E.S. Bernhardt, A.M. Helton, J.A. Stanford, B.R. Boer, and T.J. Beechie. 2008. Hydrologic spiralling: the role of multiple interactive flow paths in stream ecosystems. River Research and Applications 24 (7): 1018–1031.

Poole, G.C. 2010. Stream hydrogeomorphology as a physical science basis for advances in stream ecology. Journal of the North American Benthological Society 29 (1): 12–25.

Rieman, B.E., D.C. Lee, and R.F. Thurow. 1997. Distribution, status, and ikely future trends of bull trout within the Columbia River and Klamath River basins. North American Journal of Fisheries Management 17 (4): 1111–1125.

Rieman, B.E., D. Isaak, S. Adams, D. Horan, D. Nagel, C. Luce, and D. Myers. 2007. Anticipated climate warming effects on bull trout habitats and populations across the interior Columbia River Basin. Transactions of the American Fisheries Society 136 (6): 1552–1565.

Rieman, B.E., and J.D. McIntyre. 1993. Demographic and Habitat Requirements for Conservation of Bull Trout. USDA General Technical Report.

Santhi, C., P.M. Allen, R.S. Muttiah, J.G. Arnold, and P. Tuppad. 2008. Regional estimation of base flow for the conterminous United States by hydrologic landscape regions. Journal of Hydrology 351 (1): 139–153.

Sauter, S.T., J. McMillan, and J. Dunham. 2001. Salmonid behavior and water temperature. US Environmental Protection Agency Report EPA-910-D0-01-001.

Schlumberger, 2011. AquiferTest 2011.1 software package.

Shapiro, S.S., and M.B. Wilk. 1965. An analysis of variance test for normality (complete samples). Biometrika 52 (3/4): 591–611.

Shellberg, J.G. 2002. Hydrologic, geomorphic, and biologic influences on redd scour in bull char (*Salvelinus confluentus*) spawning streams. M.S. thesis, University of Washington , College of Forest Resources.

Shellberg, J.G., S.M. Bolton, and D.R. Montgomery. 2010. Hydrogeomorphic effects on bedload scour in bull char (*Salvelinus confluentus*) spawning habitat, western Washington, USA. Canadian Journal of Fisheries and Aquatic Sciences 67 (4): 626–640.

Shields, A. 1936. Anwendung der Aehnlichkeitsmechanik und der Turbulenzforschung auf die Geschiebebewegung, Mitt. Preuss. Versuchsanst. Wasserbau Schiffbau, 26.

Stanford, J.A, and J.V. Ward. 1993. An ecosystem perspective of alluvial rivers: connectivity and the hyporheic corridor. Journal of the North American Benthological Society 12 (1): 48–60.

Swanson, T.E., and M.B. Cardenas. 2011. Ex-Stream: a MATLAB program for calculating fluid flux through sediment-water interfaces based on steady and transient temperature profiles. Computers & Geosciences 37 (10): 1664–1669.

Tague, C., G. Grant, M. Farrell, J. Choate, and A. Jefferson. 2008. Deep groundwater mediates streamflow response to climate warming in the Oregon Cascades. Climatic Change 86 (1): 189–210.

Tennant, L. 2010. Spawning and early life-history characteristics of bull trout in a headwater-lake ecosystem. M.S. thesis, Montana State University, Fish and Wildlife Management.

Tonina, D., and J. M. Buffington. 2009a. Hyporheic exchange in mountain rivers I: mechanics and environmental effects. Geography Compass 3 (3): 1063–1086.

Tonina, D., and J.M. Buffington. 2009b. A three-dimensional model for analyzing the effects of salmon redds on hyporheic exchange and egg pocket habitat. Canadian Journal of Fisheries and Aquatic Sciences 66 (12): 2157–2173.

Tonina, D., and J.M. Buffington. 2011. Effects of stream discharge, alluvial depth and bar amplitude on hyporheic flow in pool-riffle channels. Water Resources Research 47.

USFWS, 2008. Montana bull trout distribution. Draft map created by the US Fish and Wildlife Service (USFWS) Montana Ecological Services Field Office.

U.S. Office of the Federal Register. 1998. Endangered and threatened wildlife and plants; determination of threatened status for the Klamath River and Columbia River distinct population segments of bull trout. *Federal Register* 63: 111: 31647-31674.

U.S. Office of the Federal Register. 2010. Endangered and threatened wildlife and plants; revised sesignation of critical habitat for bull trout in the coterminous United States; final rule. Federal Register 75: 200: 63898-64070.

Van Grinsven, M., A. Mayer, and C. Huckins. 2011. Estimation of streambed groundwater fluxes associated with coaster brook trout spawning habitat. Ground Water 50 (3): 432–441.

Vuke, S.M., K.W. Porter, J.D. Conn, and D.A. Lopez. 2007. Geologic Map of Montana. Montana Bureau of Mines and Geology Geologic Map 62.

Weaver, T., and J. Fraley. 1991. Flathead Basin forest practices water quality and fisheries cooperative program: fisheries habitat and fish populations. Flathead Basin Commission, Kalispell, Montana.

Weaver, T.M., and R.G. White. 1985. Coal Creek fisheries monitoring study number III. Quarterly progress report to USDA FS, Montana State Cooperative Fisheries Research Unit, Bozeman, Montana.

Wilcock, P.R., J. Pitlick, and Y. Cui. 2009. Sediment transport primer: estimating bed-material transport in gravel-bed rivers. USDA Rocky Mountain Research Station, Fort Collins, CO.

Wilcox, A.C. 2012. GEO560 Fluvial Geomorphology lecture notes. The University of Montana Geosciences Department.

Wolman, M.G. 1954. A method of sampling coarse river-bed material. American Geophysical Union.

Wolman, M.G., and J.P. Miller. 1960. Magnitude and frequency of forces in geomorphic processes. Journal of Geology 68 (1): 54-74.

Wolock, D.M., T.C. Winter, and G. McMahon. 2004. Delineation and evaluation of hydrologic-landscape regions in the United States using geographic information system tools and multivariate statistical analyses. Environmental Management 34: 71–88.

Yalin, M.S., and E. Karahan. 1979. Inception of sediment transport. Journal Hydraulics Division of the American Society of Civil Engineers 105: 1433–1443.

APPENDIX 1A: Reach-scale Geomorphology

1.A.i. Study reach stream discharge estimation

Q_{spawn} is the discharge measured in the field via float tests in late August. Float tests was not conducted in TRL or WHL_{sc}. Estimation of TRL Q_{spawn} was described in the methods section. To estimate stream channel cross sectional area for the discharge float tests, water depth was measured every 0.5 m across a specified cross section. Flow velocity was estimated by measuring the float time of a small stick as it traveled from 10 m above the measured cross section to 10 m below the cross section. The average velocity of three float tests was multiplied by 0.8 to estimate the average velocity of the in-stream water according to standard methods (Embody, 1927). Discharge was estimated by multiplying this average flow velocity estimate by the total cross sectional area.

For Q_2 (Q_{bf}) estimation using the USGS Montana ungaged basin flood-frequency calculator (Parrett and Johnson, 2004), drainage area was calculated from 30 m DEMs at the locations where the field discharge measurements were conducted. Two different SNOTEL sites (Emery Creek #469, elevation 1326 m; Graves Creek #500, elevation 1311 m) were used to estimate the average annual precipitation (AAP) in the basins of our study streams. Both SNOTELs are within the elevation range of our study reaches (~1250 m – 1372 m); Emery is proximal to and believed to be representative of Ole, and Grave is proximal to and believed to be representative of Whale, Trail, and Quartz. AAP over the last 20 years has been 102 cm at Emery and 122 cm at Graves. Therefore, AAP at Ole is estimated to be 102 cm while AAP at Whale, Trail, and Quartz is estimated to be 122 cm. Field observations of vegetation density and type agree with the estimation that Ole receives less precipitation than the other study streams.

Percent forest cover, the final parameter used in the USGS discharge calculator was only a required parameter for the Western Region streams (Quartz, Trail, and Whale). Field and aerial photo observations suggest that Whale, Trail, and Quartz are all heavily forested. Decreased forest cover density in Whale and Trail compared to Quartz due to road construction and other anthropogenic factors are assumed to be countered by the steeper valley walls and more prominently outcropping bedrock in Quartz which also decrease forest cover density. Therefore, I estimated Whale, Trail, and Quartz to have 80% forest cover within their drainage basin upstream of the field measured discharge cross section. It is noted that a fire about 10 years ago in the lower portion of the Whale drainage has substantially decreased the forest cover density in that section; however, that burned section is several kilometers downstream of the study area and therefore does not factor into the forest cover density estimation for these discharge calculations.

Q_{peak} in each study stream Twas obtained by proportionally scaling the 2011 peak discharges of the North and Middle Forks of the Flathead River to the study streams by their respective contributing areas. (e.g. Discharge of North Fork at USGS gage/Contributing area above the North Fork USGS gage = Discharge of Trail Creek at bottom of study reach/Contributing area above the bottom of the Trail Creek study reach).

Table 1A1. Study reach stream discharge estimates.

	Q_{spawn} (m^3/s)	Q_{bf} (m^3/s)	Q_{peak} 2011 (m^3/s)
$OLE_{mc\ and}\ OLE_{sc}$ combined	3.4	14.3	24.7
QTZ	2.4	15	19.3
TRL	3.9	15.9	20.5
WHL_{mc}	3.5	4.1	4.6

1.A.ii. Gaged basin flood recurrence interval analyses

Table 1A2. Middle Fork Flathead River peak annual flow flood frequency analysis. (USGS gage number 12358500: M F Flathead River near West Glacier MT). The 2011 peak flow information is bold.

Rank 1940-2011	Date	Q (cfs)	Recurrence interval (RI)	Probability (%)
1	6/9/1964	140000	73	1
2	6/20/1975	63600	37	3
3	5/19/1991	35000	24	4
4	5/20/1954	34500	18	5
5	11/12/1989	33700	15	7
6	5/17/1997	33000	12	8
7	5/23/1948	32600	10	10
8	6/18/1974	31900	9	11
9	5/19/2008	30700	8	12
10	3/2/1972	29600	7	14
11	5/22/1956	28300	7	15
12	5/23/1967	27900	6	16
13	5/27/1961	27100	6	18
14	6/6/1959	25800	5	19
15	**6/8/2011**	**25200**	**5**	**21**
16	6/13/1953	24800	5	22
17	5/5/1957	24200	4	23
18	5/28/1971	23900	4	25
19	5/9/1947	23600	4	26
20	6/6/1950	23600	4	27
21	6/5/1970	23400	3	29
22	6/9/1996	23300	3	30
23	5/11/1976	22600	3	32
24	6/16/2006	22500	3	33
25	5/31/2002	22400	3	34
26	5/27/1979	21600	3	36
27	6/4/1960	21500	3	37
28	6/19/1965	20900	3	38
29	5/26/1982	20800	3	40
30	6/18/1943	20600	2	41
31	5/26/1980	20500	2	42
32	5/26/1999	20400	2	44
33	6/8/1985	20200	2	45
34	5/12/1951	20100	2	47
35	5/15/1993	19900	2	48
36	5/26/2003	19800	2	49

37	5/22/1981	19600	2	51
38	5/14/1949	19500	2	52
39	5/13/1958	19400	2	53
40	5/30/1986	19400	2	55
41	5/31/2009	19100	2	56
42	5/11/1989	19000	2	58
43	5/1/1987	18700	2	59
44	11/8/2006	18700	2	60
45	5/29/1946	18500	2	62
46	5/31/1966	18400	2	63
47	5/31/1984	18200	2	64
48	4/28/1952	18100	2	66
49	6/3/1968	18000	1	67
50	5/18/1973	17900	1	68
51	6/6/1978	17600	1	70
52	6/14/1955	17500	1	71
53	5/27/1983	17400	1	73
54	6/1/1945	16400	1	74
55	5/24/1942	15700	1	75
56	5/23/2000	15300	1	77
57	5/13/1994	15200	1	78
58	6/7/1995	14900	1	79
59	5/19/2010	14300	1	81
60	5/15/1969	14200	1	82
61	5/20/1962	13900	1	84
62	5/13/1988	13100	1	85
63	5/1/1992	13000	1	86
64	5/26/2001	13000	1	88
65	5/12/1940	12800	1	89
66	5/27/1998	12800	1	90
67	6/4/2005	12800	1	92
68	5/31/1963	12700	1	93
69	5/20/1944	11300	1	95
70	5/5/2004	11100	1	96
71	5/11/1977	10400	1	97
72	5/14/1941	7620	1	99

Table 1A3. North Fork Flathead River peak annual flow flood frequency analysis. (USGS gage number 12355500: N F Flathead River nr Columbia Falls MT). The 2011 peak flow information is bold.

Rank 1911-2011	Date	Q (cfs)	Recurrence interval (RI)	Probability (%)
1	6/9/1964	69100	91	1
2	6/7/1995	59200	46	2

3	6/18/1974	34300	30	3
4	5/21/1954	31500	23	4
5	6/2/1972	31400	18	5
6	6/21/1975	30700	15	7
7	6/20/1916	30100	13	8
8	5/28/1961	29900	11	9
9	5/22/1956	29700	10	10
10	5/17/1997	29300	9	11
11	5/24/1948	26400	8	12
12	6/9/1996	26400	8	13
13	5/23/1967	26000	7	14
14	5/20/1991	25800	7	15
15	6/17/1917	25400	6	16
16	6/6/1959	25200	6	18
17	6/17/1933	24400	5	19
18	5/11/1976	24200	5	20
19	5/28/1938	24000	5	21
20	6/2/1913	23800	5	22
21	6/14/1953	23800	4	23
22	5/19/2008	23600	4	24
23	5/10/1947	23500	4	25
24	6/19/1965	23300	4	26
25	5/7/1957	23000	4	27
26	5/29/1986	22900	4	29
27	5/31/2002	22600	3	30
28	5/28/1971	22200	3	31
29	5/29/1946	22000	3	32
30	5/20/2006	21600	3	33
31	5/23/1932	21200	3	34
32	**6/8/2011**	**21100**	**3**	**35**
33	6/23/1950	21000	3	36
34	5/24/1935	20800	3	37
35	5/12/1951	20800	3	38
36	6/4/1960	20700	3	40
37	5/26/1999	20500	2	41
38	5/13/1958	20400	2	42
39	5/24/1929	20300	2	43
40	5/27/1983	20000	2	44
41	5/14/1949	19900	2	45
42	5/26/1982	19900	2	46
43	6/1/1966	19500	2	47
44	4/26/1934	19400	2	48
45	6/1/1990	19300	2	49

46	11/8/2006	19200	2	51
47	5/16/1936	19000	2	52
48	6/14/1955	18700	2	53
49	5/15/1993	18700	2	54
50	5/18/1973	18600	2	55
51	5/27/1979	18600	2	56
52	5/25/1985	18600	2	57
53	5/2/1987	18600	2	58
54	5/27/1970	18400	2	59
55	5/26/1980	18400	2	60
56	4/28/1952	18100	2	62
57	5/27/1942	18000	2	63
58	6/6/1978	18000	2	64
59	5/23/1981	18000	2	65
60	5/14/1969	17600	2	66
61	6/4/1968	17500	1	67
62	5/31/2009	16900	1	68
63	5/30/2003	16800	1	69
64	5/10/1989	16500	1	70
65	5/23/2000	16500	1	71
66	5/28/1998	16400	1	73
67	6/2/1945	15400	1	74
68	5/31/1984	15400	1	75
69	5/28/1943	15300	1	76
70	6/14/1911	15100	1	77
71	5/17/1931	15000	1	78
72	5/13/1994	14300	1	79
73	5/29/1962	14200	1	80
74	6/8/2005	14200	1	81
75	4/30/1939	14000	1	82
76	5/28/1937	13900	1	84
77	5/12/1940	13900	1	85
78	5/31/1963	13800	1	86
79	6/4/1914	13300	1	87
80	6/22/2010	13200	1	88
81	5/13/1988	12300	1	89
82	5/31/1930	11800	1	90
83	5/17/1912	11700	1	91
84	5/26/2001	11300	1	92
85	5/8/1992	10900	1	93
86	5/5/2004	10700	1	95
87	6/27/1915	8540	1	96
88	5/11/1977	8520	1	97

89	5/3/1941	8010	1	98
90	5/17/1944	7850	1	99

1.A.iii. Study reach textural facies analyses

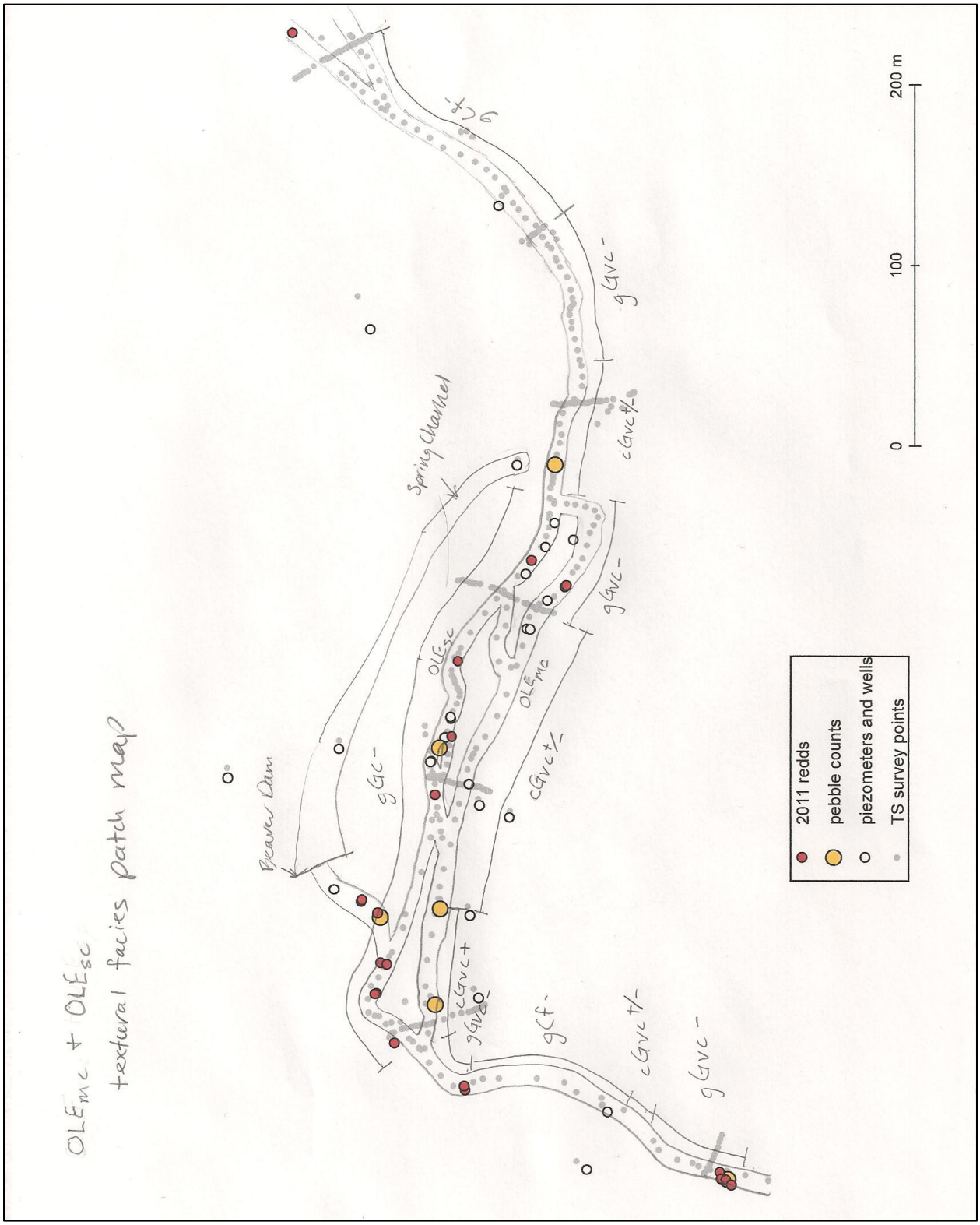

Figure 1A1. OLE_{mc} and OLE_{sc} textural facies patch maps.

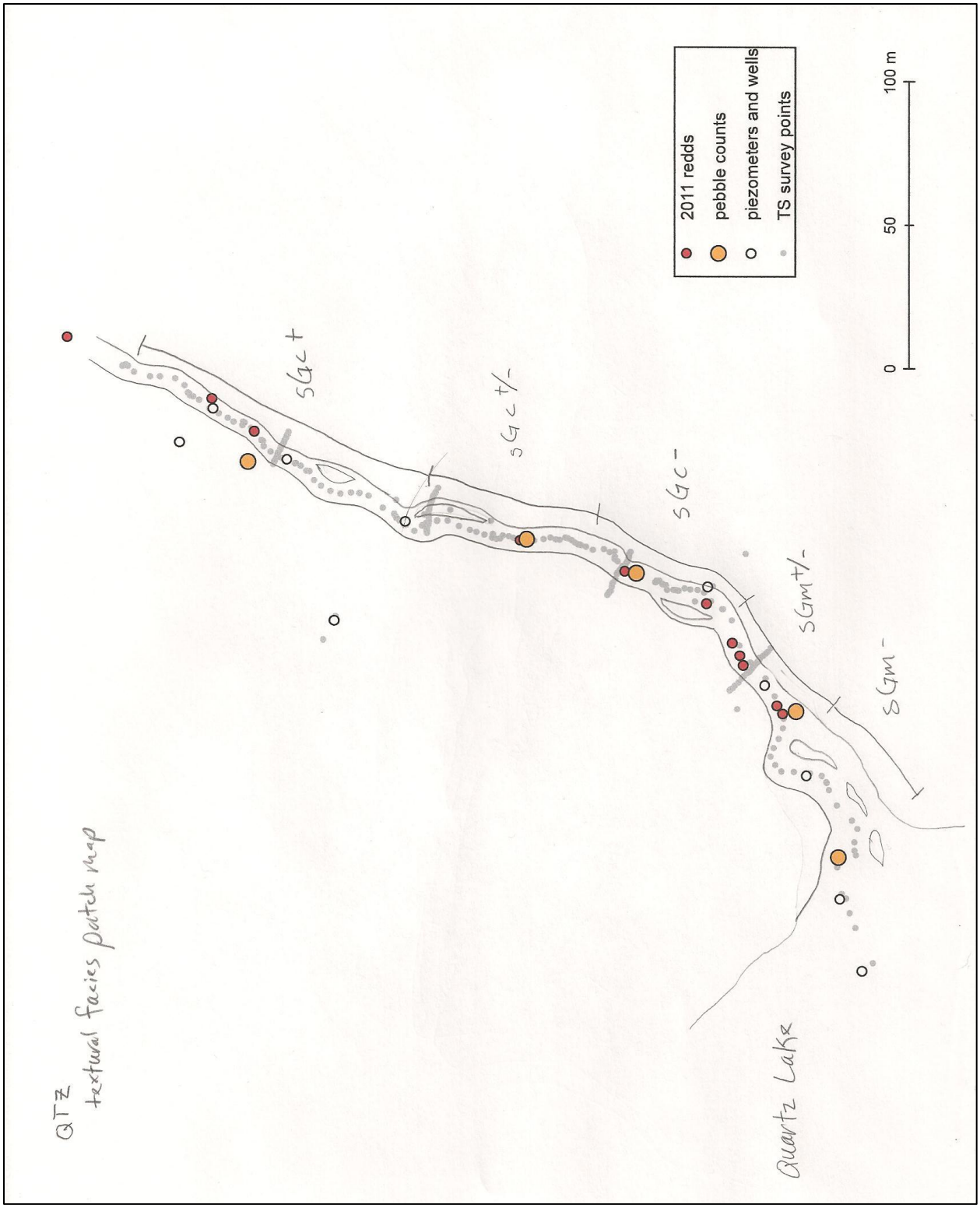

Figure 1A2. QTZ textural facies patch map.

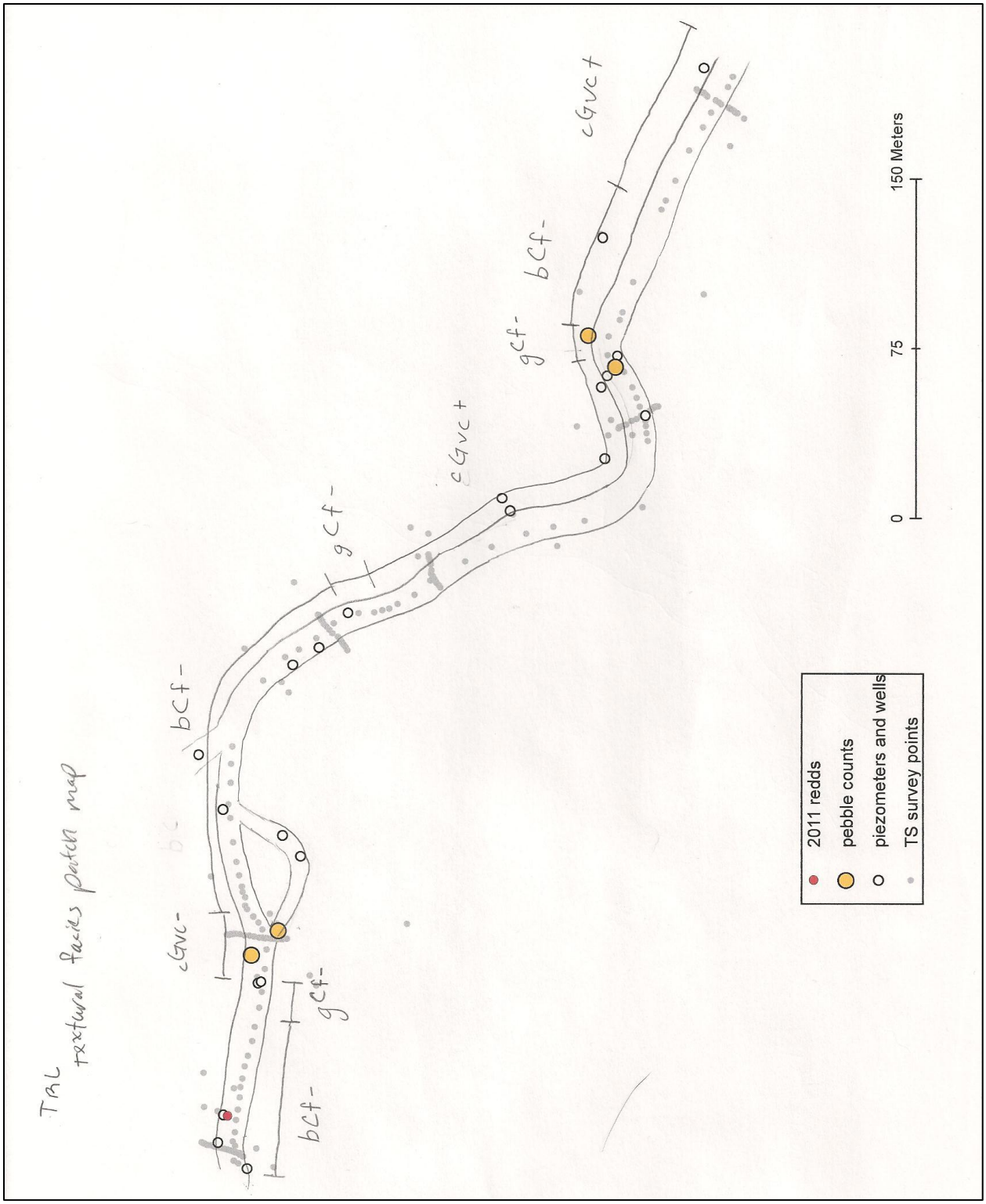

Figure 1A3. TRL textural facies patch map.

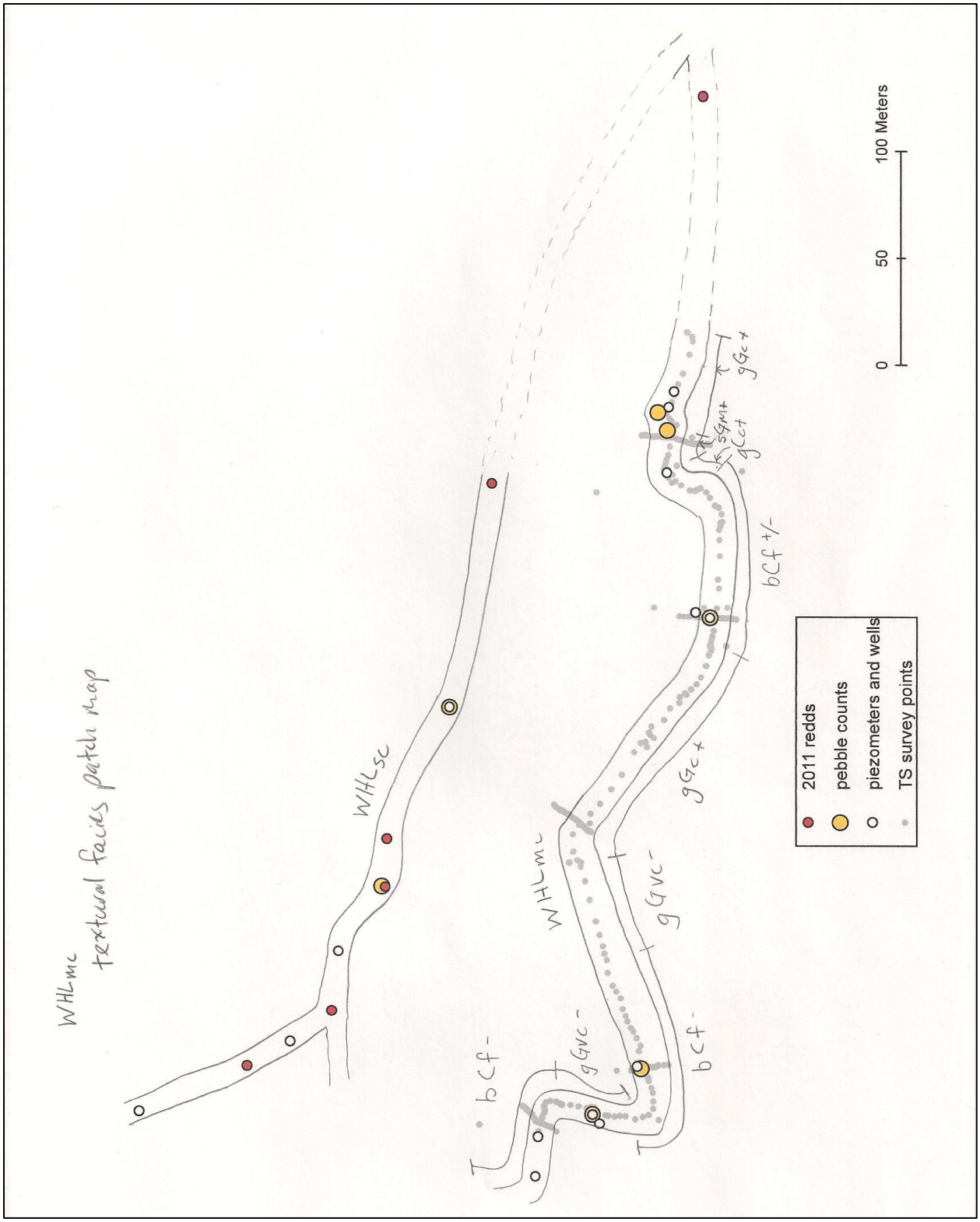

Figure 1A4. WHL_{mc} textural facies patch map.

Table 1A4. Summary of OLE_{mc} and OLE_{sc} patch map textural facies and the pebble count (PC) source of the D_{50} values.

Code[a]	D_{50} (m)	PC name
gCf-	0.064	(inferred)[b]
cGvc+	0.058	pc89
cGvc+/-	0.045	pc51, pc86[c]
gGvc-	0.035	pc101
gGc-	0.018	pc85

[a] Textural facies descriptions are based on the system described by Buffington and Montgomery (1999a). The supplemental +,+/-, and – symbols indicate whether the grain size distribution lies within the coarser, middle, or finer end of the spectrum of the dominant grain size fraction descriptors (e.g. gCf- means gravelly cobble and that the cobbles are near the fine end of the fine cobble spectrum (0.064 m – 0.128 m).

[b] No pebble counts were conducted in the gCf- patches, so I estimated the D_{50} value. I chose 0.064 because the patches appeared to be at the fine end of the cobble spectrum, and 0.064 m is the boundary between cobble and boulder.

[c] The textural facies of both the pc51 (D_{50} = 0.046 m) and pc86 (D_{50} = 0.043 m) pebble counts was cGvc+/-. Therefore, these D_{50} values were averaged to obtain the cGvc+/- D_{50} value.

Table 1A5. OLE_{mc} and OLE_{sc} textural facies and D_{50}s per HEC-RAS subreach channel section.

HEC-RAS		Textural facies		D_{50}	
River Station	τ_{obf} (N/m^2)	OLE_{mc}	OLE_{sc}	OLE_{mc} (m)	OLE_{sc} (m)
7	62.25	gCf-		0.064	
6.875*	58.78	gCf-		0.064	
6.75*	62.55	gCf-		0.064	
6.625*	57.43	gCf-		0.064	
6.5*	68.07	gCf-		0.064	
6.375*	61.06	gCf-		0.064	
6.25*	75.78	gCf-		0.064	
6.125*	45.91	gCf-		0.064	
6	25.73	gCf-		0.064	
5.8*	23.96	gGvc-		0.035	
5.6*	25.18	gGvc-		0.035	
5.4*	29.24	gGvc-		0.035	
5.2*	38.59	gGvc-		0.035	
5	101.87	cGvc+/-		0.045	
4.833*	86.80	cGvc+/-		0.045	
4.666*	65.45	cGvc+/-		0.045	
4.5*	50.35	gGvc-		0.035	
4.333*	42.50	gGvc-	gGc-	0.035	0.018
4.166*	41.61	gGvc-	gGc-	0.035	0.018
4	47.64	gGvc-	gGc-	0.035	0.018
3.833*	44.19	gGvc-	gGc-	0.035	0.018
3.666*	43.53	cGvc+/-	gGc-	0.045	0.018

3.5*	39.55	cGvc+/-	gGc-	0.045	0.018
3.333*	36.36	cGvc+/-	gGc-	0.045	0.018
3.166*	39.23	cGvc+/-	gGc-	0.045	0.018
3	68.07	cGvc+/-	gGc-	0.045	0.018
2.857*	76.98	cGvc+/-	gGc-	0.045	0.018
2.714*	74.30	cGvc+/-	gGc-	0.045	0.018
2.571*	70.50	cGvc+/-	gGc-	0.045	0.018
2.428*	63.35	cGvc+/-	gGc-	0.045	0.018
2.285*	63.46	cGvc+/-	gGc-	0.045	0.018
2.142*	49.35	cGvc+	gGc-	0.058	0.018
2	71.42	cGvc+	gGc-	0.058	0.018
1.888*	77.22	cGvc+	gGc-	0.058	0.018
1.777*	83.60	gGvc-		0.035	
1.666*	89.26	gCf-		0.064	
1.555*	93.37	gCf-		0.064	
1.444*	99.42	gCf-		0.064	
1.333*	103.48	gCf-		0.064	
1.222*	106.20	cGvc+/-		0.045	
1.111*	110.41	gGvc-		0.035	
1	118.85	gGvc-		0.035	

Table 1A6. OLE_{mc} and OLE_{sc} textural facies distribution.

	HEC-RAS subreach sections per textual facies		Ole patch map textural facies				
	OLE_{mc}	OLE_{sc}	Code	D_{16} (m)	D_{50} (m)	D_{84} (m)	PC name
	13	0	gCf-	0.027	0.064	0.118	inferred
	3	0	cGvc+	0.015	0.058	0.112	pcpz89
	14	0	cGvc+/-	0.021	0.045	0.080	avg(pcpz51,pcpz86)
	12	0	gGvc-	0.013	0.035	0.085	pcpz101
	0	17	gGc-	0.004	0.018	0.032	pcpz85
Total X.S.s	42	17					

[a] These sections were coarser than cGvc+. The D_{50} of 0.064 m was selected b/c it is the boundary between gravel and cobble. D_{16} and D_{84} were estimated by taking the largest measured D_{16} and D_{84} and adding the difference in measured D_{50} between gCf- and cGvc+ (0.064 m - 0.058 m).

Table 1A7. Summary of Quartz patch map textural facies and the pebble count source of the D50 values.

Code	D_{50} (m)	PC name
sGc+	0.03	pc42
sGc+/-	0.025	pc25
sGc-	0.016	pc19
sGm+/-	0.011	pc07

Table 1A8. QTZ textural facies and D_{50}s per HEC-RAS subreach channel section.

HEC-RAS		Textural facies	D_{50} (m)
River Station	τ_{obf} (N/m^2)		
4	33.35	sGc+	0.030
3.666*	29.75	sGc+	0.030
3.333*	33.53	sGc+	0.030
3	22.76	sGc+/-	0.025
2.75*	16.44	sGc+/-	0.025
2.5*	12.83	sGc+/-	0.025
2.25*	12.30	sGc-	0.016
2	24.43	sGc-	0.016
1.666*	26.86	sGc-	0.016
1.333*	21.89	sGc-	0.016
1	17.26	sGm+/-	0.011

Table 1A9. QTZ textural facies distribution.

	HECRAS X.S.s	Quartz patch map textural facies				
	per patch	Code	D_{16} (m)	D_{50} (m)	D_{84} (m)	PC name
	3	sGc+	0.010	0.030	0.050	pcpz42
	3	sGc+/-	0.010	0.025	0.040	pcpz25
	4	sGc-	0.005	0.016	0.034	pcpz19
	1	sGm+/-	0.005	0.011	0.031	pcpz07
Total X.S.s	11					

Table 1A10. Summary of Trail patch map textural facies and the pebble count source of the D50 values.

Code	D_{50} (m)	PC name
bCf-	0.09	(inferred)[a]
gCf-	0.075	pc18
cGvc+	0.064	pc2
cGvc-	0.04	pc51

[a] No pebble counts were conducted in the bCf- patches, so I estimated the D50 to be about 0.09 based on field observations and comparisons with the other pebble count D50 values.

Table 1A11. TRL textural facies and D_{50}s per HEC-RAS subreach channel section.

HEC-RAS		Textural facies	D_{50} (m)
River Station	τ_{obf} (N/m^2)		
6	86.95	bCf-	0.090
5.8*	74.43	bCf-	0.090
5.6*	63.17	bCf-	0.090
5.4*	52.90	gCf-	0.075

5.2*	41.38	cGvc-	0.040
5	36.21	cGvc-	0.040
4.857*	41.84	bCf-	0.090
4.714*	50.40	bCf-	0.090
4.571*	57.98	bCf-	0.090
4.428*	69.21	bCf-	0.090
4.285*	78.63	bCf-	0.090
4.142*	90.91	bCf-	0.090
4	94.07	bCf-	0.090
3.666*	90.25	gCf-	0.075
3.333*	84.84	cGvc+	0.064
3	56.85	cGvc+	0.064
2.833*	59.13	cGvc+	0.064
2.666*	59.02	cGvc+	0.064
2.5*	61.55	cGvc+	0.064
2.333*	65.21	cGvc+	0.064
2.166*	68.84	cGvc+	0.064
2	81.24	cGvc+	0.064
1.875*	81.85	gCf-	0.075
1.75*	82.45	bCf-	0.090
1.625*	82.77	bCf-	0.090
1.5*	82.34	bCf-	0.090
1.375*	80.58	bCf-	0.090
1.25*	75.54	cGvc+	0.064
1.125*	65.81	cGvc+	0.064
1	52.47	cGvc+	0.064

Table 1A12. TRL textural facies distribution.

	HECRAS X.S.s	Trail patch map textural facies				
	per patch	Code	D_{16} (m)	D_{50} (m)	D_{84} (m)	PC name
	14	bCf-	0.055	0.090	0.125	inferred[a]
	3	gCf-	0.040	0.075	0.110	pcpz18
	11	cGvc+	0.025	0.064	0.110	pcpz2
	2	cGvc-	0.006	0.040	0.090	pcpz51
Total X.S.s	30					

[a] The grain sizes of this textural facies were estimated based on the other pebble count data. Pebble counts were not conducted in this textural facies because the streambed appeared far to coarse for spawning and in several places the stream was too deep or fast to wade and conduct the pebble counts. The D_{50} was first estimated; then the D_{16} and D_{84} were estimated by taking the coarsest measured D_{16} or D_{84} and adding the difference in D_{50} between bCf- and gCf- (0.09 m - 0.075 m).

Table 1A13. Summary of Whale patch map textural facies and the pebble count source of the D50 values.

Code	D_{50} (m)	PC name
bCf+/-	0.076	pcpz20

bCf-	0.065	pcxs3
gGvc-	0.035	pcpz36
gGc+	0.027	pcpz09
sGm+	0.016	pcpz19+9m

Table 1A14. WHL_{mc} textural facies and D_{50}s per HEC-RAS subreach channel section.

HEC-RAS		Textural facies	D_{50} (m)
River Station	τ_{obf} (N/m^2)		
5	40.48	bCf-	0.065
4.666*	36.15	gGvc-	0.035
4.333*	28.22	bCf-	0.065
4	17.42	bCf-	0.065
3.833*	15.55	bCf-	0.065
3.666*	14.05	gGvc-	0.035
3.5*	12.85	gGvc-	0.035
3.333*	11.87	gGvc-	0.035
3.166*	11.07	gGc+	0.027
3	10.41	gGc+	0.027
2.833*	12.09	gGc+	0.027
2.666*	14.18	gGc+	0.027
2.5*	17.01	gGc+	0.027
2.333*	19.7	gGc+	0.027
2.166*	25.98	gGc+	0.027
2	62.65	bCf+/-	0.076
1.8*	50.75	bCf+/-	0.076
1.6*	45.77	bCf+/-	0.076
1.4*	31.48	bCf+/-	0.076
1.2*	14.18	gGc+	0.027
1	6.31	sGm+	0.016

Table 1A15. WHLmc and WHLsc textural facies distribution.

	HECRAS X.S.s per patch	Whale patch map textural facies				
		Code	D_{16} (m)	D_{50} (m)	D_{84} (m)	PC name
WHL_{mc}	4	bCf+/-	0.016	0.076	0.119	pcpz20
	4	bCf-	0.020	0.065	0.125	pcxs3
	4	gGvc-	0.008	0.035	0.065	pcpz36
	8	gGc+	0.013	0.027	0.050	pcpz09
	1	sGm+	0.006	0.016	0.029	pcpz09+9m
Total X.S.s	21					
WHL_{sc}	10.5	sGm+ (2)	0.010	0.016	0.028	pc at redd 2/3
	10.5	sGm+ (3)	0.004	0.015	0.030	pzsc16stdns

Total equivalent X.S.s	21

[a] The grain sizes of this textural facies were estimated based on the other pebble count data. Pebble counts were not conducted in this textural facies because the streambed appeared far to coarse for spawning and in several places the stream was too deep or fast to wade and conduct the pebble counts. The D_{50} was first estimated; then the D_{16} and D_{84} were estimated by taking the coarsest measured D_{16} or D_{84} and adding the difference in D_{50} between bCf- and gCf- (0.09 m - 0.075 m).

Each HEC-RAS measured and interpolated cross section was assigned a textural facies; and each textural facies is described by a pebble count. The corresponding D_{16}, D_{50}, and D_{84} of these pebble counts were then assigned to each HEC-RAS cross section and average D_{16}, D_{50}, and D_{84} per study reach were calculated.

Table 1A16. Spatially weighted grain size distributions in each study stream based on textural facies classifications and pebble count data.

	D_{16} (m)	D_{50} (m)	D_{84} (m)
OLE_{mc}	0.020	0.049	0.095
OLE_{sc}	0.004	0.018	0.032
QTZ	0.008	0.022	0.040
TRL	0.039	0.076	0.116
WHL_{mc}	0.014	0.045	0.079
WHL_{sc}	0.007	0.016	0.029

Table 1A17. Study reach wetted channel width estimates at Q_{spawn}. Widths were estimated to the nearest meter from visual observations of the Q_{spawn} profile in HEC-RAS.

River station	OLE_{mc}	OLE_{sc}	QTZ	TRL	WHL_{mc}	
7	17					
6	10			14		
5	10			22	13	
4	9	8	9	15	11	
3	15	6	10	11	14	
2	9	8	7	18	13	
1	10		6	15	16	
	OLE_{mc}	OLE_{sc}	QTZ	TRL	WHL_{mc}	WHL_{sc}
Avg wetted width	11.4	7.3	8.0	15.8	13.4	
Avg wetted width	11	7	8	16	13	6[a]

[a] Visual field estimate.

1.A.iv. HEC-RAS

The maximum channel distance between HEC-RAS cross-sections (measured and interpolated) was set to 20 m. Channel roughness values were iterated between 0.024-0.075 until modeled water level was < 10% of measured water level for the spawning discharge. Manning's n values 0.024-0.075 were used because that is the range of channel conditions reported for Western US by Barnes, 1967:http://wwwrcamnl.wr.usgs.gov/sws/fieldmethods/Indirects/nvalues/index.htm).

Overbank roughness values were estimated from Chow (1959) recommended values based on field observations (Table 3-1 in the HEC-RAS help file link). Relative ranking of the study reaches based on wood (tree and brush) roughness from most rough to least rough is Quartz, Whale, Ole, then Trail. Medium to dense brush normally ranges from 0.07 in winter to 0.1 in summer; heavy timber ranges from 0.1 with little undergrowth to 0.12 with flow through low branches (Chow, 1959). Based on this range, and the relative ranking of the streams, overbank roughness for each stream was assigned as follows: Quartz = 0.11; Whale = 0.10; Ole = 0.09; Trail = 0.08. For simplicity and to minimize "hand-waviness", these overbank roughness values were kept constant per cross section in each stream.

For plotting and spatial comparison purposes, distance between the HEC-RAS measured and interpolated cross sections were scaled to match the distances measured by the total station long profile using the following procedure (see the "HECRAS simulation results.xlsx" file for the actual calculations).

1. the long profile distance downstream of each measured cross section was calculated and recorded; if the cross section did not plot on a long profile point, the distance upstream or downstream from the most proximal long profile point was added or subtracted to obtain the appropriate distance downstream of the measured cross section.
2. the distance from one measured cross section to the subsequent downstream cross section was then divided by the number of interpolated cross sections in between yielding the scaled incremental distance from the upstream measured cross section to each of the downstream interpolated cross sections
3. this process was repeated between each of the measured cross sections to obtain distances downstream in the total station long profile of each measured and interpolated cross section.

To scale the HEC-RAS output data to the topographic survey long profile data and relate the HEC-RAS data to true redd locations, I used the following process. In ArcMap 10.0, each cross section was assigned a total station long profile distance downstream based on its location within the long profile data points. The difference between the downstream distance of adjacent cross sections was divided by the number of interpolated cross sections (+1 for the downstream cross section) in order to obtain constant incremental distances downstream between each interpolated cross section. These distances were added consecutively to the downstream distance of the upstream measured cross section. The process was repeated between each set of measured cross sections.

Table 1A18. Summary of HEC-RAS input details for bankfull discharge in each stream.

Study reach	HEC-RAS River Station[a]	Channel length (m)	Cumulative channel length (m)	Channel elevations			Manning's n[e]	
				Min.[b] (m)	LOB[c] (m)	ROB[d] (m)	Main channel	Overbank
OLE_{mc} and OLE_{sc}	7	18.37	0.00	1271.30	1272.33	1272.41	0.040	0.090
	6.875*	18.37	18.37	1270.98	1271.99	1272.08	0.039	0.090
	6.75*	18.37	36.74	1270.65	1271.65	1271.75	0.039	0.090
	6.625*	18.37	55.11	1270.33	1271.31	1271.41	0.038	0.090
	6.5*	18.37	73.48	1270.00	1270.97	1271.08	0.038	0.090
	6.375*	18.37	91.85	1269.68	1270.62	1270.75	0.037	0.090

	6.25*	18.37	110.22	1269.35	1270.28	1270.42	0.036	0.090
	6.125*	18.37	128.59	1269.03	1269.94	1270.08	0.036	0.090
	6	19.57	146.96	1268.70	1269.60	1269.75	0.035	0.090
	5.8*	19.57	166.53	1268.61	1269.54	1269.73	0.042	0.090
	5.6*	19.57	186.10	1268.52	1269.48	1269.71	0.049	0.090
	5.4*	19.57	205.67	1268.42	1269.41	1269.69	0.056	0.090
	5.2*	19.57	225.24	1268.33	1269.35	1269.67	0.063	0.090
	5	19.34	244.81	1268.24	1269.29	1269.65	0.070	0.090
	4.833*	19.34	264.15	1267.97	1269.10	1269.45	0.067	0.090
	4.666*	19.34	283.49	1267.70	1268.91	1269.24	0.063	0.090
	4.5*	19.34	302.83	1267.44	1268.72	1269.04	0.060	0.090
	4.333*	19.34	322.17	1267.17	1268.53	1268.84	0.057	0.090
	4.166*	19.34	341.51	1266.90	1268.34	1268.63	0.053	0.090
	4	17.97	360.85	1266.63	1268.15	1268.43	0.050	0.090
	3.833*	17.97	378.82	1266.53	1267.94	1268.18	0.051	0.090
	3.666*	17.97	396.79	1266.43	1267.73	1267.94	0.052	0.090
	3.5*	17.97	414.76	1266.33	1267.52	1267.69	0.052	0.090
	3.333*	17.97	432.73	1266.22	1267.30	1267.44	0.053	0.090
	3.166*	17.97	450.70	1266.12	1267.09	1267.20	0.054	0.090
	3	19.72	468.67	1266.02	1266.88	1266.95	0.055	0.090
	2.857*	19.72	488.39	1265.75	1266.60	1266.81	0.054	0.090
	2.714*	19.72	508.11	1265.49	1266.32	1266.67	0.052	0.090
	2.571*	19.72	527.83	1265.22	1266.04	1266.53	0.051	0.090
	2.428*	19.72	547.55	1264.95	1265.76	1266.38	0.049	0.090
	2.285*	19.72	567.27	1264.68	1265.48	1266.24	0.048	0.090
	2.142*	19.72	586.99	1264.42	1265.20	1266.10	0.046	0.090
	2	19.24	606.71	1264.15	1264.92	1265.96	0.045	0.090
	1.888*	19.24	625.95	1263.73	1264.52	1265.50	0.048	0.090
	1.777*	19.24	645.19	1263.30	1264.11	1265.04	0.052	0.090
	1.666*	19.24	664.43	1262.88	1263.71	1264.59	0.055	0.090
	1.555*	19.24	683.67	1262.46	1263.31	1264.13	0.058	0.090
	1.444*	19.24	702.91	1262.03	1262.90	1263.67	0.062	0.090
	1.333*	19.24	722.15	1261.61	1262.50	1263.21	0.065	0.090
	1.222*	19.24	741.39	1261.19	1262.10	1262.76	0.068	0.090
	1.111*	19.24	760.63	1260.76	1261.69	1262.30	0.072	0.090
	1		779.87	1260.34	1261.29	1261.84	0.075	0.090
QTZ	4	19.33	0	1356.04	1356.62	1357.16	0.035	0.11
	3.666*	19.33	19.33	1355.78	1356.4	1356.75	0.035	0.11
	3.333*	19.33	38.66	1355.52	1356.18	1356.34	0.035	0.11
	3	17.76	57.99	1355.26	1355.96	1355.93	0.035	0.11
	2.75*	17.76	75.75	1355.16	1355.85	1355.84	0.035	0.11
	2.5*	17.76	93.51	1355.07	1355.74	1355.75	0.035	0.11
	2.25*	17.76	111.27	1354.97	1355.63	1355.65	0.035	0.11
	2	19.21	129.03	1354.87	1355.52	1355.56	0.035	0.11
	1.666*	19.21	148.24	1354.73	1355.33	1355.35	0.031	0.11
	1.333*	19.21	167.45	1354.58	1355.14	1355.13	0.028	0.11
	1		186.66	1354.44	1354.95	1354.92	0.024	0.11
TRL	6	18.99	0	1252.34	1253.32	1253.3	0.075	0.08
	5.8*	18.99	18.99	1252.24	1253.16	1253.17	0.066	0.08
	5.6*	18.99	37.98	1252.14	1253.01	1253.03	0.057	0.08
	5.4*	18.99	56.97	1252.05	1252.85	1252.9	0.048	0.08
	5.2*	18.99	75.96	1251.95	1252.7	1252.76	0.039	0.08
	5	19.56	94.95	1251.85	1252.54	1252.63	0.03	0.08

	4.857*	19.56	114.51	1251.56	1252.31	1252.35	0.036	0.08
	4.714*	19.56	134.07	1251.26	1252.09	1252.07	0.043	0.08
	4.571*	19.56	153.63	1250.97	1251.86	1251.79	0.049	0.08
	4.428*	19.56	173.19	1250.67	1251.64	1251.5	0.056	0.08
	4.285*	19.56	192.75	1250.38	1251.41	1251.22	0.062	0.08
	4.142*	19.56	212.31	1250.08	1251.19	1250.94	0.069	0.08
	4	16.46	231.87	1249.79	1250.96	1250.66	0.075	0.08
	3.666*	16.46	248.33	1249.47	1250.61	1250.48	0.062	0.08
	3.333*	16.46	264.79	1249.15	1250.27	1250.31	0.048	0.08
	3	19.44	281.25	1248.83	1249.92	1250.13	0.035	0.08
	2.833*	19.44	300.69	1248.71	1249.76	1249.95	0.042	0.08
	2.666*	19.44	320.13	1248.58	1249.6	1249.78	0.048	0.08
	2.5*	19.44	339.57	1248.46	1249.44	1249.6	0.055	0.08
	2.333*	19.44	359.01	1248.34	1249.28	1249.42	0.062	0.08
	2.166*	19.44	378.45	1248.21	1249.12	1249.25	0.068	0.08
	2	17.91	397.89	1248.09	1248.96	1249.07	0.075	0.08
	1.875*	17.91	415.8	1247.88	1248.75	1248.88	0.075	0.08
	1.75*	17.91	433.71	1247.66	1248.53	1248.68	0.075	0.08
	1.625*	17.91	451.62	1247.45	1248.32	1248.49	0.075	0.08
	1.5*	17.91	469.53	1247.23	1248.1	1248.3	0.075	0.08
	1.375*	17.91	487.44	1247.02	1247.89	1248.1	0.075	0.08
	1.25*	17.91	505.35	1246.8	1247.67	1247.91	0.075	0.08
	1.125*	17.91	523.26	1246.59	1247.46	1247.71	0.075	0.08
	1		541.17	1246.37	1247.24	1247.52	0.075	0.08
WHL_{mc}	5	18.38	0	1277.74	1278.62	1278.85	0.035	0.1
	4.666*	18.38	18.38	1277.65	1278.54	1278.86	0.031	0.1
	4.333*	18.38	36.76	1277.56	1278.47	1278.87	0.028	0.1
	4	19.65	55.14	1277.47	1278.39	1278.88	0.024	0.1
	3.833*	19.65	74.79	1277.42	1278.38	1278.79	0.024	0.1
	3.666*	19.65	94.44	1277.37	1278.36	1278.69	0.024	0.1
	3.5*	19.65	114.09	1277.33	1278.35	1278.6	0.024	0.1
	3.333*	19.65	133.74	1277.28	1278.33	1278.51	0.024	0.1
	3.166*	19.65	153.39	1277.23	1278.32	1278.41	0.024	0.1
	3	19.25	173.04	1277.18	1278.3	1278.32	0.024	0.1
	2.833*	19.25	192.29	1277.16	1278.18	1278.24	0.026	0.1
	2.666*	19.25	211.54	1277.13	1278.06	1278.15	0.028	0.1
	2.5*	19.25	230.79	1277.11	1277.94	1278.07	0.03	0.1
	2.333*	19.25	250.04	1277.09	1277.81	1277.98	0.031	0.1
	2.166*	19.25	269.29	1277.06	1277.69	1277.9	0.033	0.1
	2	17.42	288.54	1277.04	1277.57	1277.81	0.035	0.1
	1.8*	17.42	305.96	1276.85	1277.48	1277.72	0.033	0.1
	1.6*	17.42	323.38	1276.67	1277.39	1277.63	0.031	0.1
	1.4*	17.42	340.8	1276.48	1277.3	1277.54	0.028	0.1
	1.2*	17.42	358.22	1276.3	1277.21	1277.45	0.026	0.1
	1		375.64	1276.11	1277.12	1277.36	0.024	0.1

[a] An asterisk (*) indicates an interpolated cross-section; no * indicates a measured cross-section.
[b] Minimum channel elevation.
[c] Left overbank station elevation.
[d] Right overbank station elevation.
[e] See text above for a description of the channel and overbank roughness designations.

Table 1A19. Summary of HEC-RAS output for bankfull discharge in each stream.

Study Reach	River station	Ch. shear stress (N/m^2)	Energy grade slope	Flow velocity (m/s)	Max. flow depth (m)	Top width (m)	Flow area (m^2)	Froude # Ch.
OLE_{mc}	7	62.25	1.55%	1.72	0.54	20.01	8.33	0.85
and	6.875*	58.78	1.41%	1.72	0.59	19.19	8.31	0.84
OLE_{sc}	6.75*	62.55	1.61%	1.75	0.64	20.23	8.15	0.88
	6.625*	57.43	1.49%	1.72	0.68	20.81	8.30	0.87
	6.5*	68.07	1.76%	1.88	0.68	19.00	7.62	0.95
	6.375*	61.06	1.39%	1.87	0.71	16.81	7.67	0.88
	6.25*	75.78	1.69%	2.14	0.70	14.29	6.67	1.00
	6.125*	45.91	0.76%	1.75	0.87	12.67	8.15	0.70
	6	25.73	0.30%	1.43	1.15	14.45	10.21	0.48
	5.8*	23.96	0.27%	1.16	1.21	20.69	13.02	0.38
	5.6*	25.18	0.29%	1.01	1.26	27.49	15.34	0.34
	5.4*	29.24	0.36%	0.94	1.30	33.57	16.86	0.33
	5.2*	38.59	0.55%	0.94	1.31	34.66	16.95	0.35
	5	101.87	2.20%	1.28	1.16	28.87	11.94	0.59
	4.833*	86.80	1.81%	1.25	1.05	24.81	11.74	0.56
	4.666*	65.45	1.30%	1.16	1.03	24.89	12.41	0.51
	4.5*	50.35	1.00%	1.07	1.08	25.62	13.38	0.47
	4.333*	42.50	0.87%	1.03	1.17	27.34	13.91	0.46
	4.166*	41.61	0.93%	1.08	1.26	28.09	13.25	0.50
	4	47.64	0.91%	1.26	1.33	20.27	11.39	0.53
	3.833*	44.19	1.08%	1.14	1.26	29.39	12.58	0.55
	3.666*	43.53	1.09%	1.10	1.17	31.34	12.97	0.55
	3.5*	39.55	0.96%	1.06	1.09	33.17	13.63	0.52
	3.333*	36.36	0.75%	1.02	1.05	30.23	14.42	0.46
	3.166*	39.23	0.71%	1.07	1.02	32.17	14.90	0.45
	3	68.07	1.35%	1.36	0.92	28.81	12.73	0.60
	2.857*	76.98	1.54%	1.47	0.88	23.67	10.57	0.65
	2.714*	74.30	1.55%	1.49	0.83	21.27	9.82	0.67
	2.571*	70.50	1.54%	1.46	0.80	20.65	9.76	0.68
	2.428*	63.35	1.44%	1.44	0.77	21.95	9.96	0.68
	2.285*	63.46	1.54%	1.45	0.75	23.22	9.86	0.71
	2.142*	49.35	1.19%	1.34	0.75	44.37	11.51	0.65
	2	71.42	2.15%	1.58	0.68	48.50	10.04	0.86
	1.888*	77.22	2.13%	1.57	0.69	37.16	9.46	0.82
	1.777*	83.60	2.12%	1.53	0.72	31.40	9.54	0.76
	1.666*	89.26	2.09%	1.51	0.74	27.44	9.55	0.73
	1.555*	93.37	2.02%	1.48	0.77	25.03	9.70	0.69
	1.444*	99.42	1.98%	1.45	0.82	24.00	9.94	0.64

	1.333*	103.48	1.92%	1.43	0.86	23.58	10.16	0.61
	1.222*	106.20	1.82%	1.40	0.93	23.24	10.49	0.58
	1.111*	110.41	1.74%	1.37	1.02	22.88	10.93	0.54
	1	118.85	1.77%	1.38	1.10	20.31	10.96	0.52
QTZ	4	33.35	1.22%	1.35	0.57	14.28	3.14	0.79
	3.666*	29.75	1.11%	1.27	0.62	12.72	3.25	0.76
	3.333*	33.53	1.39%	1.32	0.63	12.12	3.10	0.84
	3	22.76	0.86%	1.11	0.70	13.27	3.71	0.67
	2.75*	16.44	0.56%	0.96	0.69	14.00	4.28	0.55
	2.5*	12.83	0.40%	0.86	0.70	16.19	4.81	0.48
	2.25*	12.30	0.40%	0.84	0.73	20.70	5.09	0.47
	2	24.43	0.93%	1.15	0.69	16.93	3.69	0.69
	1.666*	26.86	1.14%	1.33	0.61	12.55	3.08	0.86
	1.333*	21.89	0.72%	1.39	0.58	9.37	2.95	0.79
	1	17.26	0.41%	1.52	0.60	6.37	2.72	0.72
TRL	6	86.95	1.13%	1.21	1.05	16.46	13.19	0.43
	5.8*	74.43	1.08%	1.24	0.93	17.79	12.78	0.47
	5.6*	63.17	1.03%	1.30	0.82	19.11	12.20	0.52
	5.4*	52.90	0.98%	1.39	0.71	20.48	11.47	0.59
	5.2*	41.38	0.87%	1.48	0.62	21.90	10.76	0.67
	5	36.21	0.94%	1.73	0.51	23.24	9.18	0.88
	4.857*	41.84	0.97%	1.58	0.63	22.62	10.05	0.76
	4.714*	50.40	1.06%	1.48	0.74	21.86	10.75	0.67
	4.571*	57.98	1.12%	1.41	0.82	21.04	11.27	0.62
	4.428*	69.21	1.24%	1.37	0.90	20.20	11.64	0.57
	4.285*	78.63	1.31%	1.33	0.94	19.34	11.95	0.54
	4.142*	90.91	1.41%	1.30	0.98	18.47	12.24	0.51
	4	94.07	1.34%	1.24	1.01	17.65	12.89	0.46
	3.666*	90.25	1.36%	1.45	1.07	15.75	10.97	0.55
	3.333*	84.84	1.40%	1.79	1.10	13.79	8.89	0.71
	3	56.85	0.93%	2.01	1.19	12.13	7.91	0.79
	2.833*	59.13	0.90%	1.73	1.17	13.27	9.20	0.66
	2.666*	59.02	0.85%	1.52	1.15	14.44	10.43	0.57
	2.5*	61.55	0.86%	1.37	1.12	15.63	11.64	0.50
	2.333*	65.21	0.89%	1.25	1.08	16.80	12.70	0.46
	2.166*	68.84	0.94%	1.17	1.04	17.95	13.56	0.43
	2	81.24	1.15%	1.15	0.96	19.00	13.85	0.43
	1.875*	81.85	1.15%	1.15	0.97	18.76	13.77	0.43
	1.75*	82.45	1.15%	1.16	0.98	18.51	13.70	0.43
	1.625*	82.77	1.14%	1.17	0.99	18.28	13.65	0.43
	1.5*	82.34	1.12%	1.16	1.01	18.06	13.66	0.43
	1.375*	80.58	1.07%	1.16	1.02	17.87	13.77	0.42

	1.25*	75.54	0.97%	1.13	1.06	17.74	14.14	0.40
	1.125*	65.81	0.79%	1.06	1.12	17.80	15.01	0.37
	1	52.47	0.57%	0.97	1.22	19.29	16.62	0.31
WHL_{mc}	5	40.48	0.72%	1.67	0.96	15.63	9.13	0.68
	4.666*	36.15	0.64%	1.79	0.91	14.36	8.43	0.73
	4.333*	28.22	0.46%	1.77	0.90	12.95	8.48	0.69
	4	17.42	0.26%	1.65	0.94	12.03	9.08	0.61
	3.833*	15.55	0.23%	1.56	0.96	12.98	9.62	0.58
	3.666*	14.05	0.21%	1.48	0.97	13.96	10.13	0.55
	3.5*	12.85	0.19%	1.41	0.98	14.93	10.62	0.53
	3.333*	11.87	0.18%	1.35	1.00	15.90	11.07	0.52
	3.166*	11.07	0.17%	1.30	1.02	16.85	11.50	0.50
	3	10.41	0.17%	1.26	1.04	17.79	11.90	0.49
	2.833*	12.09	0.19%	1.26	1.02	17.45	11.89	0.49
	2.666*	14.18	0.21%	1.28	1.01	17.87	11.81	0.48
	2.5*	17.01	0.25%	1.31	0.98	17.43	11.58	0.49
	2.333*	19.70	0.29%	1.36	0.95	16.74	11.14	0.51
	2.166*	25.98	0.38%	1.47	0.90	15.88	10.39	0.56
	2	62.65	1.23%	2.05	0.68	14.26	7.36	0.90
	1.8*	50.75	1.09%	1.93	0.69	16.26	7.79	0.88
	1.6*	45.77	1.08%	1.92	0.68	17.67	7.83	0.92
	1.4*	31.48	0.77%	1.75	0.73	19.78	8.57	0.85
	1.2*	14.18	0.29%	1.30	0.88	22.18	11.53	0.58
	1	6.31	0.11%	0.97	1.07	25.44	15.52	0.39

Table 1A20. Bankfull and bankfull adjusted Shields stress compilation. Red numbers in the HEC-RAS river station column indicate that that subreach channel section hosted one or more 2011 bull trout redds.

Study reach	HEC-RAS river station	Textural facies D_{50} (m)	HEC-RAS Q_{bf} output					
			Slope	U (m/s)	τ_{obf} (N/m^2)	τ'_{bf} (N/m^2)	τ^*_{bf}	τ^{**}_{bf}
OLE_{mc}	7	0.064	1.55%	1.72	62.25	40.5	0.060	0.039
	6.875*	0.064	1.41%	1.72	58.78	39.6	0.057	0.038
	6.75*	0.064	1.61%	1.75	62.55	42.0	0.060	0.041
	6.625*	0.064	1.49%	1.72	57.43	40.1	0.055	0.039
	6.5*	0.064	1.76%	1.88	68.07	47.8	0.066	0.046
	6.375*	0.064	1.39%	1.87	61.06	44.7	0.059	0.043
	6.25*	0.064	1.69%	2.14	75.78	57.5	0.073	0.056
	6.125*	0.064	0.76%	1.75	45.91	34.8	0.044	0.034
	6	0.064	0.30%	1.43	25.73	20.5	0.025	0.020
	5.8*	0.035	0.27%	1.16	23.96	12.5	0.042	0.022
	5.6*	0.035	0.29%	1.01	25.18	10.3	0.044	0.018

	5.4*	0.035	0.36%	0.94	29.24	9.8	0.052	0.017
	5.2*	0.035	0.55%	0.94	38.59	10.8	0.068	0.019
	5	0.045	2.20%	1.28	101.87	26.0	0.140	0.036
	4.833*	0.045	1.81%	1.25	86.80	23.9	0.119	0.033
	4.666*	0.045	1.30%	1.16	65.45	19.7	0.090	0.027
	4.5*	0.035	1.00%	1.07	50.35	15.3	0.089	0.027
	4.333*	0.035	0.87%	1.03	42.50	14.0	0.075	0.025
	4.166*	0.035	0.93%	1.08	41.61	15.2	0.074	0.027
	4	0.035	0.91%	1.26	47.64	19.1	0.084	0.034
	3.833*	0.035	1.08%	1.14	44.19	17.2	0.078	0.030
	3.666*	0.045	1.09%	1.10	43.53	17.4	0.060	0.024
	3.5*	0.045	0.96%	1.06	39.55	15.9	0.054	0.022
	3.333*	0.045	0.75%	1.02	36.36	14.1	0.050	0.019
	3.166*	0.045	0.71%	1.07	39.23	15.0	0.054	0.021
	3	0.045	1.35%	1.36	68.07	25.2	0.094	0.035
	2.857*	0.045	1.54%	1.47	76.98	29.3	0.106	0.040
	2.714*	0.045	1.55%	1.49	74.30	29.9	0.102	0.041
	2.571*	0.045	1.54%	1.46	70.50	29.0	0.097	0.040
	2.428*	0.045	1.44%	1.44	63.35	27.9	0.087	0.038
	2.285*	0.045	1.54%	1.45	63.46	28.7	0.087	0.039
	2.142*	0.058	1.19%	1.34	49.35	25.4	0.053	0.027
	2	0.058	2.15%	1.58	71.42	37.8	0.076	0.040
	1.888*	0.058	2.13%	1.57	77.22	37.3	0.082	0.040
	1.777*	0.035	2.12%	1.53	83.60	31.6	0.148	0.056
	1.666*	0.064	2.09%	1.51	89.26	35.9	0.086	0.035
	1.555*	0.064	2.02%	1.48	93.37	34.6	0.090	0.033
	1.444*	0.064	1.98%	1.45	99.42	33.3	0.096	0.032
	1.333*	0.064	1.92%	1.43	103.48	32.4	0.100	0.031
	1.222*	0.045	1.82%	1.40	106.20	28.4	0.146	0.039
	1.111*	0.035	1.74%	1.37	110.41	25.5	0.195	0.045
	1	0.035	1.77%	1.38	118.85	25.9	0.210	0.046
OLE_{sc}	4.166*	0.018	0.93%	1.08	41.61	12.9	0.143	0.044
	4	0.018	0.91%	1.26	47.64	16.2	0.164	0.056
	3.833*	0.018	1.08%	1.14	44.19	14.6	0.152	0.050
	3.666*	0.018	1.09%	1.10	43.53	13.8	0.150	0.048
	3.5*	0.018	0.96%	1.06	39.55	12.7	0.136	0.044
	3.333*	0.018	0.75%	1.02	36.36	11.2	0.125	0.039
	3.166*	0.018	0.71%	1.07	39.23	11.9	0.135	0.041
	3	0.018	1.35%	1.36	68.07	20.0	0.234	0.069

	2.857*	0.018	1.54%	1.47	76.98	23.3	0.264	0.080
	2.714*	0.018	1.55%	1.49	74.30	23.8	0.255	0.082
	2.571*	0.018	1.54%	1.46	70.50	23.0	0.242	0.079
	2.428*	0.018	1.44%	1.44	63.35	22.2	0.218	0.076
	2.285*	0.018	1.54%	1.45	63.46	22.8	0.218	0.078
	2.142*	0.018	1.19%	1.34	49.35	19.0	0.170	0.065
	2	0.018	2.15%	1.58	71.42	28.2	0.245	0.097
	1.888*	0.018	2.13%	1.57	77.22	27.9	0.265	0.096
QTZ	4	0.030	1.22%	1.35	33.35	22.0	0.069	0.045
	3.666*	0.030	1.11%	1.27	29.75	19.6	0.061	0.040
	3.333*	0.030	1.39%	1.32	33.53	21.9	0.069	0.045
	3	0.025	0.86%	1.11	22.76	14.3	0.056	0.035
	2.75*	0.025	0.56%	0.96	16.44	10.3	0.041	0.026
	2.5*	0.025	0.40%	0.86	12.83	8.1	0.032	0.020
	2.25*	0.016	0.40%	0.84	12.30	7.0	0.048	0.027
	2	0.016	0.93%	1.15	24.43	13.8	0.094	0.053
	1.666*	0.016	1.14%	1.33	26.86	18.0	0.104	0.070
	1.333*	0.016	0.72%	1.39	21.89	17.2	0.085	0.066
	1	0.011	0.41%	1.52	17.26	15.5	0.097	0.087
TRL	6	0.090	1.13%	1.21	86.95	24.0	0.060	0.017
	5.8*	0.090	1.08%	1.24	74.43	24.7	0.051	0.017
	5.6*	0.090	1.03%	1.30	63.17	26.2	0.043	0.018
	5.4*	0.075	0.98%	1.39	52.90	27.3	0.044	0.022
	5.2*	0.040	0.87%	1.48	41.38	24.9	0.064	0.038
	5	0.040	0.94%	1.73	36.21	32.1	0.056	0.050
	4.857*	0.090	0.97%	1.58	41.84	34.5	0.029	0.024
	4.714*	0.090	1.06%	1.48	50.40	32.0	0.035	0.022
	4.571*	0.090	1.12%	1.41	57.98	30.2	0.040	0.021
	4.428*	0.090	1.24%	1.37	69.21	29.7	0.048	0.020
	4.285*	0.090	1.31%	1.33	78.63	28.8	0.054	0.020
	4.142*	0.090	1.41%	1.30	90.91	28.3	0.062	0.019
	4	0.090	1.34%	1.24	94.07	26.0	0.065	0.018
	3.666*	0.075	1.36%	1.45	90.25	31.6	0.074	0.026
	3.333*	0.064	1.40%	1.79	84.84	42.0	0.082	0.041
	3	0.064	0.93%	2.01	56.85	45.0	0.055	0.044
	2.833*	0.064	0.90%	1.73	59.13	35.7	0.057	0.034
	2.666*	0.064	0.85%	1.52	59.02	29.0	0.057	0.028
	2.5*	0.064	0.86%	1.37	61.55	24.8	0.059	0.024
	2.333*	0.064	0.89%	1.25	65.21	21.9	0.063	0.021

	2.166*	0.064	0.94%	1.17	68.84	20.1	0.067	0.019
	2	0.064	1.15%	1.15	81.24	20.6	0.079	0.020
	1.875*	0.075	1.15%	1.15	81.85	21.4	0.067	0.018
	1.75*	0.090	1.15%	1.16	82.45	22.7	0.057	0.016
	1.625*	0.090	1.14%	1.17	82.77	22.9	0.057	0.016
	1.5*	0.090	1.12%	1.16	82.34	22.5	0.057	0.015
	1.375*	0.090	1.07%	1.16	80.58	22.3	0.055	0.015
	1.25*	0.064	0.97%	1.13	75.54	19.2	0.073	0.019
	1.125*	0.064	0.79%	1.06	65.81	16.6	0.064	0.016
	1	0.064	0.57%	0.97	52.47	13.4	0.051	0.013
WHL_{mc}	5	0.065	0.72%	1.67	40.48	32.1	0.039	0.031
	4.666*	0.035	0.64%	1.79	36.15	29.6	0.064	0.052
	4.333*	0.065	0.46%	1.77	28.22	31.4	0.027	0.030
	4	0.065	0.26%	1.65	17.42	24.4	0.017	0.023
	3.833*	0.065	0.23%	1.56	15.55	21.8	0.015	0.021
	3.666*	0.035	0.21%	1.48	14.05	16.9	0.025	0.030
	3.5*	0.035	0.19%	1.41	12.85	15.4	0.023	0.027
	3.333*	0.035	0.18%	1.35	11.87	14.2	0.021	0.025
	3.166*	0.027	0.17%	1.30	11.07	12.4	0.025	0.028
	3	0.027	0.17%	1.26	10.41	11.7	0.024	0.027
	2.833*	0.027	0.19%	1.26	12.09	12.0	0.028	0.028
	2.666*	0.027	0.21%	1.28	14.18	12.7	0.032	0.029
	2.5*	0.027	0.25%	1.31	17.01	13.7	0.039	0.031
	2.333*	0.027	0.29%	1.36	19.70	15.0	0.045	0.034
	2.166*	0.027	0.38%	1.47	25.98	18.2	0.060	0.042
	2	0.076	1.23%	2.05	62.65	51.9	0.051	0.042
	1.8*	0.076	1.09%	1.93	50.75	46.0	0.041	0.037
	1.6*	0.076	1.08%	1.92	45.77	45.6	0.037	0.037
	1.4*	0.076	0.77%	1.75	31.48	36.4	0.026	0.030
	1.2*	0.027	0.29%	1.30	14.18	14.1	0.032	0.032
	1	0.016	0.11%	0.97	6.31	6.3	0.024	0.024

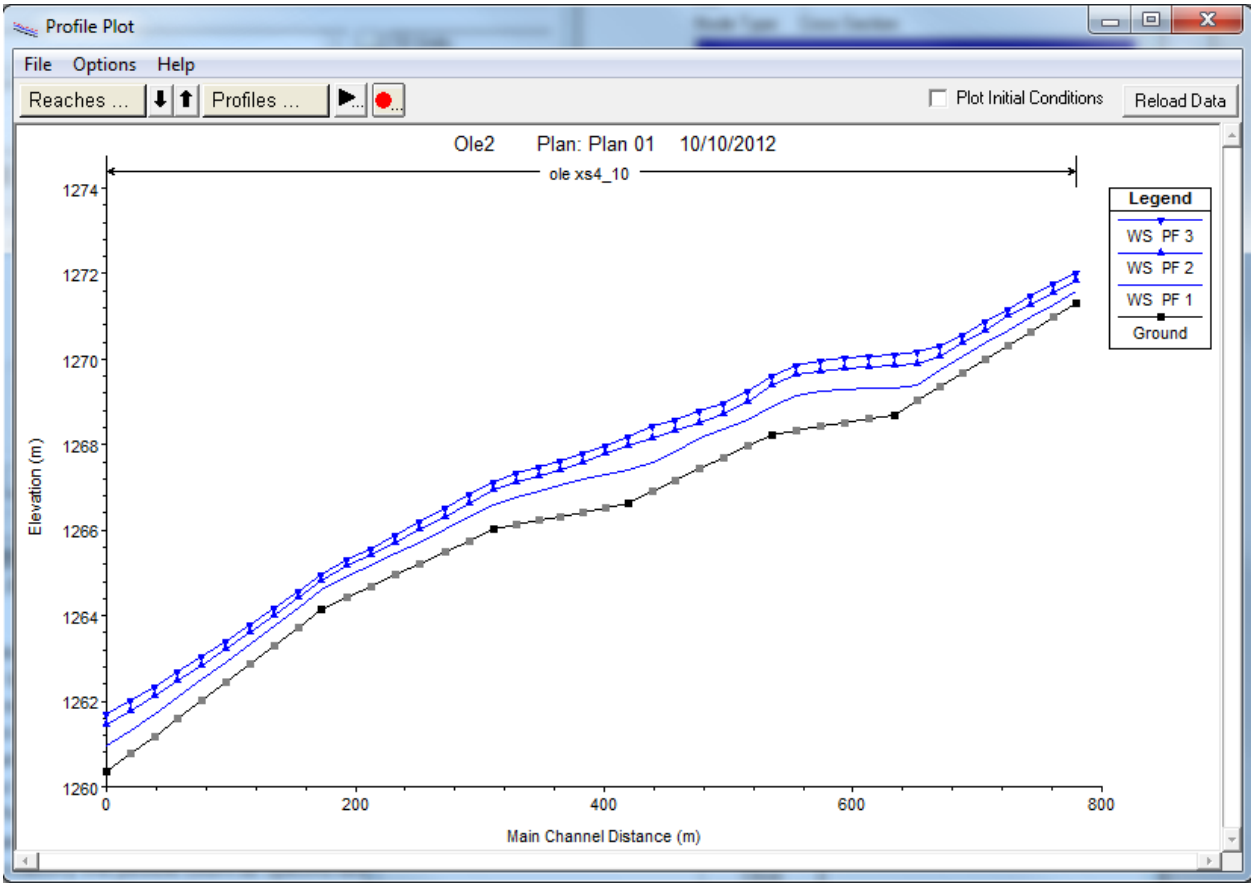

Figure 1A5. OLE_{mc} and OLE_{sc} HEC-RAS modeled water surface profiles.

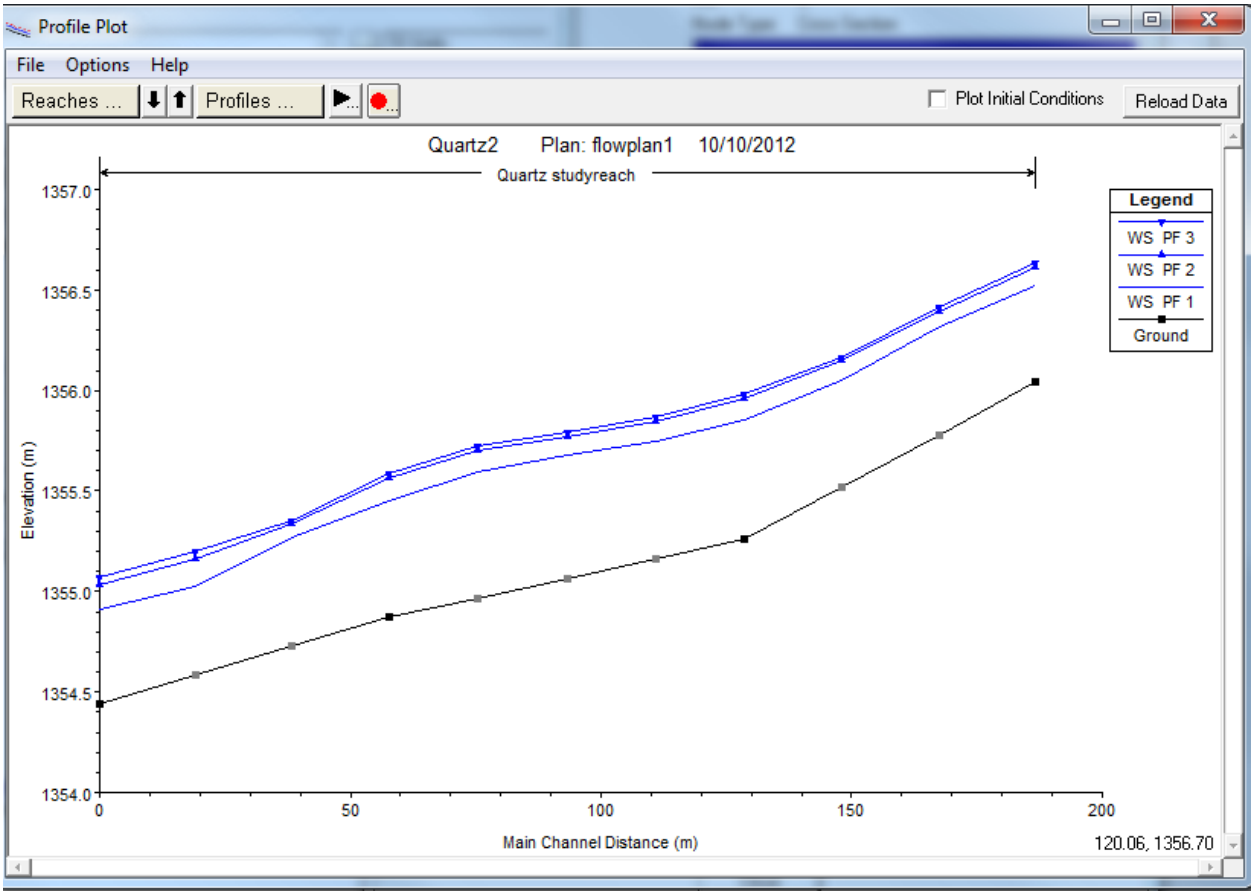

Figure 1A6. QTZ HEC-RAS modeled water surface profiles.

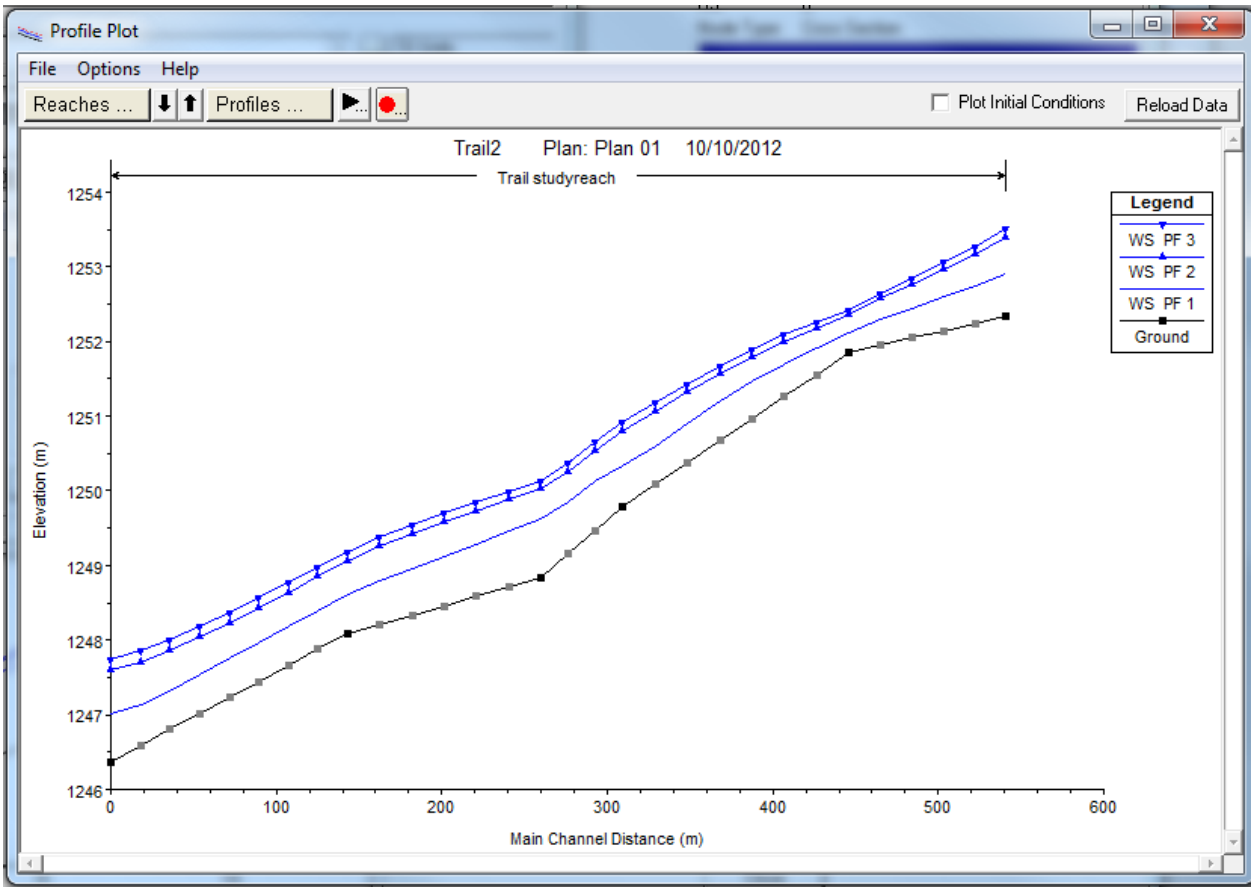

Figure 1A7. TRL HEC-RAS modeled water surface profiles.

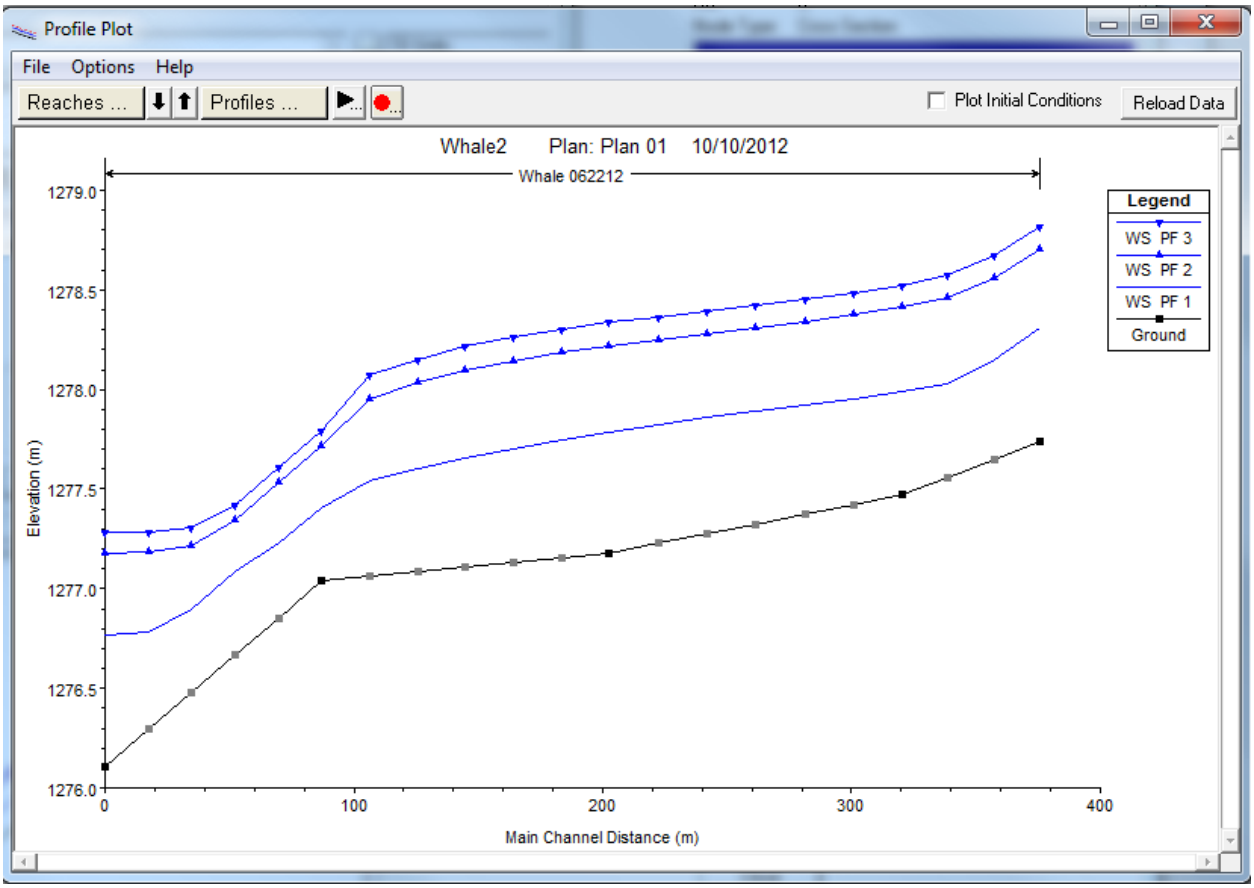

Figure 1A8. WHL_{mc} HEC-RAS modeled water surface profiles.

APPENDIX 1B: Reach-scale hydrogeology

1.B.i. Slug tests

Falling head slug tests were conducted by introducing a slug of 100 ml of water and measuring the water level change in 1 second or 0.5 second increments with a Solinst Levelogger Gold (Model 3001). Every effort was made to introduce the slug instantaneously as recommended by Butler (1998). The pre-analysis processing guidelines of Bulter (1998) were followed. Because of non-instantaneous slug introduction, the translation method was utilized (Pandit and Miner, 1986). For almost all data sets, H_o was determined by standard methods of examining the data, then background static water level was determined by averaging the water levels of a 6 s window that ended 4 s prior to the determined peak. The 4 s gap between the data used to calculate static water level and initialization of the test was implemented in order to avoid water level values affected by the initial introduction of the slug of water. Water level deviations for static were then normalized (initial displacement = 1) which Bulter (1998) instructs is essential when dealing with transducer data.

For non-instantaneous slug introduction, estimation of initial head displacement (H_o) and initiation time (t_o) of the test can be difficult to determine. Of the common approaches utilized to estimate H_o and t_o, Butler (1998) reports that the translation method (Pandit and Miner, 1986) is the best approach. However, Butler (1998) notes that, "the translation method is only appropriate when a plot of the logarithm of the response data vs. time is approximately linear. In cases where the response plot has a pronounced concave-upward curvature, the translation method can introduce considerable error into the hydraulic conductivity estimate." In terms of slug test setup and design, Butler (1998) states the following:

1. slug out is better than slug in
2. at least three slug tests should be performed per trial; and the first and last slugs should be the same amount while the middle amount(s) should be a different volume; comparison of the first and last slug tests' data allows for better assessment of well development and potential skin effects.

AquiferTest data analyses

AquiferTest software (Schlumberger 2011) was used to calculate hydraulic conductivity from our slug test data. All slug test piezometers were constructed and installed in similar fashions to similar depths. Therefore, well and aquifer dimension parameters in AquiferTest were made the same for all analyses. This was done to minimize the number of variables in the slug test data analyses. Aquifer thickness (b) was set at 10 m depth for all analyses; however, calculations of K did not appear to be dependent on b because all other variables were held constant, changes in b between 1 m and 100 m had minimal to no effect on the hydraulic conductivity calculation. Piezometers were indicated as partially penetrating an unconfined aquifer of thickness 10 m. Screen and casing radius = 1.5 cm; length of screen = 20 cm; distance from the top of the aquifer to the bottom of the screen = 60 cm (~ average for all slug test piezometers). Data windows from peak to equilibrium ranged from 4 s to 20 s depending on the dataset and amount of apparent noise. The Butler High-K analyses method was used to calculate K. In most cases the auto-fit curve provided an acceptable best-fit curve (obtained by selecting the play button "fit"). If further manual adjustment of the auto-fitted curve resulted in a new K value that was more than ~2x10-4 m/s different from the auto-fitted curve, then the manually adjusted curve and resulting K value was used instead of the auto-fitted curve and K value. Only two slug test curves needed manual adjustment (Ole pz86_12 and pz44_11). See the summary tables below for the AquiferTest derived K_h values.

Table 1B1. OLE$_{mc}$ AquiferTest K_h values from slug test data.

	auto-fit		manual adjust		Data window	
	(m/d)	(m/s)	(m/d)	(m/s)	data points	total time (s)
pz101_11	237	2.74E-03			5	5
pz101_12	90	1.04E-03			4	4
pz101_51	238	2.76E-03			11	5
pz101_52	125	1.45E-03			21	10
pz101_11 b=100m[a]	237	2.74E-03			5	4
pz101_11 b=1m[a]	262	3.03E-03			5	4
pz86_11	120	1.39E-03			16	15
pz86_12	~~107~~	~~1.24E-03~~	85	9.84E-04	26	25
pz86_51	125	1.45E-03			11	5
pz86_52	162	1.88E-03			21	10
pz81_11	129	1.49E-03			6	5
pz81_12	107	1.24E-03			8	7
pz51_11	104	1.20E-03			4	3
pz51_12	77	8.93E-04			6	5
pz44_11	~~588~~	~~6.81E-03~~	693	8.02E-03	6	5
pz44_12	274	3.17E-03			3	2
pz58_51ns	112	1.30E-03			8	3.5
pz58_52ns	115	1.33E-03			9	4

[a] These tests utilized the pz101_11 slug test data, but the aquifer thickness parameter was changed from 10 m (the default b for all my slug test analyses) to 100 m and 1 m in order to test the sensitivity of the Kh determination on aquifer thickness. Since the difference between the derived Kh values is small; Kh determination in AquiferTest is assumed to be mostly insensitive to aquifer thickness, and b=10 m is used for all analyses.

Table 1B2. QTZ Creek. AquiferTest K_h values from slug test data.

	auto-fit		Data window	
	(m/d)	(m/s)	data points	total time (s)
pz42_12	147	1.70E-03	8	7
pz42_11	119	1.38E-03	9	8
pz39_12	226	2.62E-03	7	6
pz39_11	106	1.23E-03	8	7
pz25_12	224	2.59E-03	11	10
pz25_11	114	1.32E-03	12	11
pz09_12	62	7.22E-04	10	9
pz09_11	51	5.90E-04	9	8
pz07_12	135	1.56E-03	9	8
pz07_11	150	1.74E-03	5	4

Table 1B3. TRL AquiferTest K_h values from slug test data.

	auto-fit		Data window	
	(m/d)	(m/s)	data points	total time (s)
pz51_11	60	6.99E-04	12	11
pz51_12	61	7.01E-04	10	9
pz51_51[a]	35	4.06E-04	60	30
pz51_52[a]	67	7.75E-04	60	30
pz24_11	78	9.08E-04	9	8
pz24_12	65	7.57E-04	9	8
pz24_51	50	5.75E-04	30	15
pz24_52	48	5.51E-04	20	10
pz2_11	138	1.60E-03	10	9
pz2_12	95	1.10E-03	12	11
pz2_51	38	4.43E-04	60	30
pz2_52	43	5.03E-04	60	30
pz19_11	134	1.55E-03	8	7
pz19_12	108	1.25E-03	5	4
pz19_51[a]	26	3.04E-04	40	20
pz19_52[a]	25	2.95E-04	40	20
pz1_11	26	3.04E-04	9	8
pz1_12	37	4.33E-04	19	18
pz1_51	34	3.95E-04	40	20
pz1_52	34	3.91E-04	40	20
pz58sl1sg_51[b]	18	2.04E-04	120	60
pz58sl1sg_52[b]	18	2.05E-04	120	60

[a] Noisy data and poor curve fit. AquiferTest derived Kh value not used.

[b] The only redd in the Trail Creek study section was located less than 1 m from pz58. pz58 was not intended to be a slug test well; however I conducted one anyway due to the proximity of the redd. Due to the different dimensions of the well, the slug test data is not considered suitable for comparison to slug test data from the other slug tests.

Table 1B4. WHL_{mc} AquiferTest K_h values from slug test data.

	auto-fit		Data window	
	(m/d)	(m/s)	data points	total time (s)
pz41_51	35	4.08E-04	33	16.5
pz41_52	34	3.91E-04	33	16.5
pz36_51	89	1.03E-03	11	5.5
pz36_52	94	1.09E-03	11	5
pz19_51	103	1.19E-03	11	5
pz19_52	82	9.45E-04	21	10
pz09_51	577	6.68E-03	21	10
pz09_52	750	8.68E-03	20	9.5

1.B.ii. Streambed flux analyes

iButton calibration

Vertical arrays of thermistor dataloggers (Maxim iButton, model DS1921Z) measured stream and streambed temperatures. Manufacturer accuracy limits are +/- 1 °C; however, prior to deployment, all iButtons were calibrated in a laboratory grade temperature controlled water bath and exposed to the full range of expected temperatures. After comparing the water bath temperature to each iButton's recorded temperature, correction factors were applied to each individual iButton. Corrected iButton temperatures were accurate to within +/- 0.2°C when compared with the bath temperatures.

Ex-Stream

Vertical iButton array dataloggers recorded water temperatures at 30 minute intervals. The dataloggers are capable of storing 2048 temperature recordings with time stamps; therefore, measuring and recording temperature at 30 minutes intervals the memory capacity fills after 42.67 days. The temperature datasets were used to calculate vertical streambed flux using the MATLAB program Ex-Stream, developed by Swanson and Cardenas (2010). Sensor spacing is an input parameter for Ex-Stream and array designs and sensor spacings are explained below. For all designs, the temperature recorded by the stream dataloggers was assumed to be representative of the streambed sediment at the stream – streambed interface. The top of the upper baffle was placed flush with the streambed. The distance from the top of this upper baffle to the center point of the middle iButton pair in design 1 and 2 was ~8 cm. A second baffle is positioned between the middle and lower iButton pairs in designs 1 and 2. The distance from the top of the upper baffle to the center point of the lower iButton pair in designs 1 and 2 was ~25 cm. Since sensor spacing for design 3 was variable, each the spacing was measured individually for each array and these datasets were run individually in Ex-Stream to allow for more accurate flux calculations by using true sensor spacing distances. Sensor spacing for design 3 arrays was measured as the distance from the top of the streambed to the center point of the hanging iButton pair. The hanging iButton pair was tapped to a ~15 cm bolt; ~10 cm up from the iButton pair, a baffle consisting of two 2.5 cm diameter washers was held in place by three nuts.

Ex-Stream requires 1 min interval input data; so I linearly interpolated my 30 min interval iButton temperature datasets to 1 min using Excel. The Hatch (2006) and Keery (2007) methods (hereafter, these will be referred to as the 'Hatch method' and 'Keery method') were the appropriate analytical models to use on my data; in Ex-Stream both models assess amplitude ratio differences (Ar method) and phase differences (Dp method) between vertically separated temperature datasets to calculate daily averaged vertical streambed flux (q_v, in m/d). The Ar method reliably estimates flux magnitude and direction within a range of -5 to 3 m/d (Hatch, 2006). The Dp method calculates only flux magnitude and reliably estimates flux in a range of -7 to 7 m/d (Hatch, 2006). The Keery method is more straightforward that the Hatch method in that it does not consider thermomechanical dispersion.

Swanson and Cardenas (2010) model synthetic fluid fluxes varying between +/- 0.27 m/d and found that the Hatch model (with thermal dispersivity turned off) and Keery model output the same flux value. Ar method error was ~10^{-4} m/d, while the Dp method error was ~10^{-1} m/d. The Dp method is more sensitive and therefore produces more error (Swanson and Cardenas, 2010).

In calculating flux with my data, the Hatch model constantly produced errors (e.g. Amplitude ratio too high) and was unable to analyze my data. The Keery method, however, rarely if ever produced errors and was able to output flux values for all my input temperature data. Due to the simplicity and similar performance of the Keery method compared to the Hatch method (Swanson and Cardenas, 2010), I used the Keery method for all my flux calculations. Additionally, the Ar method calculated fluxes were the only fluxes considered. Dp method calculated fluxes were not considered due to incoherent output values, high sensitivity and error associated with the method, and lack of flux direction in the output.

Below is a screen-shot of the input parameters and selected options I used in model runs. Default model parameters for thermal conductivity, fluid density, specific heat and grain density were used for all model runs. Mixed sand and gravel ranges in porosity from 20-35% while well-sorted sand and gravel ranges from 25-50%. The streambed sediments in the four study sections are best characterized as mixed sand and gravel; therefore, the conservative estimate of 20% porosity was used for all Ex-Stream model runs. In Ex-Stream, porosity influences the outputted flux estimation because porosity is included in the calculation of bulk density and other thermal properties (Swanson and Cardenas, 2010b: Ex-Stream Help File). In assessing how Ex-Stream responds to changes in porosity, I found that computed flux values for the Keery method had a positive correction and the Hatch method a negative correlation with changes in porosity (e.g. increase in n caused increase in q for Keery but a decrease in q for Hatch).

Fitted curve data only outputs to the fit_data folder if "Use CurveFit" is left unselected. Therefore, in order to conduct QA&QC on the fitted data, CurveFit was not used. The same 38 day temperature dataset was run through Ex-Stream with and without CurveFit; there was effectively no difference in the computed flux values.

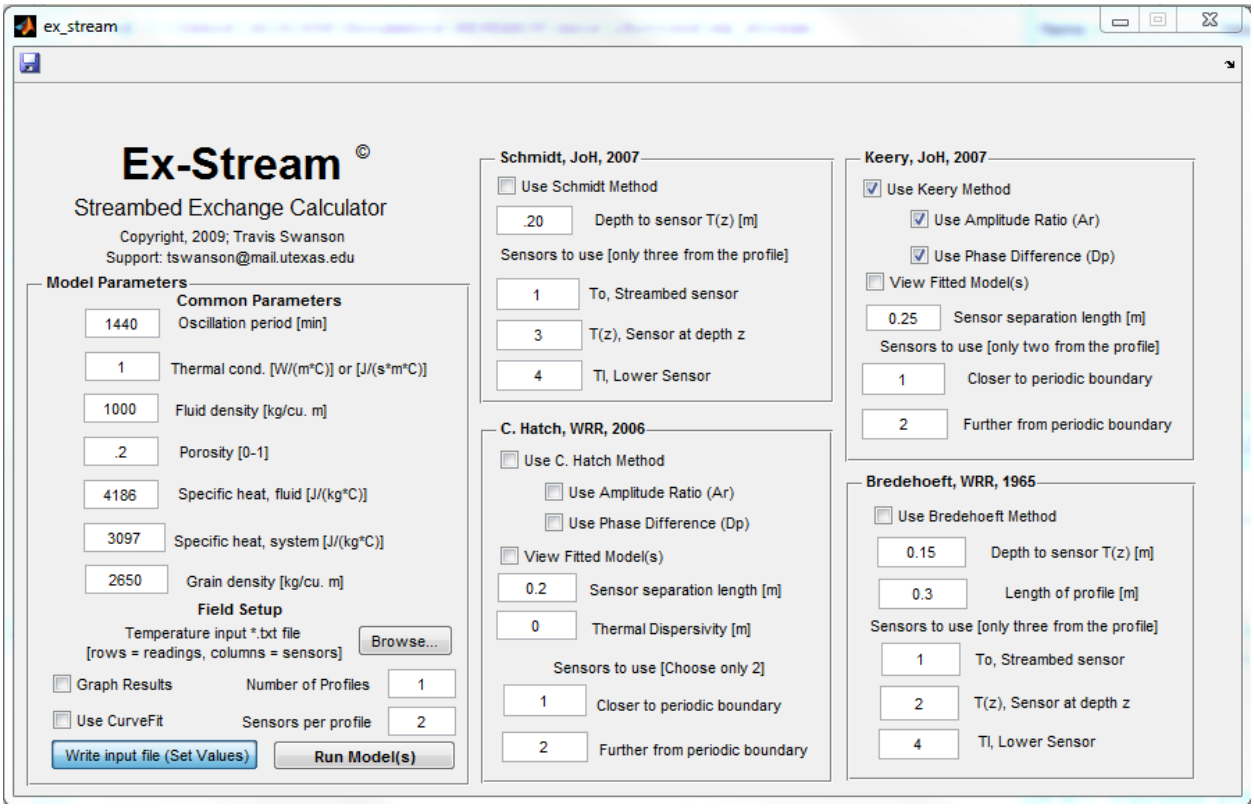

Figure 1B1. Screen-shot of Ex-Stream input parameters and selected options used to obtain vertical streambed flux.

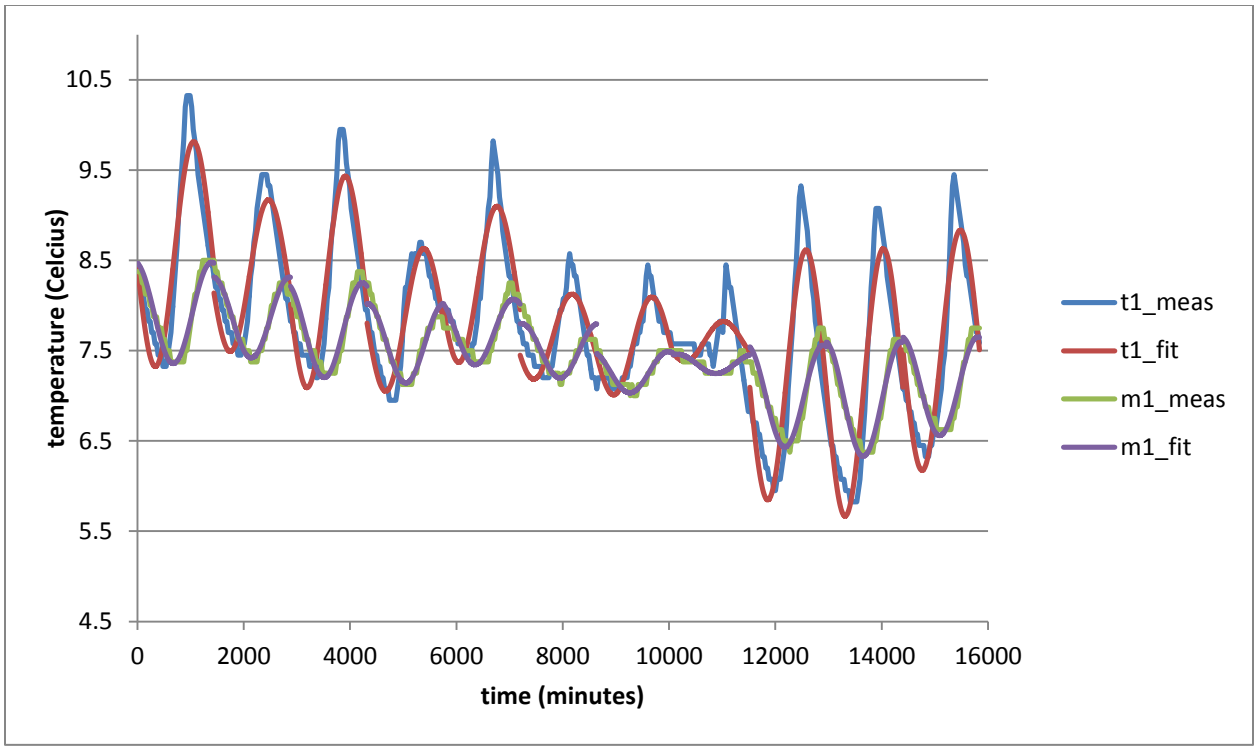

Figure 1B2.Plot of interpolated iButton data and ExStream curve fitted lines for Ole pz44sr3sgst from 9/12/11-9/22/11 (the t1 is the stream temperature sensor; m1 is the upper streambed sensor).

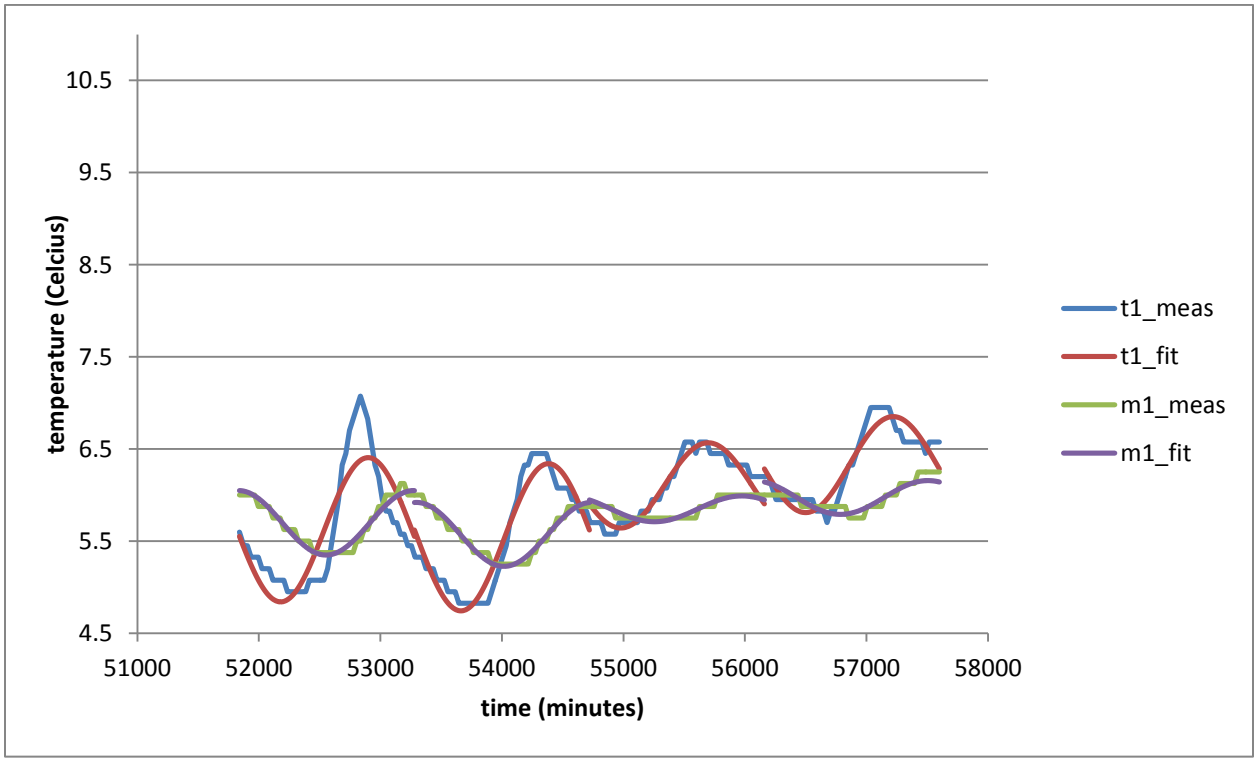

Figure 1B3. Plot of interpolated iButton data and ExStream curve fitted lines for Ole pz44sr3sgst from 10/18/11-10/21/11 (the t1 is the stream temperature sensor; m1 is the upper streambed sensor).

Nonhydrostatic and hydrostatic drivers of streambed flux

Vertical streambed flux (q_v) magnitude and direction are controlled by streambed pressure gradients caused by nonhydrostatic and hydrostatic conditions (e.g. Janssen, et al., 2012). A primary driver of nonhydrostatic contribution to hyporheic flow arises from turbulent flow over bedforms, which causes redirection in fluid momentum (e.g. Janssen, et al 2012). This process is known as "pumping". Nonhydrostatic ("pumping") conditions cause increased streambed flux (and decreased hyporheic residence time) with increased stream discharge (Janssen, et al. 2012). In contrast, hydrostatic conditions cause decreased streambed flux with increased stream discharge due to flattening of the water surface profile in relation to bedform curvature (Tonina and Buffington, 2009a). Therefore, this balancing of streambed pressure gradient changes with small changes in stream stage due to precipitation events during the study period can help explain the lack of change in vertical q_v at my sites.

1.B.iii. Hydraulic conductivity (K) and redd occurrence

To plot the distance downstream of slug test piezometers (and obtained horizontal hydraulic conductivity values) in relation to redd occurrence, the piezometers and redds were matched with the most proximal long profile topographic survey point. The piezometer or redd was then assigned this distance downstream within the topographically surveyed long profile. Distance downstream within the long profile is calculated by applying the distance formula to the northing and easting coordinates of adjacent long profile points and then adding the cumulative distances between points starting with the first long profile point as zero.

Table 1B5. Slug test piezometer longitudinal study section position was estimated by matching the piezometer location with the nearest total station surveyed long profile point using Arc10.0.

		Long Profile	
	Slug test piezometer	Surveyed point name	Distance downstream (m)
Ole	pz44	89	129
	pz51	164	301
	pz58	245	395
	pz81	362	534
	pz86	370	597
	pz101	458	871
Quartz	pz42	237	59
	pz39	242	69
	pz25	71	166
	pz09	125	277
	pz07	129	292
Trail	pz51	157	100
	pz24	48,23	417
	pz2	31	472
	pz19	33	483
	pz1	29	619
Whale	pz41	39	0
	pz36	62	41
	pz19	179	338

	pz09	267	456

Table 1B6. Bull trout redd longitudinal study section position was estimated by matching the redd location (or redd cluster location) with the nearest total station surveyed long profile point using Arc10.0.

			Long Profile	
	Redd name	Total # of redds	surveyed point name	distance downstream
Ole	3	1		-20
	4	1	245	395
	16, 17	2	440	706
	18, 19, 20, 21	4	458	871
Quartz	10	1	225	36
	9	1	234	56
	8	1	71	166
	7	1	96	206
	6	1	118	243
	5, 4, 3	3	123	262
	2, 1	2	128	290
Trail	7	1	144	18

APPENDIX 2A: Valley-scale geomorphology

2.A.i. Valley-confinement

Delineations of unconfined and confined valleys were conducted for all catchments of the Flathead River basin by Wenger et al. (2011). Shapefiles of these delineations were shared with me courtesy of David Nagel and Sharon Parkes with the US Forest Service Rocky Mountain Research Station in Boise, Idaho.

Editing Trail Creek VBclass=0, FID 152:

Most of the upstream portion of this polygon is the delineation of a terrace above Trail Creek. I have edited the polygon to include only the Trail Creek valley bottom portions.

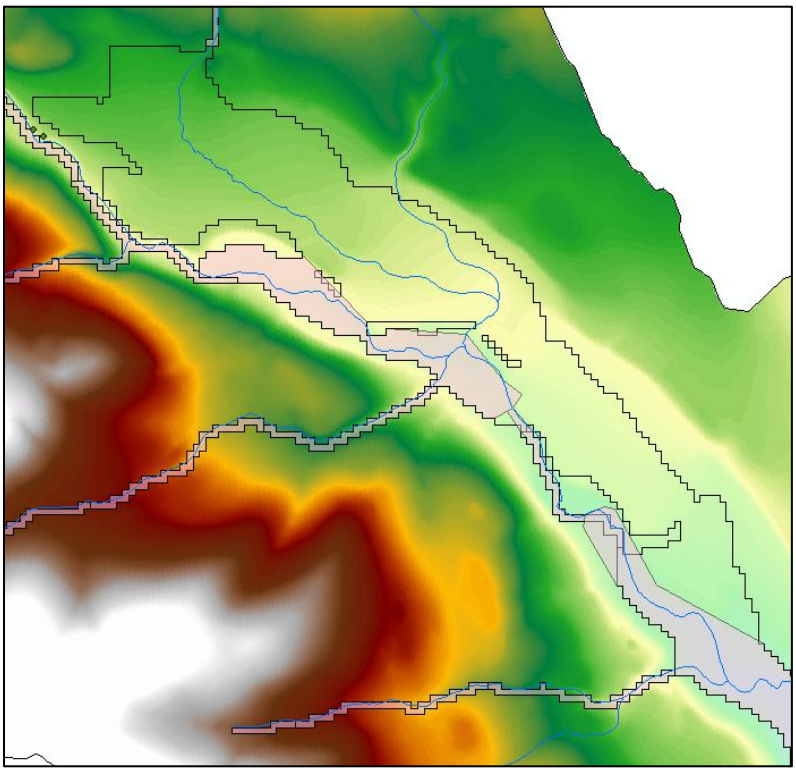

Figure 2A1. The original Trail Creek valley bottom polygon (FID 152) which falsely includes a terrace above the Trail Creek valley floor is indicated by the hollow outline. The pink polygons show the new, edited, more accurate valley bottom delineation.

Extended notes and observations about valley confinement and distribution of 2011 redds

In the Ole catchment, there are 2 unconfined valley segments – both are ~4 km long and are located near the midpoint of the catchment. Bull trout spawning and rearing is not known to extend into the upstream unconfined valley (USFWS, 2008). Bull trout redds observed in 2011 were clustered near the downstream extent of the lower unconfined valley (n=21) as well as 50-1500 m downstream of this unconfined valley in the confined valley segment (n=19, Figure 19a, Table 7). The furthest downstream ~3 km+ of Ole Creek is coarser and steeper and has narrower valley walls than the rest of the drainage of the highlighted spawning and rearing area. Redds are rarely observed in this section (John Fraley, 2011, personal communication).

In the Quartz catchment, there is a 1.5 km long unconfined valley that extends from the confluence of Rainbow and Quartz Creeks to Quartz Lake (Figure 19b). The majority of 2011 bull trout

redds were distributed fairly evenly throughout this unconfined valley (n=35); several redds were located 100-280 m downstream of Cerulean Lake in the confined valley section (n=8; Figure 19, Table 7). The bull trout spawning in Rainbow Creek may be a separate resident population of Cerulean Lake (Tennant, 2010); however, genetics studies indicate that the Quartz and Cerulean Lake populations are connected (Clint Muhlfeld, 2011, personal communication).

In the Trail catchment, there is a 1 km long unconfined valley segment in the known spawning and rearing reach (Figure 19c) (USFWS, 2008). Migratory spawning bull trout are unable to access much of the Trail Creek drainage because of an intermittent stream section that acts as a migration barrier during late summer and fall baseflow conditions (the bottom of the intermittent stream section is indicated by the yellow star in Figure 19c). The majority of 2011 redds in Trail were dispersed in a confined valley ranging from 60 m to 2500 m downstream from the migration barrier (n=7); the furthest downstream redd was located in the aforementioned unconfined valley segment (Figure 19c; Table 7).

In the Whale catchment, there are two unconfined valley segments – the larger of which is about 12 km long and hosted all the 2011 bull trout redds observed in the Whale drainage (n=43, Figure 19d, Table 7). Whale Creek Falls, located just upstream of the upstream extent of the large unconfined valley, presents a barrier to further upstream fish migration in Whale Creek (the barrier is indicated by the yellow star in Figure 19d). Bull trout can however migrate up the adjacent tributaries near the upstream extent of the large alluvial valley. These adjacent tributaries are not included in the annual "index stream" redd count surveys. However, the southern tributary, Shorty Creek, which hosts a ~2 km long unconfined valley, is known to annually host spawning bull trout (Tom Weaver, 2012, personal communication) (Figure 19d).

APPENDIX 2B: Valley-scale hydrogeology

2.B.i. Spatial water temperature comparisons

Stream temperature data from above, within, and below each study area was compiled to compare variability and rates of change in stream temperature during the months immediately prior to, during, and after the 2011 spawning season (mostly August, September, and October temperatures). Dr. Clint Muhlfeld and Leslie Jones of the USGS provided stream temperatures for above and below the Ole Creek study section (Ole Upper = FHR_234; Ole Lower = FHR_092) and above and within the Quartz Creek study section (Rainbow, below the mouth of Cerulean Lake = FHR_099; Quartz, above the mouth of Quartz Creek as it drains into Upper Quartz Lake = FHR_096). Pat Van Emerien of the Flathead National Forest (FNF) provided stream temperature data from above and within the Trail Creek study reach and above and below the Whale Creek study reach. All these temperature data were collected by Hobo U22-001 units. The USGS and FNF data were collected at hourly intervals; so I filtered my data to include only hourly data points for my statistical comparisons of water temperate averages, variances, standard deviations, and rates of change. *(see "All_stream_temp_spatially_compiled.xlsx" in data>water temperature>spatial comparisons.)*

Regional groundwater temperature estimation

Groundwater temperature is influenced by seasonal variations in surface heat from the sun and by the geothermal gradient (1.8-3.6˚C/100 m (Heath, 1983); mean of 2.9˚C/100 m (Todd, 1980)) – which is controlled by conductive and convective movement of heat in Earth's interior (Kasenow, 2001). Mean annual groundwater temperature at 10-25 m depth is about 1-2˚C higher than mean annual air temperature (Kasenow, 2001). In this depth range, seasonal fluctuations in groundwater temperature can occur but the temperature is relatively constant (Kasenow, 2001). Below this depth range, the increase in groundwater temperature due to the geothermal gradient is relatively constant (Kasenow, 2001). Tables 2B1 and 2B2 below show that groundwater temperate at 10-25 m depth in the study areas should therefore be ~4-6°C.

Table 2B1. Approximate elevations above mean sea level of each study reach – estimated from a 30 m DEMs obtained from the USGS seamless server.

	Elevation	
study reach	**(m)**	**(ft)**
Ole	1260	4134
Quartz	1370	4495
Trail	1260	4134
Whale	1300	4265

Table 2B2. Average annual air temperature from the SNOTEL stations closest to the study reaches.

SNOTEL					Average Annual Air Temp (°C)					
Station	**#**	**Elev. (ft)**	**Lat**	**Long**	**2007**	**2008**	**2009**	**2010**	**2011**	**5 yr Avg**
Emery Creek	469	4350	48 deg; 26 min N	113 deg; 56 min W	4.8	4.1	4.1	3.9	3.5	4.1
Grave Creek	500	4300	48 deg; 55 min N	114 deg; 46 min W	4.8	3.8	3.9	3.8	3.6	4.0
Many Glacier	613	4900	48 deg; 48 min N	113 deg; 40 min W	5.9	4.8	4.9	4.4	4.3	4.9
									Average	4.3

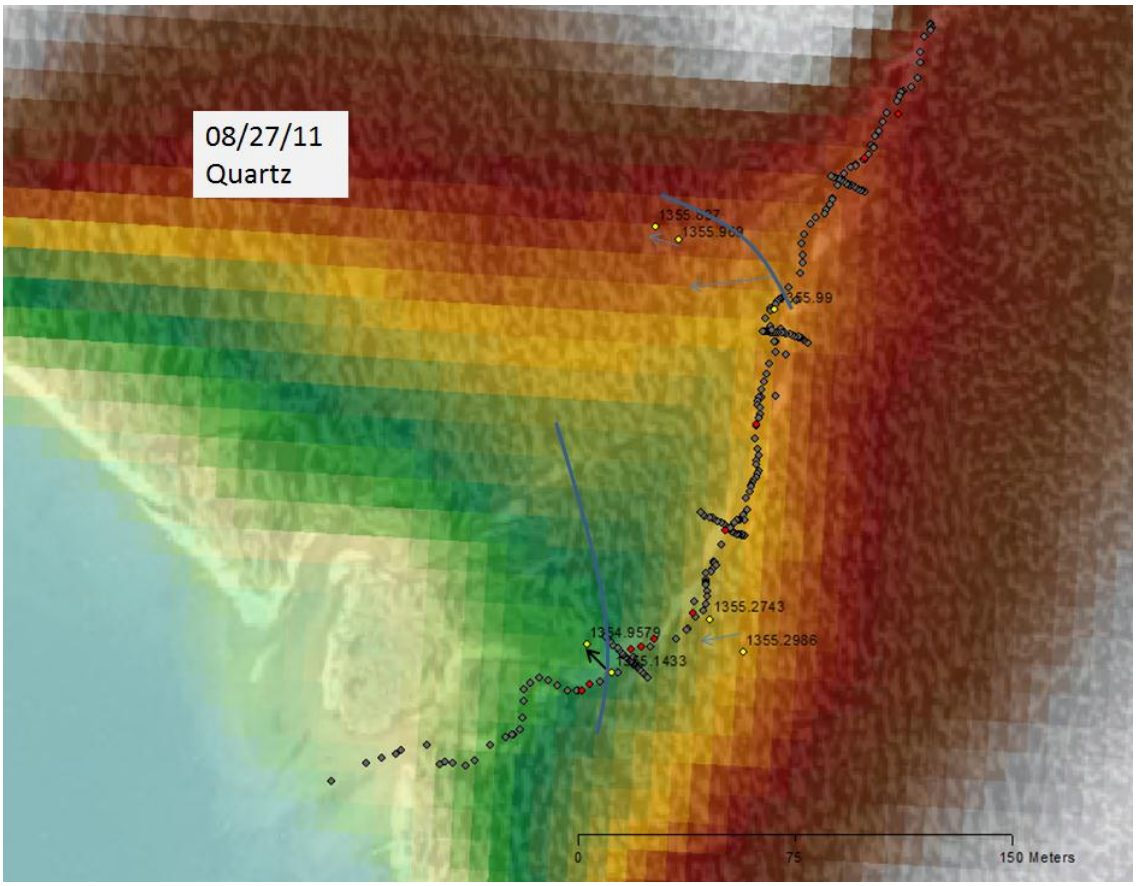

Figure 2B1. Inferred QTZ water table contour lines (blue).

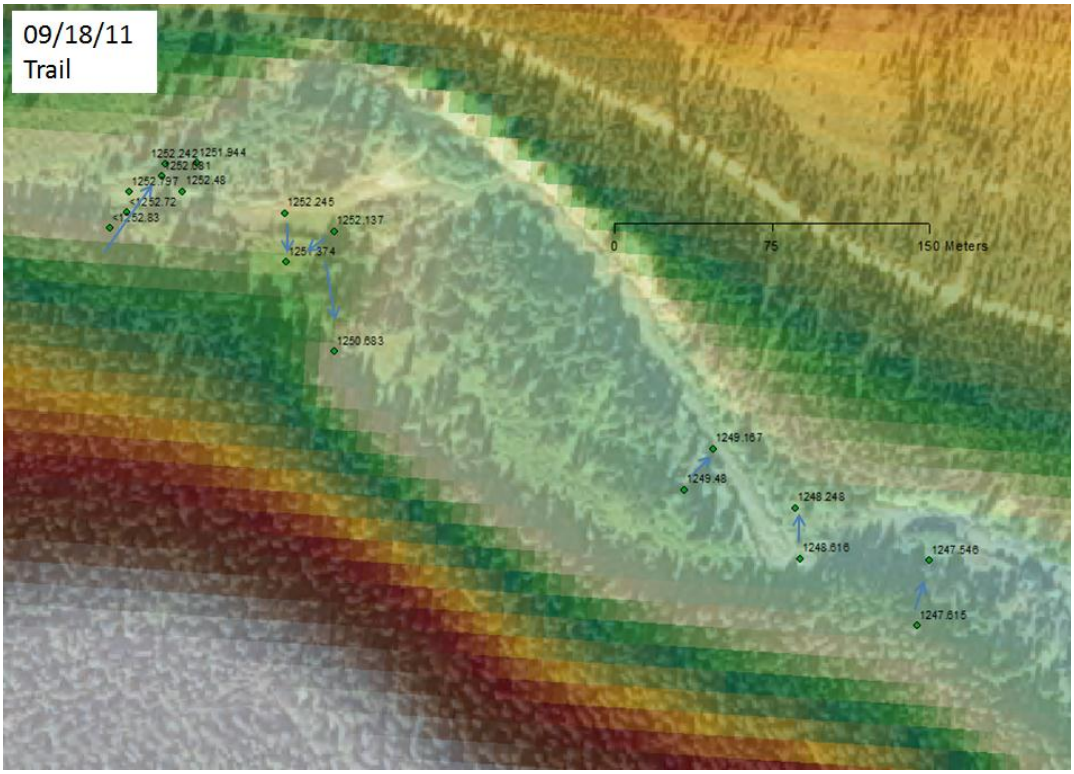

Figure 2B2. TRL stream and floodplain water elevations.

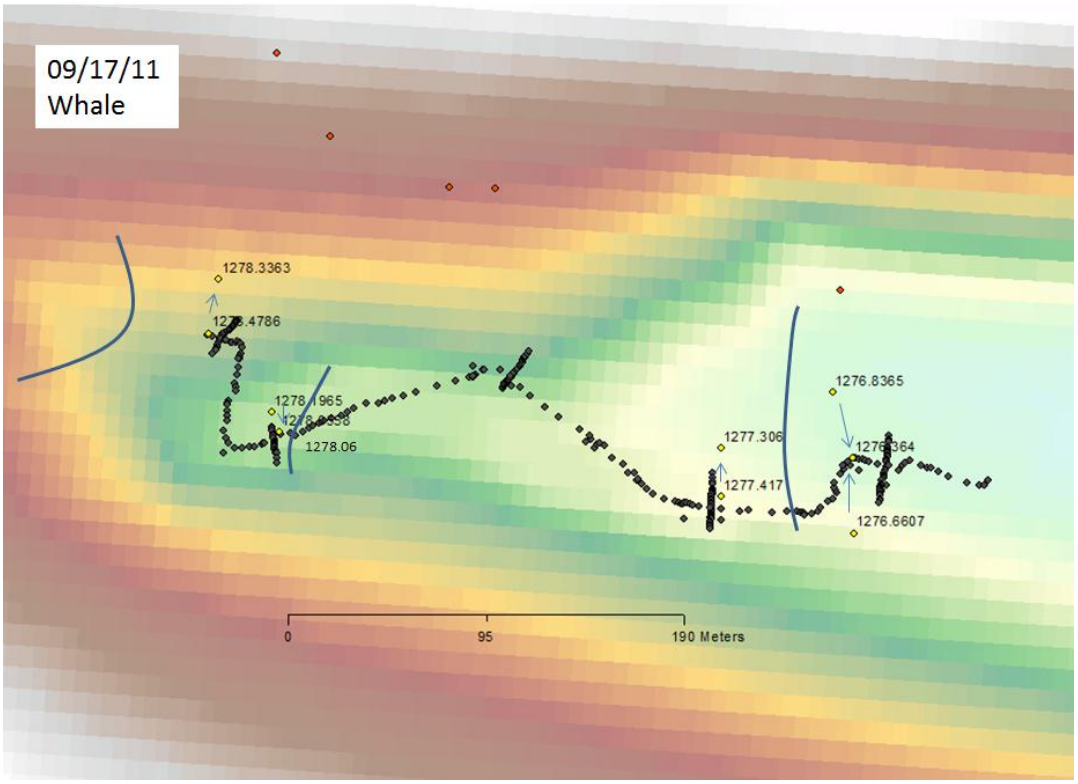

Figure 2B3. WHL_{mc} stream and floodplain water elevations.